Universiy of Pannonia
Faculty of Information Technology
Doctoral School of Information Science

Optimal Current Control for Domestic Power Converters

DOI:10.18136/PE.2021.807

Doctoral (PhD) Thesis

Author: László Richárd Neukirchner

Supervisor: dr. Attila Magyar

Made at:
Universiy of Pannonia
Doctoral School of Information Science

Veszprém
2021

Optimal Current Control for Domestic Power Converters

Thesis for obtaining a PhD degree in the Doctoral School of Doctoral School of Information Scienceof the Universiy of Pannonia

In the branch of Information Technology Sciences.

written by:
László Richárd Neukirchner

Supervisor(s): dr. Attila Magyar

propose acceptance (yes / no)

....
dr. Attila Magyar

The PhD-candidate has achieve .... % in the comprehensive exam.
Veszprém, ...

....
(Chairman of the Examination Committee)

As reviewer, I propose acceptance of the thesis:

Name of Reviewer: .... : yes / no ....
(Reviewer)

Name of Reviewer: .... : yes / no ....
(Reviewer)

The PhD-candidate has achieved .... % at the public discussion.
Veszprém, ...

....
(Chairman of the Committee)

The grade of the PhD Diploma: ....(... %).
Veszprém, ...

....
Chairman of UDHC

Acknowledgement

I would like to express my special thanks of gratitude to my supervisor and teacher Dr. Attila Magyar as well as our principal of the doctoral school Prof. Katalin Hangos who gave me the wonderful opportunity to pursue this excellent project on optimal current control, which also helped me to develop and better myself on the field of scientific work, where I could really see myself grow and develop. I really feel gratitude to them. I would like to also thank Dr. Nimród Kutasi, and his restless support and encouragement in the filed of predictive control, as well as Dr. András Kelemen in the field of power electronics. Without they unquestionable and deep technical knowledge on the field, and they helpfulness, kindness and hospitality this doctoral thesis would not have happened. I would also recognise Dr. Peter Görbe who helped me to put the subject of voltage quality in context and accelerated my progress at the start of my PhD. studies, and Dr. Attila Fodor, who helped me on the filed of current control, and system modeling, and also helped me organise my work and guide me in the forest of research. All of they contribution were invaluable to reach this stage of completion.

Any attempt at any level can't be satisfactorily completed without the support and guidance of my spouse Klaudia, my parents Anikó and László, my sister Elisabeth, and my friends. They helped me a lot with they spiritual and financial support in making this project, despite of their busy schedules. They always could find enough time and energy to give me enough attention and assistance.

I could not thank you enough!

Abstract

Starting the third decade after the millennium, in the European Union, the approach of the energy-, and with it the automotive industries has changed significantly since. The increasing governmental interventions on the industry, started with the bad reputation of diesel in passenger cars, and increasingly tighter restrictions on lead battery technologies, also Germany's renewable policies, dismantling nuclear plants encourage manufacturers and researchers for innovation in the direction of power efficiency. Solutions, which seemed to occupy the second place on the podium, have been re-assessed and re-thought in the light of this approach in terms of power topologies and algorithms alike. As the tide of renewable sources has taken the western Europe with a storm, with the high anticipation of getting rid of fossil fuels (or at least reduce they consumption), it brought down a myriad of problems to solve. The first of these is the high stochastic nature of these source, with the ever increasing demand on storage, to smoothen out the arms of the scale of supply and demand. The second comes with the incentive (policy maker, and civic alike in pursuit of "cheap" and non polluting energy) of installing these sources in residual areas, parking lots, schools, household roofs, just to name a few. On top of that, these actors have higher consumers in they disposal, using them on they whim, making the situation even worse.

This introduces two interesting, yet completely understandable phenomena, which act as the "symptoms" on the quality of our well accessible electric power for our consumers, due to the reason of these trends. The first is the harmonic distortion of the network's voltage phases, tackled with load regulations, and a wide range of active and passive filter designs. The second is the voltage phase asymmetry alias the voltage unbalance, appearing when uneven production, consumption, or distribution on the network. This is a major yet often overlooked power quality problem in low voltage residential feeders due to the random location and rating of single-phase renewable sources and uneven distribution of household loads. Here a new indicator of voltage deviation is proposed that may serve as a basis of analysis and compensation methods in this dimension of power quality. The first half of this dissertation is about indicating such voltage asymmetry and mitigating it with a complex controller and electric power conversion structure, which is integrated with an optimization based control algorithm that uses asynchronous parallel pattern search as its engine. This structure uses current control on each phase to achieve the results, on the voltage quality.

The second half is zooming down on the current control aspect itself, where

a model of a power converter device is used for an optimal, predictive controller structure, to achieve the demanded efficiency, also with the calculation capacity in check. Starting with the design of a constrained optimal control of a current source rectifier, based on a mathematical model developed in Clarke and Park frame. Despite the clean establishment of the model's differential equations, the underlying bilinearity would make further controller design complicated. To comply with the system constraints an explicit model-based predictive controller was established. To simplify the control design, and eliminate the bilinearity from the equation system, a disjointed model was utilised due to the significant time constant differences between the AC and DC side dynamics. As a result, active damping was used on the AC side, and explicit model based predictive control on the DC side. The results are compared by simulation with the performance of a state feedback control.

Tartalmi Kivonat

Az ezredév forduló utáni harmadik évtized kezdetén az Európai unió hozzáállása az autó- és energiaiparhoz nagyban megváltozott. A tagállamok rendeletekkel és megszorításokkal való beavatkozása az ipari szférába rossz színben kezdte feltüntetni a dízelautókat, illetve erős szabályozásnak tette ki az ólomsavas akkumulátor alkalmazóit. Németország megújuló energia stratégiája, és atomerőműveinek lebontása új kihívások elé állította a kutatókat az energiahatékonyság innovációja terén. Azon technológiai és algoritmikus megoldások, melyek eddig másodlagos helyen tűntek fel, most újra napvilágra kerültek átgondoltabb formában az új körülményekhez igazodva. Eközben a megújuló energia vihara meghódította nyugat Európát. Ennek melléktermék és hogy közben hogy a fosszilis üzemanyagoktól megszabaduljanak (vagy legalábbis csökkentsék használatukat), egy sor új megoldandó problémára vetett napvilágot. Az elsődleges ezek között az energiaforrások megerősödött sztochasztikus termelési és fogyasztási hajlama. Mindemellett a megnövekedett energia tárolási igény, hogy a kereslet és kínálatot szimbolizáló mérleg serpenyői egyensúlyba kerüljenek. A másodlagos az energiatakarékosság szándéka (mely törvényhozói és civil oldalon egyaránt az alsó, alacsony káros anyag kibocsátással járó energiát célozza meg), melynek során ezeket a megújuló forrásokat megnövekedett számban szerelik fel parkolókba, iskolákba, családi házak tetejére, hogy csak egy párat említsünk. Ezenfelül ezek a szereplők azóta megnövekedett energia igénnyel is rendelkeznek, tovább súlyosbítva a helyzetet. Ez két figyelemre méltó de ugyanakkor teljesen érthető jelenséget enged mutatni, melyek a fogyasztók által oly könnyen hozzáférhető energiaforrásaink a "szimptómáit" reprezentálják. Az első a hálózati fázis feszültségek felharmonikus torzítása, melyek fogyasztói szabályozással, és széles körű aktív és passzív szűréssel igyekeznek orvosolni. A második a fázis feszültség vektorok aszimmetriája, vagy más szóval feszültség aszimmetria, mely a fogyasztók és termelők kiegyensúlyozatlan hálózati eloszlásán alapulnak. Ez a fontos, ugyanakkor sokszor elhanyagolt energiaminőségi probléma főként annak tudható be, hogy a kisfeszültségű hálózatok háztartási termelőinek és fogyasztóinak időbeli és topológiai eloszlása véletlenszerű. Ebben a disszertációban egy új indikátor kerül bemutatásra a feszültség aszimmetria detektálására, mely alapul szolgálhat annak kompenzálására egyaránt, hozzájárulva az áram minőségi kérdés ezen dimenziójához. A dolgozat első fele ennek a jelenségnek a detektálására, és kompenzálására helyezi a hangsúlyt. Mindezt egy komplex teljesítményelektronikai struktúra segítségével, mely optimalizáción alapuló szabályozási algoritmussal lett ellátva, mely aszimmetrikus párhuzamos mintakereső

algoritmust (APPS) használ. Ez a struktúra fázisonkénti áram szabályozást alkalmaz, hogy elérje a kiszabott minőségjavulási határértéket.
A dolgozat második fele magára az áramszabályozási aspektusra fókuszál. Ennek során egy "buck" típusú áram vezérelt egyenirányító konverter kapcsolás differenciál egyenlet rendszerét, modell alapú prediktív szabályozásnak lett alávetve, a hatékonyság és a számítási kapacitás kritériumának jegyében. Ez a típusú konverter nem annyira elterjedt (a "boost" típusú, a feszültség-átalakítóhoz, a feszültség-inverterhez képest), de jelentős előnyei vannak, mert feszültség-csökkentő kapcsolásként használható. A kapott modellt alapul véve, és a rendszert érintő korlátozásnak eleget téve, egy explicit modell alapú prediktív szabályozó került megtervezésre. Itt modell differencia egyenleteinek letisztultsága ellenére, a beágyazott bilinearitás további szabályozótervezési komplikációkhoz vezetett volna. A tervezési nehézségek és ezáltal az egyenlet rendszer bilinearitásának feloldására, egy egyen és váltakozó áramú oldalt szétcsatoló alkalmazás lett megvalósítva, felhasználva az AC és DC oldal időállandóbeli különbözőségét. Ennek eredményeképp aktív szűrés került implementálásra az AC, míg explicit modell alapú prediktív szabályozás lett megvalósítva a DC oldalon. Az eredmények szimulációs környezetben kerültek összehasonlításra egy állapotvisszacsatoláson alapuló szabályozás teljesítményével.

Rezumat

La începutul deceniului trei după trecerea de mileniu, se observă o abordare radical diferită a Uniunii Europene față de industria auto și energie. Intervenția statelor membre în sfera industrială prin restricții și norme din ce în ce mai stricte, a condus la o reputație proastă a mașinilor diesel și a restricționat drastic utilizarea acumulatoarelor cu plumb. Strategia Germaniei în domeniul energiilor regenerabile, închiderea centralelor nucleare, a impulsionat cercetările privind eficientizarea consumului de energie. Soluțiile existente de optimizare, algoritmii existenți dar aflați pe plan secund au fost regândite și folosite cu succes în noul context. Între timp în occident se observă răspândirea furtunoasă a soluțiilor de energie regenerabile. Aceste tehnologii, precum și dorința de a reduce la minim folosirea resurselor de energie fosile, a condus la un șir întreg de probleme noi de rezolvat. Problema primară este caracterul aleatoriu atât a surselor de producție precum și a consumatorilor de energie. Totodată se impune o capacitate ridicată de stocare a energiei, pentru a putea echilibra cererea și oferta în orice situație. Problema secundară se datorează dorinței de reduce consumul de energie (atât legislativ cât și prin activități civice se dorește reducerea emisiilor poluante și folosirea energiilor regenerabile), astfel se montează aproape în orice loc posibil generatoare de energie verde, cum ar fi pe acoperișul școlilor, caselor, a locurilor de parcare, etc. Aceste tendințe noi de producție și consum de energie conduc la cel puțin două fenomene importante în distribuția energiei electrice. Prima problemă majoră este conținutul armonicilor în tensiunile de fază din rețelele de alimentare, aceste distorsiuni armonici fiind eliminați sau reduși prin reglementări către consumatori și aplicarea unor filtre active și pasive către rețea. A doua problemă este asimetria tensiunilor de fază, care se datorează consumului și mai nou a producției dezechilibrate de energie raportat la cele trei faze din rețea. Acest aspect important, dar neglijat de multe ori se datorează în principiu faptului că producătorii și consumatorii de joasă tensiune sunt distribuiți aleatoriu atât în timp, cât și topologic. În această teză se introduce un nou indicator pentru detectarea asimetriilor de tensiune din rețeaua de alimentare, acesta contribuind la soluțiile de compensare a acestor asimetrii. Prima parte a tezei abordează această problematică de detectare și compensare a asimetriilor de tensiune din rețelele de alimentare. Problema se tratează pe o structură complexă de electronică de putere, în care s-a implementat un algoritm de reglare optimal, folosind un algoritm de căutare asimetric paralel de eșantioane(APPS). Această soluție folosește reglarea curenților de fază pentru a obține indiciile de performanță impuse.

Partea a doua a lucrării abordează metode de reglare evoluate pentru un convertor electronic de putere AC-DC, tip buck cu invertor de curent. Acest tip de convertor nu este atât de răspândit (comparativ cu convertorul tip boost, ridicător de tensiune, cu invertor de tensiune) dar are avantaje semnificative, deoarece se poate folosii ca și redresor coborâtor de tensiune. În teză am abordat modelarea matematică a convertorului și am studiat metode de reglare predictive bazate pe model a convertorului. Am constatat că metoda abordabilă este o reglare separată a părții AC (curenții de fază) și reglare separată a mărimilor electrice din partea DC (tensiune și curent). Se pot utiliza regulatoare separate din cauza dinamicii diferite a celor două părți din convertor, diferența fiind de câteva ordini de mărime. Pe partea AC am implementat un filtru activ, iar pe partea DC un regulator bazat pe model explicit (Exp-MPC). Rezultatele sunt demonstrate prin simulări și am realizat o comparație cu un regulator după stare.

List of contents

Chapter 1

Introduction

Growth of distributed generation from renewable energy sources and the nature of the electrical power grid initiated a trend to alter from a passive network to an active one. So called smart grids have the ability to provide much more in depth observable measurement results of their customers, grid operators and energy traders alike. Through voltage and current measurements, the habits of each actor (household, station, or industrial- commercial facility) can be easily mapped and taken into account. Moreover, the potential failure could be indicated and preemptively acted upon, before irreversible malfunction, significant amount of wear, or generally, the efficiency of energy consuming actor's power electric consumer's diminishes. In most cases, only smart metering is present, whilst central control and measurement is not an option.

In this new environment, the importance and difficulty of maintenance and operational stability and cost effective control of the distribution system are increasing together. With this in mind local solutions are the most convenient solutions, and as opposed to this expectation most of a household's possible renewable sources and loads are unevenly distributed, without mindful control over single phase power converters. Some of these could represent an unevenly high power consumption, or worse a locally significant energy source in times where it's most unnecessary, especially outside peak zones of consumption. The situation is further exacerbated by the stochastic on/off switching of the different types of loads. This cause stochastic disturbing unbalance in the load currents which cases unbalanced load of the low voltage transformer, and amplitude- and phase unbalance in the voltage phasor trough the serial impedance of the low voltage transportation line wires and connecting devices cables.

If we observe the opposite side, ideal generators supply symmetrical three-phase sinusoidal positive sequence voltages, which are balanced in terms of their amplitudes phase differences at a single frequency. With this in mind voltage (as such consumption- and production-) unbalance occurs on the network. The terminology of unbalance can be divided into amplitude unbalance, phase difference unbalance, and unbalanced harmonic disturbance. The occurrence of at least one of these features is enough for a distribution network to

become unbalanced.
Many countries have changed their regulating laws about power supply to allow for grid-tie inverter systems to provide spare power from renewable sources to local low voltage grids.The unbalance of the grid is further increased by using single phase grid tie inverter systems in the size of typical small household power plants (1 - 5 kVA) and the produced electrical power originating from renewable power source (wind and solar) also admits stochastic behavior. This unbalance yields to a suboptimal operation of low voltage three phase transformers and machines to generate undesirable additional yield loss and increase in the probability of malfunction of the low voltage energy transportation system's components, or the effective current unbalance could cause additional power loss of the transportation line resistances or in the end complete shutdown.
To mitigate or avoid such situations an approach is required, where the system where aforementioned phenomena occurs is an optimization problem. However to formulate an optimization problem, many things should be established to formulate it properly. Most importantly, a cost function should be established which can be served as a measure of goodness for solving the question. For instance, if voltage unbalance would be eliminated, than the correct indicator of unbalance should serve as basis, moreover the deviation from the optimum could be quadratic.
Such tasks can not be achieved without proper instrumentation. To be able to apply control, where he voltage levels are designated, and the end user has no direct control (only the plant or transformer level has such), deviations can be addressed, and current control can be used as actuation. This way a control structure can be imagined for a power electric converter, where every step should count towards the optimum state, with respect to the energy (or control reserves), wear of the device (sub components, namely gates have finite switching capabilities), and safety constraints (designated level of current and voltage should not trespass a given hard constraint for the sake of malfunction avoidance, and soft constraint for the sake of reducing wear). Additionally it should not be forgotten, that with all the above, the device should operate in the domains of kHz or above, and it should be run on a cheap device, like an embedded micro-controller chip or digital signal processor (DSP). With all this in mind a power electric structure can be designed to fulfill the high standards of today's requirements. The problem is, conventional controllers can not achieve al this requirements. The methodology based on optimal control, was originally designed for highly complex, and safety critical systems, with huge amount of inputs and outputs, power plants, and chemical- or refinery plants. These systems though, have an incomparably lower time constant, which renders conventional model based predictive controllers useless in the domain of power electronics.
To marry the two approaches together, a solution came up from the automotive industry. A car is also a highly safety critical multiple-input, multiple-output (MIMO) system with obvious constraints, in increasingly changing environment. The main point is, to map the state and input space of the environment,

significantly reducing calculation demands based on the system complexity. Where constraints are present, finite states can be defined, either by hand (e.g. state machines) or by advanced mapping algorithms, and then in every state of operation, a relatively simple (linear if possible) rule where one state of the system dynamics could be substituted, then to make sure stepping on to the next most applicable rule can be achieved very fast. This way, by choosing the resolution of the mapping correctly (too fine resolution gives too high processing requirements, too low gives suboptimal dynamics), the predictive control approach can be applied in both worlds.

Chapter 2

Voltage unbalance indication

2.1 Motivation and aim of research

The motivation of the research was that the evolution of voltage unbalance as a general concept had it's stages through the years coming up with more and more sophisticated variations, suspecting that the topic of voltage quality indicator development may not be a settled debate. After examining the various approaches and the latest solution in use the voltage unbalance factor (VUF), it can be seen that more and more factors are taken into account, with VUF relying on the negative and positive symmetrical components in the end. However, detaching from the great utility symmetrical components hold, and examining the calculation from purely geometrical perspective, non of the indicators are hard coded to achieve a complete overlap to the ideal state of the voltage phasor it is aimed for. As such the aim is to come up and validate the utility of a voltage unbalance indicator, that takes as much information into account as possible (without the subharmonic components and as such harmonic distortion in scope), and still hold the value that the previous approaches especially VUF made, in terms of utility.

2.2 Literature overview

Single phase power injections to the grid are mainly generated by domestic photovoltaic-(PV) and wind power plants. For off-grid, sometimes more complex solutions integrating diesel generators, PV and wind generators. Such as proposed, in [1], and [2], where presented the economical aspects of a PV system. The economic results are strongly influenced by the annual average insolation value, which encourages the areas most exposed to the sun and the southern areas. The consumption of consumers is not critically important, but the design principle used has as significant effect on the maximization of the performance of PV plants. In the paper [3] it is worth noticing, that autonomous photovoltaic systems are strongly responsible of their reactive energy requirements. To support photovoltaic systems with sufficient battery banks one should be able to establish that their reactive energy requirement share fairly compensated by the corresponding energy yield. Additionally, in

[4] the author emphasizes that PV systems are increasingly being deployed in all over the world, and this is the source of a wide range of power quality problems. With a view on consistently measuring and assessing the power quality characteristics of PV systems, they had presented an in-depth overview and discussion of this topic.
The study [5] explored implementation issues of electric vehicle battery packs. They suggest that high voltage battery packs with large format cells has advantages in assembly, thermal management, monitoring and control, services and maintenance. On the other hand, quality, reliability and limited specific energy of large format cells are obstacles need to overcome. Solving these problems will further affect the cost, performance, reliability and safety of the electric vehicles. Smart energy systems in specially in urban areas are discussed in [6] where a design methodology has been suggested.
A numerical study was done by [7] on the distribution network faults and the effects on unbalance factor and the matrix representation of network impedances with the symmetrical component and phase component method. The study concluded, that during fault voltages and currents are greatly affected by the system unbalance and the fault impedance. The increase of the system unbalance causes an increase of the during-fault voltages and currents variation. The increase of the fault impedance reduces the fault current and therefore the effect of the system unbalance on during fault voltages and current diminishes. For each system there is a characteristic value of fault impedance that is related to the load impedances. Larger fault impedances values produce fault currents similar to nominal load currents and therefore the effect of these faults in terms of during-fault voltages and currents cannot be differentiate from nominal operation conditions. Variation of power quality in non-faulty scenarios leads to thermal transients in electrical machines. This problem can be especially important in the case of low-power machines, because they have shorter time constants than high-power ones. The rate of thermal responses of a machine also significantly depends on the type of power quality disturbances. Voltage unbalance can cause machine overheating within a mere few minutes. Furthermore, fluctuating unbalance could cause an extraordinary rise in windings temperature and additional thermo-mechanical stress. Consequently, voltage unbalance is found to be more harmful to induction motors than the results from previous work [8]. Additionally beside the heat factor, voltage unbalance can cause increased reactive power [9], various copper loss [10] torque pulsation in electric motors [11]. The authors of [12] were discussing the effects of unbalanced voltage on a three-phase induction motor, one has to consider not only negative-sequence voltage but also the positive-sequence voltage. With the same voltage unbalance factor, the status of voltage unbalance could be judged by the magnitude of positive sequence voltage. Also the effect of voltage unbalance has been studied on three-phase four-wire distribution networks for different control strategies for three-phase inverter-connected distributed generation units on voltage unbalance in distribution networks [13]. Here the negative-sequence component and the zero sequence component were studied where unbalance conditions could lower stability margin and increasing the

power losses. On the other hand, the adaptive coordination of distribution systems included distributed generation is also an emerging problem as it was discussed by [14]. A small voltage unbalance might lead to a significant current unbalance because of low negative sequence impedance as highlighted in [15]. As such a previous work of [16] a complex control unit has been proposed that is capable of lowering extant harmonic distortion. In the work of [17] the effect of a small domestic (photovoltaic) power plant on the power quality, mainly the total harmonic distortion has been examined. The aim of this work is to examine and compensate three phase voltage asymmetry of the electrical network based on the extended simulation model proposed by [16]. Further control methods were applied for the solution for balancing of the most sensitive with regard to electric energy quality part of power system in [18], minimizing the active power losses, stabilization of three-phase voltages, enhancement of asynchronous machine performance stability and reduction of errors occurring in power consumption measuring circuits.
In many articles the authors presents a different viewpoint of calculating unbalance on the network. [19] showed to assess the harmonic distortion and the unbalance introduced by the different loads connected to the same point of common coupling have been applied to an experimental distribution network. By [20] the focus was to bring out the ambiguity that crops up when we refer to a particular value of voltage unbalance that exists in the system. By making use of the complex nature of voltage unbalance, the voltage combinations that lead to the calculation of complex voltage unbalance factor could be narrowed down to a great extent. A fast and accurate algorithm for calculating unbalance has been presented by [21]. The magnitudes of zero, positive, and negative sequences are obtained through simple algebraic equations based on the geometric figure, which is also called as 4 and 8 geometric partitions. Also a three-phase optimal power flow calculation methodology has been presented by [22], that is suitable for unbalanced power systems. The optimal algorithm uses the primal-dual interior point method as an optimization tool in association with the three-phase current injection method in rectangular coordinates.

2.3 Definitions of voltage unbalance

In a symmetric three-phase power supply system, three conductors each carry an alternating current of the same frequency and voltage amplitude relative to a common reference but with a phase difference of one third of a cycle between each. The common reference is usually connected to ground and often to a current-carrying conductor called the neutral. Due to the phase difference, the voltage on any conductor reaches its peak at one third of a cycle after one of the other conductors and one third of a cycle before the remaining conductor. This phase delay gives constant power transfer to a balanced linear load.
In general symmetric three-phase systems described, are simply referred to as three-phase systems because, although it is possible to design and implement

asymmetric three-phase power systems (i.e., with unequal voltages or phase shifts), they are not used in practice because they lack the most important advantages compared to the symmetric. In a three-phase system feeding a balanced and linear load, the sum of the instantaneous currents of the three conductors is zero. In other words, the current in each conductor is equal in magnitude to the sum of the currents in the other two, but with the opposite sign. The return path for the current in any phase conductor is the other two phase conductors.
Constant power transfer and cancelling phase currents would in theory be possible with any number (greater than one) of phases, maintaining the capacity-to-conductor material ratio that is twice that of single-phase power. However, two-phase power results in a less smooth (pulsating) torque in a generator or motor (making smooth power transfer a challenge), and more than three phases complicates infrastructure unnecessarily.
Three-phase systems may also have a fourth wire, particularly in low-voltage distribution. This is the neutral wire. The neutral allows three separate single-phase supplies to be provided at a constant voltage and is commonly used for supplying groups of domestic properties which are each single-phase loads. The connections are arranged so that, as far as possible in each group, equal power is drawn from each phase. Further up the distribution system, the currents are usually well balanced. Transformers may be wired in a way that they have a four-wire secondary but a three-wire primary while allowing unbalanced loads and the associated secondary-side neutral currents [23].
The voltage quality is described by the European standard EN-50160, which defines, and describes the main characteristics of the voltage at the network users supply terminals (or point of connection) in public networks. The most important factors are listed here:

- Frequency
  - 50 Hz ± 1 % during 99.5 % of the year.
  - 50 Hz $+4$ % or -6% during 100 % of the year.
- Supply voltage variations
  - During each period of one week 95 % of the 1 min mean r.m.s. values of the supply voltage shall be within the range of ± 10 %.
  - all 10 min average r.m.s. values of the supply voltage shall be within the range of $+10$ or -15 %.
- Rabid voltage change
  - Only flicker severity is defined. For single rapid voltage changes, an indication is given that the voltage change should not exceed 5 % of the nominal voltage.
- Flicker

  - During each period of one week, the long term flicker severity caused by voltage fluctuations should be less than or equal to 1 for 95 % of the time.

- Unbalance

  - During each period of one week, 95 % of the 10 min r.m.s. value of negative fundamental phase sequence component of the supply voltage shall be within the range of 0 and 2 % of the positive fundamental sequence as it shall be displayed in (2.9).

- Harmonics

  - During each period of one week, 95 % of the 10 min r.m.s. value of each individual harmonic voltage shall be less or equal than 5 % of the 3^rd harmonic, 6 % of the 5^th, and 2 % of the 2^nd and so forth (table is included in [24]).
  - The THD (total harmonic distortion of the supply voltage (including all harmonics until the order of 40 shall be less or equal than 8 %.)

For more information see the standard EN-50160, and [24].
In this dissertation form the listed voltage quality problems only the voltage unbalance and it's indicators shall be examined.

2.3.1 Phenomena of voltage unbalance

In a domestic network, three-phase electric power systems have at least three conductors carrying alternating voltages that are offset in time by one-third of the period. A three-phase system may be arranged in delta or star. A star system allows the use of two different voltages from all three phases, such as a 230/400 V system which provides 230 V between the neutral (center hub) and any one of the phases, and 400 V across any two phases displayed on Fig.(2.1a). The definition is the following:

$$\begin{aligned} V_a &= \hat{V}\,sin(\theta) \\ V_b &= \hat{V}\,sin(\theta + \tfrac{4}{3}\pi) \\ V_c &= \hat{V}\,sin(\theta + \tfrac{2}{3}\pi), \end{aligned} \tag{2.1}$$

where V_a, V_b, V_c are the phase voltage vectors, $\hat{V}$ is the voltage peak, and θ is the phase angle.
First, if a quality indicator is chosen and used to describe a system, in this case the three phase low voltage network, the value is used, is advised to be a norm. As such it needs to comply the mathematical definition of a norm.
A given vector space $\mathcal{V}$ over a field $\mathbb{F}$ of real (or complex) numbers, a norm on $\mathcal{V}$ is a non-negative function of $p : \mathcal{V} \to \mathbb{R}$ with the following properties:

1. Triangle inequality: $p(\phi_1 + \phi_2) \leq p(\phi_1) + p(\phi_2)$,

2. Absolute scalability: $p(a\phi) = |a|p(\phi)$,

3. Positive definite: if $p(\phi) = 0$ then $\phi = 0$,

where ϕ is a chosen norm candidate.
Secondly, the physical property needs to be identified. Voltage unbalance is a phenomena where the three phase voltages differ in amplitude normal 120 degree phase relationship shown in Fig.(2.1b). In most cases both are happening at the same time. This includes unequal voltage magnitudes at the fundamental frequency, either under, or over voltage, at the fundamental phase angle deviation.

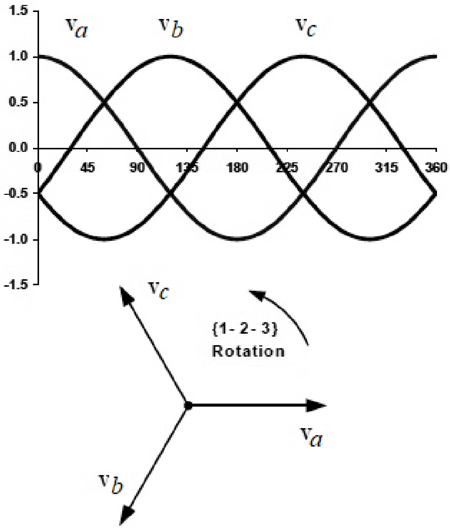

(a) Three phase sine wave of network voltage.

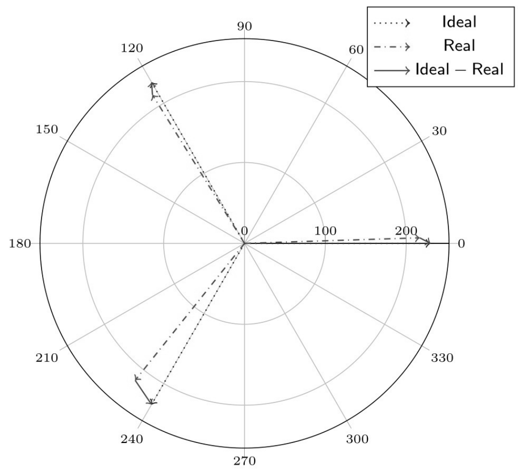

(b) The three phase voltage phasor whith *Ideal* and *Real* voltage vectors.

This is observed as a frequently cited power quality issue in low-voltage domestic distribution networks and in systems that supply large single phase loads distributed unevenly among the phases. Effects of voltage unbalance are complex, but can be categorized as structural or functional. The former refers to the asymmetry in the three-phase impedances of transmission lines, cables, transformers, etc. It occurs because it is neither economical nor necessary to maintain distribution system with perfectly symmetrical impedances. The latter refers to uneven distribution of power consumption over the three phases. Although the term voltage unbalance is unambiguous, the root phenomenon may be various as well as the standard norms used to measure unbalance.
In this section a detailed explanation is presented about the types of currently used method for indication.

2.3.2 Types of voltage deviations and norms

Voltage unbalance is not a straightforward term. To understand the concept, unbalance is when on a given frequency (mostly fundamental frequency) voltage vectors (phase or line depending on the definition) deviating from the ideal in terms of length or angle. The first fall in to the category of unbalance, namely any kind of phase deviations, and unbalanced amplitude deviations, and balanced amplitude deviations, like under-voltage. There are many different technological causes with more or less practical importance. The following conditions are examined and tested in the sequel:

Single phase under-voltage unbalance If there is a single phase uncompensated overload in the system, the voltage in the overloaded phase will be lower than the other two.

Two phase under-voltage unbalance Two of the three phases are overloaded without compensation, the two overloaded phases will have higher voltage drop than the third phase.

Balanced three phase under-voltage The loads of all three phases are overloaded in a balanced manner.

Unbalanced single phase angle If the three phase voltage amplitudes are balanced but the relative angles between them (ideally it should be equal to ± 120 degree). It is assumed, that V_a would be the reference. If one of the other two phase angles is deflected, unequal displacement.

Unbalanced two phase angles displacement Similar to the single phase angle unbalance, if the other two phase angles are both deflected, then unequal angle displacement in two phase angles occurs.

An indicator of the voltage unbalance is supposed to measure the extent of unbalance but it is not expected to classify between the above types.

2.3.3 Non standardized approximation formulas

Up to now, the following definitions have not been adopted by any standard or rule to indicate the degree of voltage unbalance, but used by various manufacturers. Firstly based on [25] recommended by the CIGRE (International Council on Large Electric Systems, in French: Conseil International des Grands Réseaux Électriques), the voltage unbalance is determined with:

$$VUFactor = \frac{\sqrt{1-\sqrt{3-6\frac{V_{ab}^4+V_{bc}^4+V_{ca}^4}{\left(V_{ab}^2+V_{bc}^2+V_{ca}^2\right)^2}}}}{1+\sqrt{3-6\frac{V_{ab}^4+V_{bc}^4+V_{ca}^4}{\left(V_{ab}^2+V_{bc}^2+V_{ca}^2\right)^2}}} \tag{2.2}$$

where, $\{V_{ab}, V_{bc}, V_{ca}\}$ are the line-to-line voltages. Note, that the CIRGE variant has no distinct notation, as such it would be indicated as $VUFactor$ in this thesis. Moreover, the author of [26] recommends two more variants, based on manufacturer recommended "standards":

$$VU = \frac{82\cdot\sqrt{(V_{ab}-V_{avg_{line}})^2+(V_{bc}-V_{avg_{line}})^2+(V_{ca}-V_{avg_{line}})^2}}{V_{avg_{line}}} \times 100 \tag{2.3}$$

$$VUR \quad = \quad \frac{max(|V_{ab}-V_{bc}|,|V_{bc}-V_{ca}|,|V_{ca}-V_{ab}|)}{V_{avg_{line}}} \times 100, \tag{2.4}$$

where the mean of line voltages is noted by $V_{avg_{line}} = \frac{V_{ab}+V_{bc}+V_{ca}}{3}$. This formulas were created with the intention to avoid the use of the complex algebra in symmetrical components and give a good approximation of the later described VUF standard. With the indicator of (2.3), and as well as (2.4). It is worth noticing, that only the voltage magnitude unbalance is reflected, completely ignoring Fortescue's method of symmetrical components [27] (shall presented later in the thesis), which considers negative sequence components as harmful on electric equipment and yield. Later it will be shown that other methods try to push the same methodology, until the currently used norm (VUF) is used.

2.3.4 LVUR

One of the first voltage unbalance in percent is defined by the National Electrical Manufacturers Association (NEMA) [28] is defined as the ratio of the maximum voltage deviation from the average line voltage magnitude to the average line-voltage magnitude.

$$LVUR \quad = \quad \frac{\max\left(|V_{ab}-V_{avg_{line}}|,|V_{bc}-V_{avg_{line}}|,|V_{ca}-V_{avg_{line}}|\right)}{V_{avg_{line}}} \times 100 \tag{2.5}$$

The LVUR assumes that the average voltage is always equal to the rated value, which is 480 volts for the US three-phase systems, and it works only with magnitudes. Phase angles are not considered in this definition.

2.3.5 PVUR

The next phase voltage unbalance in percent described in IEEE standard 141. [29] (derived from [30]), is $PVUR_{IEEE-141}$. It is defined as the ratio of the maximum voltage deviation of phase voltages from the average phase-voltage magnitude to the average phase voltage magnitude. In various fields, LVUR and $PVUR_{IEEE-141}$ are commonly used to estimate the degree of voltage unbalance due to simplicity of calculation. The two unbalance factors mentioned above cannot completely reflect system voltage unbalance effects, such as the phase displacements of unbalanced voltages.

$$PVUR_{IEEE-141} \quad = \quad \frac{\max\left(|V_a-V_{avg_{phase}}|,|V_b-V_{avg_{phase}}|,|V_c-V_{avg_{phase}}|\right)}{V_{avg_{phase}}} \times 100, \tag{2.6}$$

where the voltages $\{V_a, V_b, V_c\}$ denotes the phase-to-neutral voltages, and $V_{avg_{phase}} = \frac{V_a+V_b+V_c}{3}$. The second variant is, $PVUR_{IEEE-936}$, mentioned in [31] is defined as the ratio of the difference between the highest and the lowest phase-voltage magnitude to the average phase-voltage magnitude. Therefore, the numerical values of voltage balance quantified by $PVUR_{IEEE-936}$ are generally larger than those of $PVUR_{IEEE-141}$ and LVUR.

$$PVUR_{IEEE-936} = \frac{\max(|V_a|,|V_b|,|V_c|)-min(|V_a|,|V_b|,|V_c|)}{V_{avg_{phase}}} \times 100, \tag{2.7}$$

The number of possible combinations of three phase or line voltages that satisfy the definitions of voltage unbalance mentioned above will become infinite as only the magnitudes of voltages are considered.

2.3.6 VUF and CVUF

The voltage unbalance factor (VUF) was defined by the International Electrotechnical Commission [32], [33]. From the theorem of symmetrical components [27], voltage unbalance can be considered as a phenomenon that positive sequence voltage (V_p) is disturbed by negative (V_n) and zero-sequence (V_0) voltages:

$$\begin{bmatrix} V_0 \\ V_p \\ V_n \end{bmatrix} = \frac{1}{3} \begin{bmatrix} 1 & 1 & 1 \\ 1 & \upsilon & \upsilon^2 \\ 1 & \upsilon^2 & \upsilon \end{bmatrix} \cdot \begin{bmatrix} V_a \\ V_b \\ V_c \end{bmatrix}, \tag{2.8}$$

Where $\upsilon = e^{2j\pi/3}$ is the Fortesque operator. From that the formula of VUF can be expressed as:

$$VUF = \left|\frac{V_n}{V_p}\right| \times 100, \tag{2.9}$$

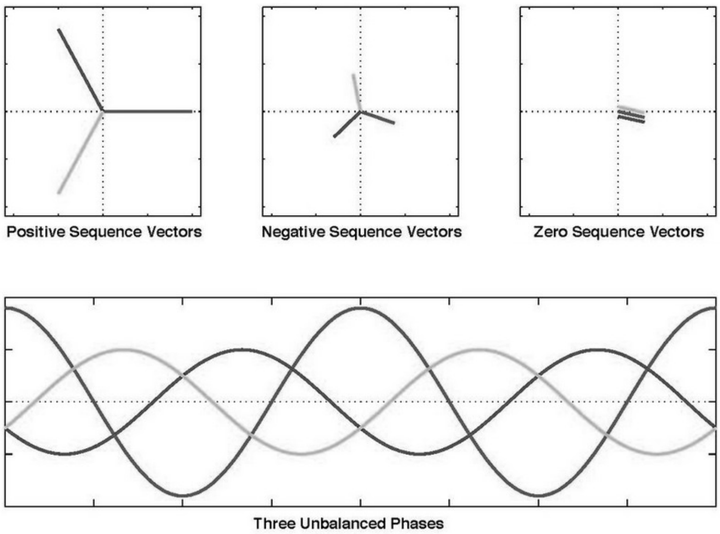

Figure 2.2: Simplified graphical display of symmetrical components.

This norm is currently in use world wide for voltage unbalance indication. The main focus in on the negative sequence component V_n, on which many studies attributes importance of the cause of negative effects the voltage unbalance causes.
As such, three-phase electric loads without path through the neutral, negative-sequence voltage is the primary cause of voltage unbalance. Normally, positive-sequence component of three-phase voltages is very close to rated value. If

expressed in per-unit quantities, the positive-sequence voltage will be very close to 1.0 p.u., and the corresponding negative-sequence voltage will be very close to the VUF. Thus, the VUF can indeed be considered as the negative-sequence component in per-unit. This explains the advantage of using the VUF as an index for analyzing the effects of voltage unbalance considering the phase deviations. An extension of the VUF is the complex voltage unbalance factor ($CVUF$) that is defined by the ratio of the negative- sequence voltage phasor to the positive-sequence voltage phasor studied in [34], and [35]. The CVUF is a complex quantity having the magnitude and the angle. Although the CVUF has not yet been widely used by practicing engineers, it has been proposed in some studies (e.g., [36], [37], [38]) due to its richness of information on unbalance. The formula of $CVUF$ is similar to VUF:

$$k_v = \tfrac{V_n}{V_p} = k_v \cdot e^{j\theta_v} = k_v \angle \theta_v, \tag{2.10}$$

where k_v is the magnitude and θ_v is the angle of $CVUF$.

It can be observed, that the previously mentioned norms (2.2), (2.3), (2.4), (2.5), (2.6), (2.7), and (2.9) indicate different values for a single case with various correlations. The first two standard indicators, $PVUR_{IEEE-936}$ and $PVUR_{IEEE-141}$, ignore the ±120 degree phase difference unbalance and only take the amplitudes into account. Additionaly, the zero-sequence components never present in the line-to-tine voltages regardless of the level of unbalance, only phase-to-neutral voltages. It has been proven, that these components are unelectable in some cases like bridge control of converters [39], or synchronous machine diagnosis [40].
The actual state of the art definition in use, VUF, is sensitive to the phase difference unbalance. Lastly $CVUF$ considers also phase and magnitude of the voltage unbalance, but the two units (k_v, and θ_v) are hard to merge together as a singular optimization cost. To be able to employ $CVUF$ as a successfully the weighting factor of the ratio of negative and positive symmetrical component's amplitude and phase shall be considered, which is non-trivial, and situation dependent (different network failure modes can be targeted with different weighting factors). Moreover, these definitions ignore zero sequence components and harmonic distortion that are always present in three-phase four-wire systems [15] hence, $CVUF$ not in the scope of this thesis.

2.3.7 Conclusion

As it was shown, establishing a straight forward definition for measuring a three phase network's voltage unbalance was not an easy task, and still not settled. With new attempts to come up with a more accurate and wholesome method e.g. $CVUF$, which paves the path for further research potential. However, going with the with the initial criteria of this thesis's level of analysis:

1. *all deviations from the ideal voltage phasor in terms of amplitude and phase are causing a decline of network quality,*

2. *the indicator shall serve as a cost function candidate, with fulfilling the definition of a norm.*

Before the standardisation the actors of the industry came up with methods, that suited they point of view of network quality with $VUFactor$, calculating an approximate double square mean of amplitude differences, and VU with a normalised square mean and VUR indicating the maximum linear amplitude deviation, neglecting all the other properties.
Later on with the need for standardisation and consensus, more sophisticated attempts were made, with $LVUR$, and $PVUR$ as the direct successor of VUR, with $PVUR_{IEEE-936}$ the most advanced one, sill indicating the largest amplitude deviation from the ideal, neglecting not considering other amplitude deviations as well as completely neglecting phase deviations. Finally after a complete rework, VUR became the standardised indicator as of today, employing the symmetrical components theorem a.k.a. the Fortescue method [27]. With this the negative sequence was identified as the main contributor of voltage unbalance caused failures from power factor distortions to increased network and machine losses. As such VUF approach with giving the ration of negative and positive symmetrical components as well as having one scalable value for control makes VUF an excellent candidate. Unfortunately, the simplicity of VUF comes with a downside, meaning the zero sequence components are neglected, as such making the indicator blind to balanced undervoltages, and dips. Finally the newest candidate the $CVUF$ attempts to further refine what VUF may omitted, with separating the angles of voltages into a second value, giving a complex result. Unfortunately this violates the second initial criteria such as since the value is complex and there is no trivial weighting ratio, $CVUF$ falls out of the scope of analysis as a cost function. This begs the question, how could voltage unbalance be measured loss-less, but resulting one (conveniently square-like) value, easily applicable for an optimization algorithm.

2.4 Proposed geometrical indicator

Hence it can be stated that every difference between the ideal and the measured voltage in both amplitude phase and sub-harmonics is caused by a form of voltage deviation from the ideal. The problem can also be investigated from a geometrical point of view as it is depicted in Figure (2.3). The three-phase voltage system's phasor diagram contains three phase-to-neutral voltage vectors which can be regarded as the points of a triangle (similarly, the three line-to-line vectors can play the role of the edges of the triangle). The two triangles (i.e. the ideal and the actual ones) always intersect except from very extreme and physically meaningless cases. The area where the two triangles do not cover each other (i.e. the difference of their union and intersection) can be used as a norm of voltage quality. In fact it is computationally more demanding compared to the previous methods, but takes every deviation into consideration [P1], [P2]. This way the error is given by (2.11).

$$G = \text{Area of } (\triangle_{Ideal} \cup \triangle_{Real} - \triangle_{Ideal} \cap \triangle_{Real}), \quad (2.11)$$

$\triangle_{Ideal}$ indicates the triangle spanned by the ideal voltage vectors and $\triangle_{Real}$ the triangle of real voltage vectors. Difference of the ideal and the real triangle's union and intersection defines the norm G. Basically, the algorithm calculates the symmetrical difference of the triangles, stretched from three phase ideal and real voltage vectors. This approach fulfills the norm definition as well, displayed in section (2.3.1).

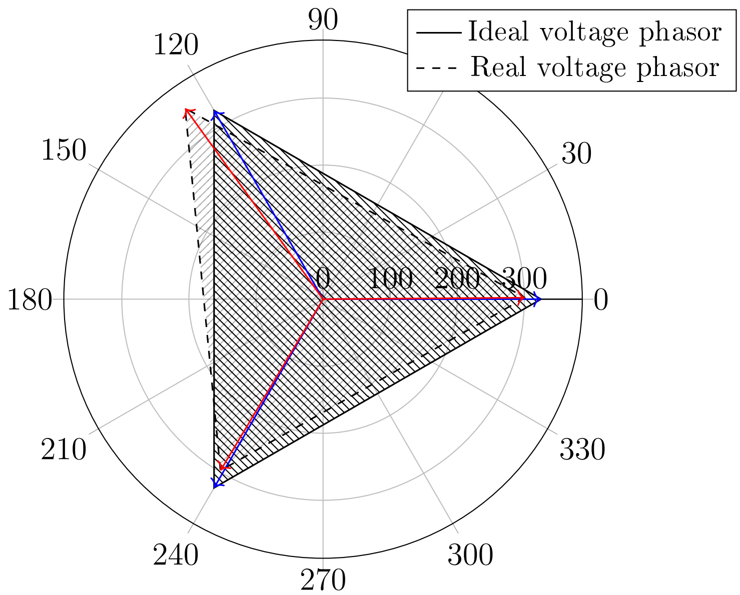

Figure 2.3: The triangles spanned by the ideal and the real peak voltage phasors. The extent of voltage deviation on the network can be measured by the sum of areas where the two triangles are not overlapping.

2.5 The method's novelty compared to VUF

When using a new norm for calculation and cost function it is reasonable to test it's viability compared to the prevalent or regulated method, the voltage unbalance factor (VUF) defined by the International Electrotechnical Commission, as discussed in section 2.3.6. In this case the geometrical norm's utility (2.11) against the currently used VUF (2.9) shall be examined.
The geometrical norm was validated experimentally, by investigating the correlation between the regulated and geometrical norms subjected to random, uniformly distributed unbalance on the voltage vector amplitude and phase values with 20 V amplitude and $1/300 \cdot \pi$ rad phase variance (Fig. (2.4), and Fig. (2.5)).

Although there is correlation between the two norm values in the general case, but for some situations the VUF indicates low, while geometrical norm still indicates high value.

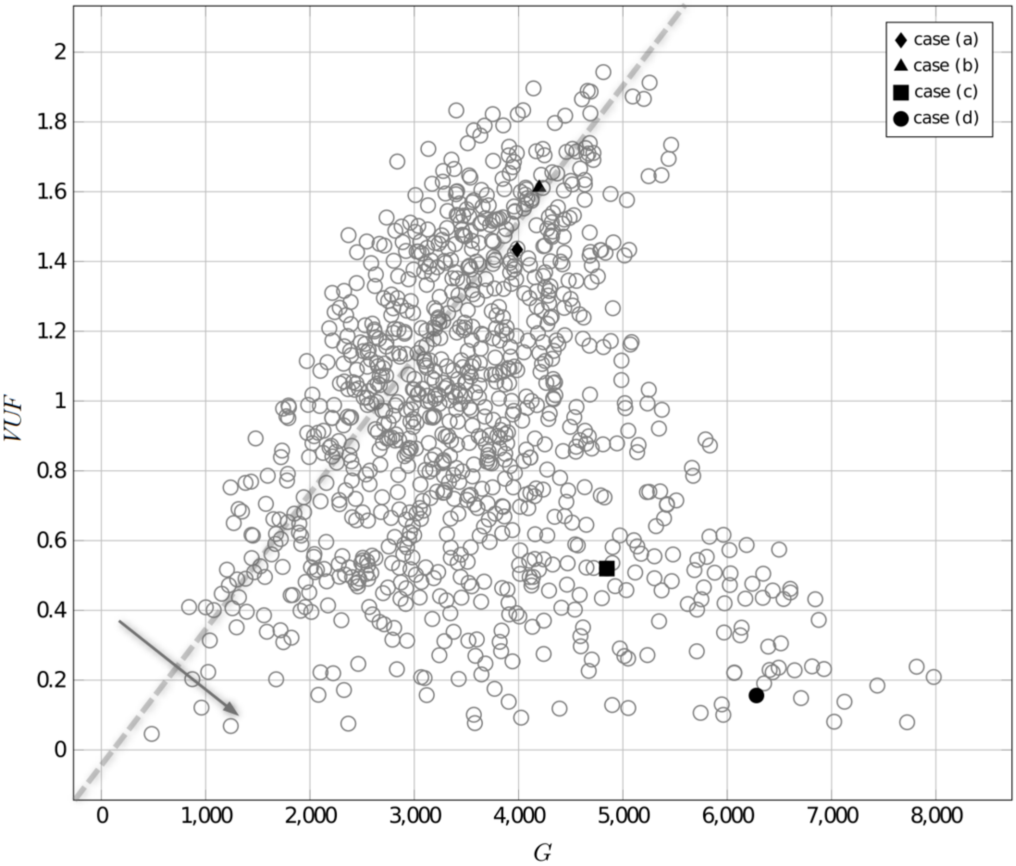

Figure 2.4: Correlation between the geometrical voltage unbalance indicator G and the regulated voltage unbalance indicator VUF using 1000 samples. In every iteration each three phase voltage vector's amplitude and phase values changed randomly, according to uniform distributions with ± 20 V amplitude and $\pm\frac{1}{3}\pi \cdot 10^{-2}$ rad phase variance. The dashed line indicates the axis across the main correlation cloud. It can be seen, that the geometric norm contains more information than VUF form the right of the dashed line. The four asymmetry cases of Figure (2.6) are denoted by black symbols on the picture. It is apparent, that in case (c), and (d) the G norm holds additional information than the VUF.

On Figure (2.6a) dominant phase deviation can be observed, while Figure (2.6b) shows amplitude deviation but with opposite direction. When there is such deviation on the grid both indicators present almost identical results. On (2.6c) there is still an observable unbalance (two phase deviate stronger than the third in terms of amplitude), but the correlation is significantly lower. In the last case in the lowest correlation area, amplitude deviation is present, but the deviation direction is identical on all phases (balanced over-voltage or under-voltage, can be observed on Figure (2.6d)), still, the VUF indicates very low values. In this case other methods are utilised in parallel in terms of network diagnostics to detect the under-voltage phenomena.[41].

To clarify this, the VUF's calculation method needs to be investigated (see (2.9)). The symmetrical component mutual impedance matrix on a three phase connection point is given by (2.12),

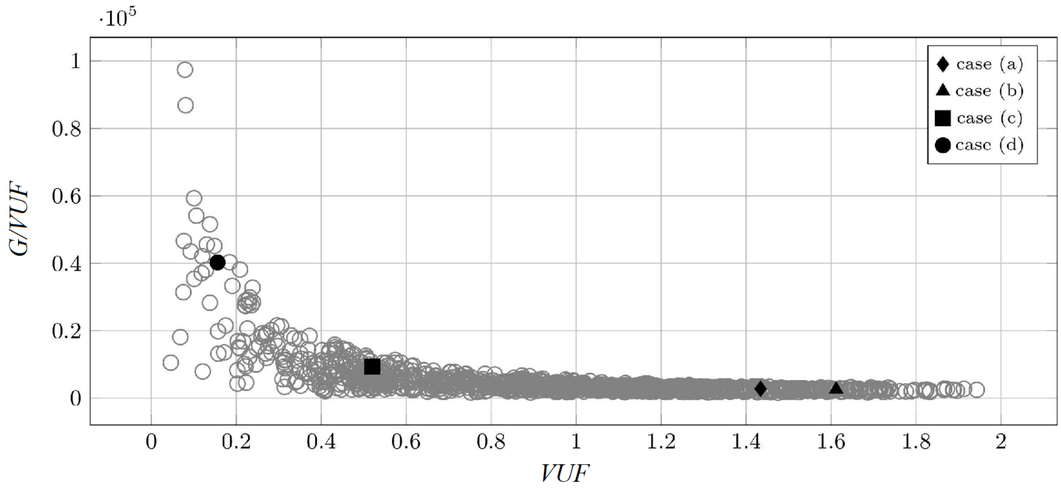

Figure 2.5: Correlation between the regulated unbalance indicator and the fraction of geometrical and regulated indicator. It can be seen that there is a functional connection between the two values.

$$\begin{aligned} Z_s &= \frac{1}{3}\begin{bmatrix} 1 & 1 & 1 \\ 1 & \upsilon & \upsilon^2 \\ 1 & \upsilon^2 & \upsilon \end{bmatrix} \cdot \begin{bmatrix} Z_{aa} & Z_{ab} & Z_{ac} \\ Z_{ba} & Z_{bb} & Z_{bc} \\ Z_{ca} & Z_{cb} & Z_{cc} \end{bmatrix} \cdot \begin{bmatrix} 1 & 1 & 1 \\ 1 & \upsilon^2 & \upsilon \\ 1 & \upsilon\upsilon^2 & \end{bmatrix} = \\ &= \begin{bmatrix} Z_{00} & Z_{01} & Z_{02} \\ Z_{10} & Z_{11} & Z_{12} \\ Z_{20} & Z_{21} & Z_{22} \end{bmatrix}, \end{aligned} \tag{2.12}$$

where Z_s is the symmetrical component mutual impedance matrix, and $\upsilon = e^{j\frac{2}{3}\pi}$. If there are both negative and zero sequence symmetrical components present on the network, the dominant part of the voltage drop's negative and zero sequence can be calculated as follows (2.13).

$$\begin{aligned} \Delta U_2 &\approx Z_{21}I_1 + Z_{22}I_2 \\ \Delta U_0 &\approx Z_{01}I_1 + Z_{00}I_0, \end{aligned} \tag{2.13}$$

ΔU_0, ΔU_1, ΔU_2 are the voltage drop's zero positive and negative sequence components, I_0, I_1, I_2 are the current's drop's zero positive and negative sequence components, and Z_{00}, Z_{01}, Z_{21}, Z_{22} are mutual impedances, respectively. If there is only positive and negative sequence present, then the right hand side's second term is zero. As such, the indication of negative and zero sequence present the network calculates (2.14):

$$\begin{aligned} m_{21} &= \mid \tfrac{Z_{21}}{Z_{11}} \mid \times 100 \\ m_{01} &= \mid \tfrac{Z_{01}}{Z_{11}} \mid \times 100, \end{aligned} \tag{2.14}$$

where m_{21} is the negative sequence factor which is identical to the VUF, and m_{01} is the zero sequence factor.
As such from (2.14), it can be derived, that the geometrical method shown in (2.11), compared to the VUF shown in (2.9) incorporates the zero sequence

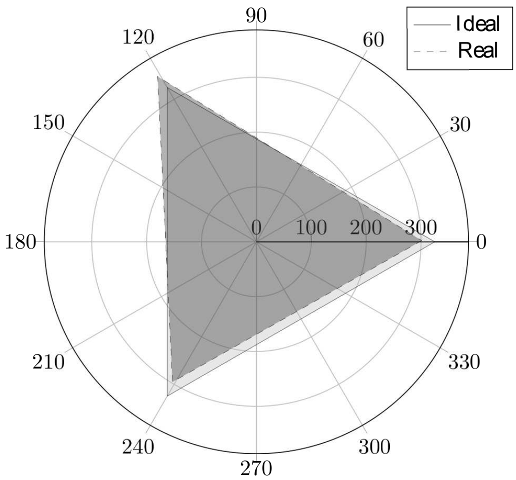

(a) High correlation with phase deviation. The norm values are $G = 3986$ and $VUF = 1.434$.

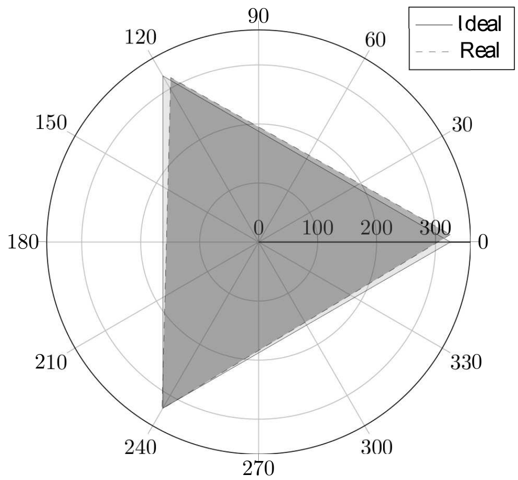

(b) High correlation with opposed amplitude deviation. The norm values are $G = 4198$ and $VUF = 1.612$.

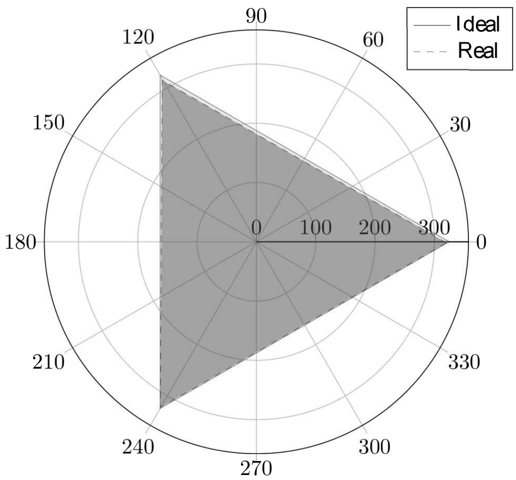

(c) Low correlation with opposed amplitude deviation. The norm values are $G = 9322$ and $VUF = 0.5198$.

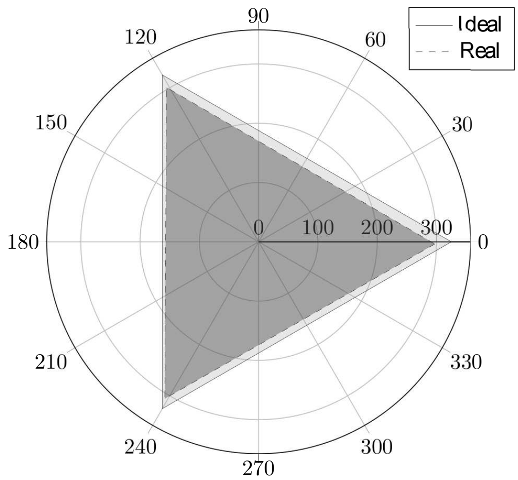

(d) Low correlation with uniform voltage drop. The norm values are $G = 6280$ and $VUF = 0.156$.

Figure 2.6: Four distinct cases of voltage triangles examining correlation between the regular VUF and geometrical G method.

Table 2.1: Comparison of different voltage unbalance indicators, according to the scope defined in section 2.3.7.

Indicating Capabilities	Amplitude deviation only	Phase deviation only	Balanced three phase under-voltage	Trivial cost candidate
$VUFactor$	Yes	No	No	Yes
VU	Yes	No	No	Yes
VUR	Yes	No	No	Yes
$LVUR$	Yes	No	No	Yes
$PVUR_{IEEE-141}$	Yes	No	No	Yes
$PVUR_{IEEE-936}$	Yes	No	No	Yes
VUF	Yes	Yes	No	Yes
$CVUF$	Yes	Yes	No	No
G	Yes	Yes	Yes	Yes

factor as well. This can be observed on Figure (2.4), with the dashed line across the main correlation cloud on the scatterplot. The perpendicular dislocation from the dashed line to the right is proportional to the uniform amplitude deviation (case (d) on Figure (2.6)). Since the geometrical method calculates with error surfaces, the approximation would be the VUF's value (including the zero sequence) squared. To understand the context, the zero sequence deviation (can be interpreted as uniform amplitude deviation from the ideal phasor) can be an indication of undervoltage, or voltage dip, which are common network errors.
As such comparing the results from Figure (2.4), as well as the observations from (2.12)-(2.14) the best cost function candidate as well as the most promising unbalance indicator would be G according to the initial criteria laid down in section 2.3.7. A comprehensive overview the can be observed in Table (2.1).

This comes from G's property of calculating the deviations based on the symmetrical difference of the voltage phasors, and since surfaces instead of numerical differences are considered the value follows a square-value nature. It is worth to keep in mind, that the definition of VUF can not be applied to the proposed method, since it was designed around the percentage difference of positive and negative symmetrical components, but this allows to establish a square-like cost function to minimize with an optimizer employed in an active, network connected filter.

2.6 Summary

At the previously described balanced over- or under-voltage case the positive sequence value is dominant, so the regular indicator will take considerably lower value. In other words, aside from indicating voltage unbalance, the geometrical method incorporates the balanced deviations as well. In a control design perspective, a general case, where notably highly unbalance values may appear, using VUF as cost function could introduce hidden errors in control due error cancellation. Additionally the geometrical solution checks electrical asymmetry, i.e. the norm of a ± 120 degree rotated version of the ideal three-phase phasor is zero in the geometrical sense. Moreover, the geometrical norm is more sensitive for small scale unbalance, as opposed to the VUF. To summarize, the geometrical indicator a more suitable solution for a more general case indicator, and a good candidate for cost function in optimal control design.

Notations used in the chapter

$CVUF$	Complex Voltage Unbalance Factor
G	Geometrical voltage unbalance indicator
$I_{0,1,2}$	Zero positive and negarive sequence of current drop
k_v	Magnitude of CVUF
$LVUR$	Voltage unbalance notation based on NEMA standard
m_{21}	negative sequence factor, identical to VUF
m_{01}	zero sequence factor
$PVUR_{IEEE-141}, PVUR_{IEEE-936}$	Voltage unbalance notation based on IEEE-141, and IEEE-936 standard
V_{ab}, V_{bc}, V_{ca}	Line-to-line voltages
$V_{avg_{line}}$	Average of line voltages
V_a, V_b, V_c	Phase-to-neutral voltages
$V_{avg_{phase}}$	Average of phase voltages
V_0, V_p, V_n	Zero, negative and positive sequence voltages based on symmetrical components theorem
$\hat{V}$	Voltage peak
$\vec{V}_a, \vec{V}_b, \vec{V}_c,$	Voltage vectors in the three phase phasor
VUF	Voltage Unbalance Factor
$VUFactor, VU, VUR$	Non standardized voltage unbalance factor based on manufacturer standards
Z	Symmetrical component mutual impedance
ΔU	Zero positive and negative sequence of voltage drop
θ	Angular displacement of the voltage or current vector
θ_v	Angle of CVUF
v	Fortesque operator

Chapter 3

Voltage unbalance compensation in three-phase networks

3.1 Motivation and aim of research

The motivation of the research was, to come up with a "plug-and-play" three phase network voltage unbalance (VU) reducing solution, assuming no priory knowledge is required from the network for connected device, only the nominal voltage, and fundamental frequency. Hence, any measurement beyond the conceptual device's connection point was infeasible, and network parameters, topology, parameters from active loads, short circuit power, or the knowledge about the distribution transformer's features were assumed as unknown. This brings an interesting subset of employable solutions namely non-model based optimizers, in terms of this thesis, the asynchronous parallel pattern search (APPS). So, the aim was twofold in this case. First the thesis aims to show, that the geometrical norm (G) could serve a valid cost function and indicator for optimization design (of course with the target of reducing VU). And second, to operate said optimizer in the described unknown and inestimable network environment, where after setup and connection, VU reduction is still feasible.

3.2 Literature overview

The phenomena of voltage unbalance (VU) has been investigated for a long time. VU of three-phase voltages results from asymmetry of line impedances and from inequality of loads in three phase networks. Efforts are in general are made to reduce the asymmetry, sprouting form network topology geometries impedance by transposition. On the other hand, voltage unbalance caused by uneven distribution of loads over three phases is more difficult to compensate. In low voltage residential and/or commercial systems, single-phase loads account for the majority of power consumption. Wherever possible, efforts are made to distribute the single phase loads uniformly over three phases, but residential areas are generally not sanctioned per household. It is unlikely that at a given time instant loads in the three phases are balanced because they vary in a random manner. In other words, even if the average loads in the three phases are kept the same, the instantaneous power demands in the three phases differ from each other, leading to unbalanced voltages at the point of common coupling. With this in mind, predictive models can not reliably established, however stochastic models has been used to aid the effort. In [42] a distribution networks were examined, and a Monte Carlo analysis with random variation of the voltage unbalance factor is modeled with the aid of correlated Gaussian random variables that represent random variations in three-phase active and reactive powers. Also this method used in [43], for single phase power plants (mainly PV plants) caused VU risk assessment and mitigation. It was shown that this unchecked plants can cause serious risk with above 2% VUF, and the maximum single-phase and uncontrolled connection of plants is unacceptably high, posing a risk for other networks as well.

The authors of [44] proposed a stochastic multi-objective optimization to model VU, where the discrete decision variables are coordinated with continuous regulation of solar reactive outputs updating they assumed covariances. For the purpose, the stochastic processes of solar active power are modelled in a scenario based framework. Stochastic processes were converted into a series of equivalent deterministic scenarios. For this purpose, a modified non-dominated sorting genetic algorithm-II was proposed, in which crossover rate and mutation rate are dynamically revised by a fuzzy logic controller.

There are different approaches of lowering the unbalance with different control techniques. Since conventional inverter topologies ar built for symmetrical, and zero offset current and voltage waveforms, the topology needed to change, to compensate the negative (and occasionally zero) sequence symmetrical components, besides normal operation. An interesting approach by [45] was introduced, where two parallel VSIs are connected to produce positive and negative sequence components side by side. The approach also utilizes optimal control to achieve both the quality of power (MPPT) within the microgrid and the quality of currents (unbalance mitigation with low THD) flowing between the microgrid and the utility system, where two parts are controlled complementarily to inject negative- and zero-sequence currents in series to balance the line currents, while generating zero real and reactive power. An other approach, is to try to estimate the required compensation geometrically by [46], where the required step in space vector modulation (SVM) is calculated by giving the assumed vectorial sum to move the measured system to a more balanced state. The authors use a series connected VSI (with common DC link) to achieve the required freedom for the operation, although the unbalance reduction is for the controlled three phase loads only, and the network is not influenced.

In the market there are devices with the sole purpose of compensation, and one of them is the static var compensator (SVC). This device is connected parallel, to the network (usually after the transformer station) to adaptively reduce the networks reactive power. However in [47] the SVC is used also for mitigating the grid's VU. In the article, as three-phase IGBT-based static synchronous compensator was proposed for voltage and/or current unbalance compensation, where an instantaneous power theory (IPT) was used for real-

time calculation and control. This control approach calculates the controller's next step from the instantaneous values of voltage and current to formulate the required power to inject in an averaged time interval.
In some cases the authors aim not to reduce the effect of unbalance on the network, but to ensure stable operation, while devices and loads are protected. In [48] the authors argue, that working under network VU, a current source inverter (CSI) holds a better strategy, than its counterpart, although the device is only operates under this condition and does not contribute to the unbalance even further. The device stands as gateway between a DC microgrid and an AC grid. Under the effect of VU the DC microgrid suffers harmonic oscillations in voltage, and possible controller tripping (one phase exceeds the current limit) if it is not mitigated. The authors mention the use of conventional VSI based structures for CSI may lead to unstable operation, as such, they inject balanced three phase currents into the AC grid under an unbalanced grid voltage. Based on the instantaneous active power theory under unbalanced grid conditions [49] proposes an optimized negative-sequence current references for eliminating the double-frequency oscillations on active power at AC side of a current source converter. The approach is similar as before, using CSI as a good topology candidate, as well as the control structure of IPT, but the goal here is also to work under unbalanced grid conditions, and only protecting the device and the load. In [50] direct control strategy with CSI model based control is shown which is simpler than the complicated IPT. The factors of unbalance are measured (negative and zero sequence as well) and the optimal current is calculated from the device model and from the factors via phase locked loop.
As an issue both [51], and [52] names the increasing PV penetration a thread for the network quality, namely the voltage balance. The former suggests that the network operators are mainly obligated to mitigate the phenomena, by the transmission systems management and control, and the former suggests a local strategy. The idea is to use the PV-VSI (voltage source inver with photovoltaic source on the DC end) as the control reserve for VU mitigation. Here also geometrical approach is used with SVI to calculate the VSI's next step and formulate the optimal voltage vector on the voltage phasor, and an intermediate PI controller to reduce parameter sensitivity. The controller's cost function is derived via current and voltage measurement based on the IPT.
The authors in [53] suggest, that current control strategies, where non harmonic currents were used deemed to have difficulties, however the CSI exhibits higher reliability and power density than the VSC with added DC-DC boost converter topology. As such a current source based strategy with only harmonic currents were used, which shall be presented in section 5.5.

3.3 Optimization-based voltage unbalance compensation

In this dissertation the approach is, that the electrical network's level of unbalance only depends on the generators and loads switching on and off the network, as such it is assumed, that *the network beyond the connection point is unknown (the amount, type and power of domestic loads are unknown), and network impedance's stochastic distribution function can not be estimated* as it shall be discussed in section 3.4.1. *Thus, the compensation's goal is to find the local optimum regardless of unknown conditions. Furthermore, the goal is to compensate the* VOLTAGE UNBALANCE (VU)*, without the option to place current controllers after the connection point.* This implies, that the grid's transformer's current (as well as any current after the connection point, including the network's short circuit power) can not be measured, to esteem the network's behaviour.

3.3.1 Problem statement

Based on the general assumptions above, an optimization-based and model-free compensation structure is suggested here. Figure (3.1) depicts the high-level structure of the compensation structure.

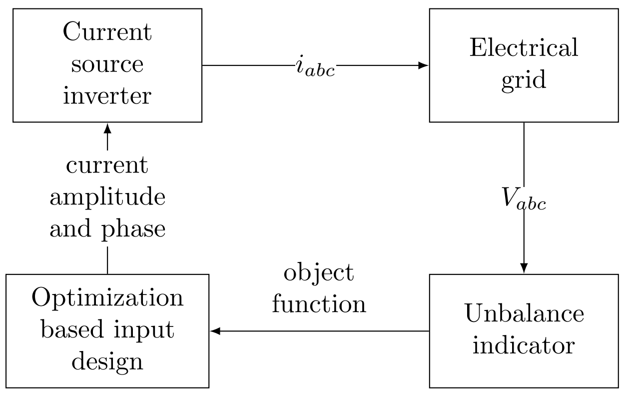

Figure 3.1: Block scheme of the voltage unbalance compensation.

From the control-theoretic point of view, the main characteristics of the problem are as follows.

- Current input to the network (three phase current phasor): $i_{abc} = [i_a, i_b, i_c]$. The current waveform is generated by a three-phase current source inverter, its implementation details are out of the scope of the thesis (see appendix chapter 5.5 for an overview).

- Measured voltage (three phase voltage phasor): $V_{abc} = [V_a, V_b, V_c]$.

- Control aim: Minimization of the selected voltage unbalance indicator value during the operation of the network.

Based on the measured quantities, the dynamic behavior of the network cannot be predicted and thus its dynamical model is supposed to be unknown. The only source of information from the network is the voltage response given by the network for the current input. Since the network actors (generators and loads) are continuously switching on and off the network in an unobservable and uncontrollable manner, the model structure as well as the modell parameters of the network cannot be determined using the tools of system identification. The above facts makes it difficult to use the model based techniques of control theory.

3.3.2 Elements of the problem

In the following paragraphs, the main functional blocks of the problem statement depicted in Figure (3.1) are detailed.

Electrical grid The electrical grid is supposed to be a three-phase grid, the only assumption is that the three-phase voltage V_{abc} can be measured at the connection point. Since the network units (generators and loads) are continuously switching on and off the network in an unobservable and uncontrollable manner, the model structure as well as the model parameters of the network cannot be determined using the tools of system identification. *An important assumption that has to be made with respect to the transient response of the network is that the effect of the input decays by the time the next input is applied to the network.* This cannot be ensured in the general case since the network is unknown.

Unbalance indicator Any suitable norm of voltage unbalance can be used as an unbalance indicator, however, to show the applicability of the proposed geometric norm in the Case study (Section (3.4)) it will be used as cost function. In accordance with the notions introduced in Section (2.3), the unbalance indicator is a mapping from the three-phase voltage phasor V_{abc} to $\mathbb{R}^+$.

Optimization based input design The optimization based input design is equivalent to the solution of an optimization problem:

$$\min_{i_{abc}} f(V_{abc}) \tag{3.1}$$

where f stands for the applied unbalance indicator. Of course, a more sophisticated input design method would take into account the constraints on the appliable current.

Ideally, the point i^q_{abc} corresponding to the local minimum, which can be calculated from the negative gradient $\nabla f(V_{abc})$, that gives the value and direction of the corresponding step in the parameter space, as such making the optimization straightforward. The next step is made in the direction of gradient with the proper sign. Most of the time, this sequence of steps, converges to local multivariate extreme value $\mathbf{x}^q$ of the function (3.2).

$$i_{abc}^{(q)} = i_{abc}^{(q-1)} - t_q \nabla f(V_{abc}^{(q-1)}), \tag{3.2}$$

where $q \in \mathbb{N}$, and t_q resembles the step size of the algorithm. Unfortunately, the controlled electrical system is described by multivariate non-linear differential equations, the optimization of which is infeasible to derive using the differentiation of an error function. Therefore, the optimization methods based on direct differentiation are not applicable. In such cases, the applied optimization method has to be a derivative-free one as the network model is not assumed to be known. A variety of optimization methods are availeble of this class, e.g. Nelder-Mead [54], Pattern search [55], [56], Simulated annealing [57], Subgradient method [58].

Current source inverter The role of this power electric device is to produce the current waveform determined by the Optimization based input design module.

Its structure and implementation may depend on the actual field of application and is not in the scope of this thesis. However, some basic power electronic components of current control is presented in the Appendix (5.5)

3.4 Case study: Voltage unbalance compensation of low voltage network

In order to illustrate the applicability of the proposed geometric norm as a cost function on an optimization based compensation method described in section (3.3.1), the compensation of voltage unbalance (VU) of an unknown low voltage domestic network, with a current source power electric device. The goal is, to reduce the VU on the network utilizing the limited resources. With this in mind, the device is connected to any three phase four wire 400V connection point, and based on only on the measured network voltage, shall formulate such constrained harmonic current waveforms, that results in unbalance reduction based on the prescribed const function (VUF, or G, described in 2.4)Unfortunately, the method cannot be examined on a real network connected to the grid, that is why *a high fidelity simulation model had been developed for the case study*. The three-phase low voltage network and all the elements of the problem statement has been implemented in Matlab Simulink environment using the Simscape Electrical toolbox. The top level structure of the Simulink model can be seen in Figure (5.4), (5.5).
The domains of the signals expected are as follows:

- Controller output (three phase current phasor): $i_{abc} = [i_a, i_b, i_c]$, the domain for each phase is [0, 20] A amplitude and $\pm 60°$ phase.
- Measured signal (three phase voltage phasor): $V_{abc} = [V_a, V_b, V_c]$, the domain for each phase is [0, 326] V (peak) amplitude and $\pm 60°$ phase.

It is important to note, that the following case study serves as a proof of concept and a simulation based benchmark problem in order to be able to compare different unbaance indicators as well as different optimization problems. *Because of the simplified nature of the problem, there are some neglected features (e.g. subharmonics, flicker) which might be interesting from the electrical engineering point of view in a real world application.*

3.4.1 Formulation

This chapter's aim to propose a model and control scheme for a three phase instrumentation, which can compensate voltage based unbalance, and as such lower the power losses and increase power quality, not only at the domestic connection point but possibly in the whole low voltage transformer area without prior knowledge of the network's topology, it's connected load's, or the transformer characteristics.

Electrical Grid The network, the proposed VU compensator supposed to be connect, is a three phase four wire low voltage domestic transformer area. For the sake of modeling and simulation simplicity, the transformer's secunder circuit is assumed as wye (star) connected, where the neutral wire is grounded, an modelled as ideal voltage sources connected to a three phase function generator or a specific input waveform in case of measurements (see section 5.4 for network setup). It is worth mentioning, that the transformer choice could convey some issues as indicated by [59], and [60], but the transformer modeling is out of scope of this thesis.

Due to the unregulated, and uneven load, or (with the emergence of affordable PV stations) possible domestic powerplant distribution, the voltage and current unbalance present in the network causes additional power loss inside the medium voltage/low voltage transformer and in the transportation line wires too. It also has undesired effects in certain three phase loads, mainly rotating machines where it causes torque reduction and pulsating torque effect. Large scale unbalance can also activate automatic protection functions of electricity dispatch system causes power outage. These negative effects lower the electric power quality and rises the cost of electrical energy and rises the carbon footprint of our everyday life, and also undesirable for the customers and adds maintenance cost to the service provider.

It can be observed in Fig. (3.3), that the actual system of interest is the power grid with all the unknown stochastic and nonlinear phenomena, represented as a black box model, with limited observability through the measured voltage (V_{abc}). Although the global network VU is observable. As already mentioned the input to the system are current signals (one current in the single phase case and three in the three phase setup), which are naturally constrained by the available energy of the household, stored in a battery pack or momentarily generated by the wind or solar generator unit. The response of the system

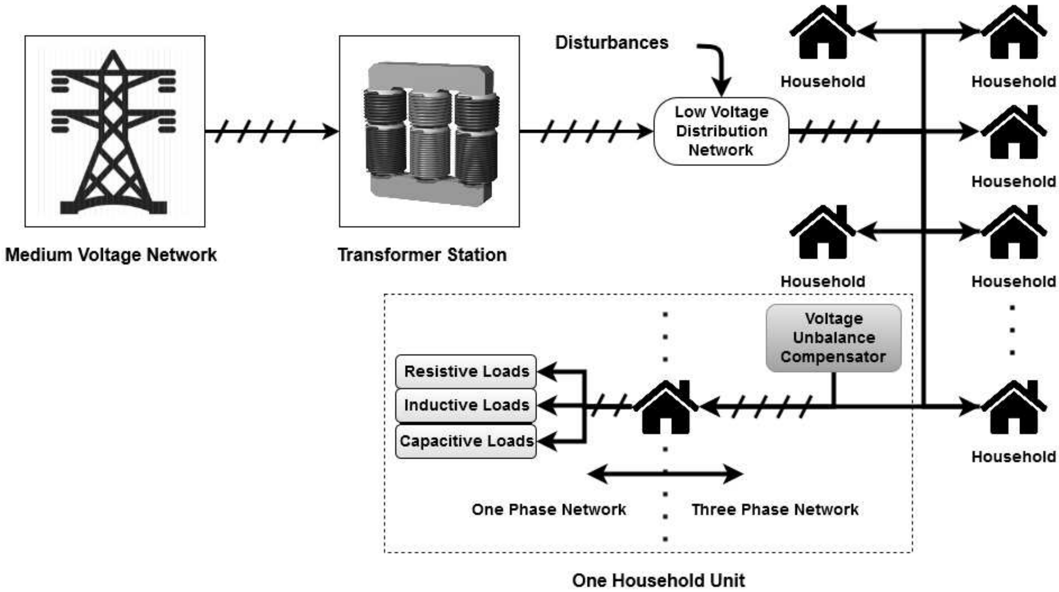

Figure 3.2: The theoretical structure of a three phase four wire low voltage network. Several regular households are representing the main loads, and connected with power line sections, subject to inductive and resistive disturbances and capacitive couplings. Domestic powerplants may connect to any connection point within the low voltage section, via an appropriate inverter - either to the three phase sections using a three phase inverter or to a single phase using a single phase inverter.

can be either the current or the voltage measured at the connection point of the inverter unit, however, the general legal regulations only allow voltage measurement for consumers.

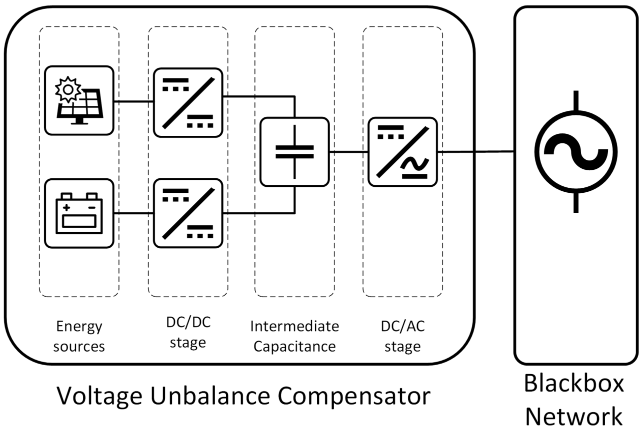

Figure 3.3: Simplified compensator perspective and overview.

For the control aim it is a natural choice to minimize the VU of the low voltage local transformer area measured at the connection point of the inverter. Several optimization based methods are available for such kind of optimal control problems, e.g. [16] where the only bottleneck is the computational efficiency since the implemented controller has to run on the commercial inverter's hardware (digital signal processor unit).

Unbalance indicator The voltage network is assumed to react to the controlled current injection i_{abc} with the three-phase voltage phasor V_{abc}. The injected current waveform's effect is assumed to be immediately observable as the change of the network's voltage, however, the uncertainty does not make the approach so straightforward as with model based controllers.

Let us define the following *mapping from the output of the optimizer* of the problem statement (i.e. a given three-phase magnitude-phase $\mathbf{x} \in \mathbb{R}^6$) to the selected *unbalance norm of three-phase voltage response* of the network as follows.

$$f_{norm}[\mathbf{x}] \tag{3.3}$$

where $norm = VUF$ is the state of the art, and $norm = G$ is the proposed geometrical indicator of VU, where VUF is described by (2.9), and G is described by (2.11). The scope of analysis is limited to only these two norms, but the principle works with any valid voltage unbalance indicator of choice.

Optimization based input design As it was mentioned in Section (3.3.1), there are several derivative-free optimization methods available in the literature for solving problems like (3.1). For such problems, pattern search methods are one possible solution technique since they neither require nor explicitly estimate derivatives. In [P1], an Asynchronous Parallel Pattern Search (APPS) method is used and is presented here. The methodology and formulation of the APPS method is described in more detail in Appendix (5.6).

With this in mind the list of processes which could be parallelized, comes from shape of the voltage phasor itself (observed in Fig. (2.3)). The ideal phasor is deviating in terms of voltage amplitudes and angles. As such, if the first phase V_a is is locked by angle, it can be assumed, that the ideal phasor can deviate by two phases and three amplitudes. As such the search algorithm has five processes (or axes) to optimize along. Basically the general strategy for the APPS method, from a single process perspective follows:

Algorithm 1: Asynchronous Parallel Pattern Search

$\mathbf{x}_i^0 = 0,\ \Delta_j^0 = 0, d_j^{(q)} = 1;$
while $f_{norm}[\mathbf{x}_j^q + \Delta_j^{(q)} d_j^{(q)}] \neq 0$ **do**
  for *j=1; j<=6; j++* **do**
    $d_j^{(q)} = 0.5(sign(N^{(q-3)} - N^{(q-2)} + sign(N^{(q-4)} - N^{(q-3)})));$
    $\Delta_j^{(q)} = n_j N^{(q-1)} \Delta_j^{(q-1)} + \Delta_j^{(q-2)} + m_j N^{(q-1)};$
    $N^{(q)} = f_{norm}[\mathbf{x}_j^{(q)} + \Delta_j^{(q)} d_j^{(q)}];$
    if $f_{norm}[\mathbf{x}_j^{(q)} + \Delta_j^{(q)} d_j^{(q)}] < f_{norm}[\mathbf{x}_j^{(q)}]$ **then**
      $\mathbf{x}_j^{(q+1)} = \mathbf{x}_j^{(q)} + \Delta_j^{(q)} d_j^{(q)};$
      $i_{abc} = f_{current}[\mathbf{x}];$
    else
    end
  end
  q++;
end

where $f_{current}$ is a mapping from the optimizer output ($\mathbf{x}$) to the three-phase current injected to the network (i.e. it represents the curent source inverter). Since the injected currents are synchronised via initial Fast Fourier Transformation (FFT), this operation could be performed. Furthermore, Δ_i the process step length aka. the value of the current vector's amplitude or angle needs to be changed for a successful step, and d_i is the corresponding step's signed direction vector, which specifies the applied changes direction. Furthermore N represents the chosen norm's value as the network's response to the current injection, and n_i, and m_i are scaler gains for the corresponding process. The algorithm is initialised with $\mathbf{x}_i^0 = 0$, $\Delta_i^0 = 0$ for a smooth start, due to lack of prior network knowledge.

The search pattern p is based on the sampling of the error function (selected norm) on V_{abc}, and it corresponds to variables or subsets of variables in each point in the independent variable or parameter space. At the same time, the norm values at these points can be calculated independently if $\Delta_q > 0$, using Algorithm (1). The parameter is $\mathbf{x}^q \in \mathbb{R}^n$, and the initial search pattern $\mathbf{p} \in \mathcal{D} = d_1, ...d_n$ is taken from a predefined finite set, and updated every iteration. In this case, the error function values of N should be calculated for each pattern $\mathbf{p}$ in the set $\mathcal{D}$. As the competing directions are different, if there is not enough computing power available for direction vector $\mathbf{p}$, synchronization should not be maintained. In this case we are talking about the asynchronous case. In the case of our controller, an individual $\mathbf{p}$ vector is defined for each output variable, and the optimization was performed in each direction asynchronously and shifted in time as it can be observed in Figure (3.5). Most likely, the error function has a single local minimum as a symmetric amplitude and phase values. Approaching the minimal value of norm, the controller uses adaptive increments that are proportional to the norm itself. Because of the complex interactions between the components of the controller, only one parameter is changed at a time, even if the values of the amplitude and phase

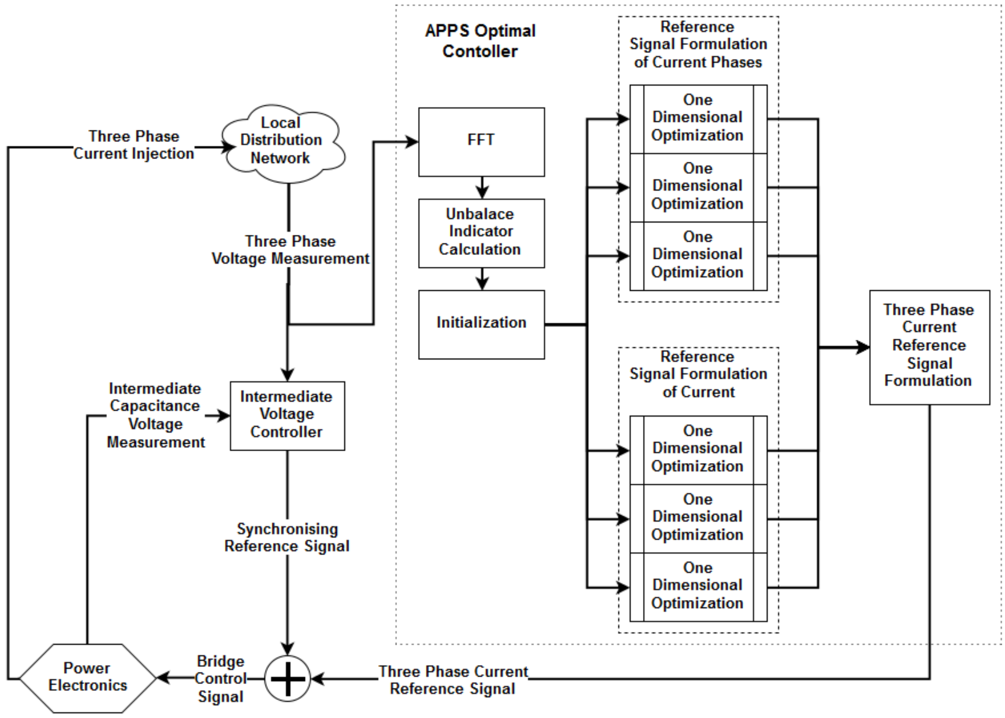

Figure 3.4: The optimization algorithm implemented for current control. A one dimensional linear optimization step is being solved in each dimension of the six dimensional parameter space, iteratively.

components in specific time slot changes. The algorithm moves along the six axes of six separate time slots close to the local minimum of the error function, however as mentioned the first step of the six is always trivial, since it is locked to the first phase.

The advantage of this controller structure that is not necessary to know the controlled value's behavior, like we could not determine the number and type of the other loads on the network [P1]. There are however three disadvantages. First is the low speed of control, due to the several necessary iterations (depending on the circumstances) to find the optimal directions in the parameter space, and the serial nature of interventions and norm calculations. The second comes from the method itself since the controller may stuck in local minima, and the third is that the sequential current injections may increase THD of the network.

Current source inverter The role of this unit is to realize the three-phase current i_{abc} demand calculated by the optimization algorithm. It is an asymmetric three-phase current scource inverter used in low voltage networks. The operation, the structure and the parameters of this unit is not in the scope of this thesis, however its structure is presented in [P1] and Appendix (5.5).

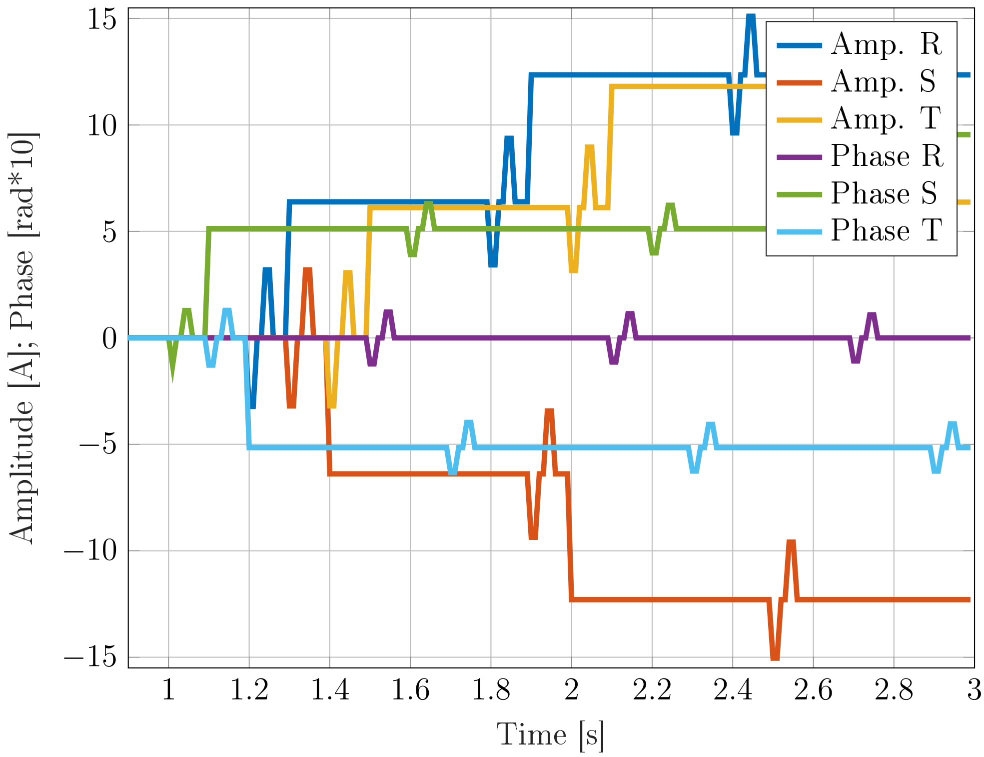

Figure 3.5: Timing and progression of individual APPS axes. It can be observed, that each optimization sequence has it's delayed time window in strict order of 0.1 second. In each step an upper and a lower directional test step is made with the with of 0.02 second from which the algorithm can decide the size and direction of the next step, based on Algorithm (1). As such 0.6 second is required for performing one optimization cycle.

3.4.2 Numerical results

In order to be able to investigate the proposed optimization based unbalance reduction with the three phase inverter on a low voltage local grid, all the elements of this complex electrical system (including the photovoltaic source, battery, and other power electronic components) has been modeled in Matlab/Simulink environment according to [P1]. The primary aim of the simulation based experiments were to serve as a proof of concept for the proposed complex control structure.

Performance analysis

The aim of performance analysis is twofold. First of all, the proposed voltage unbalance indicator has to be investigated in the control structure as the cost function of the optimization based controller, and on the other hand, the control structure itself has to be exposed against engineering expectations on a proof of concept level. The results of the first experiment can be seen in Figure (3.6) where the geometrical norm (2.11) has been used as the voltage unbalance indicator and the cost function for the optimizer on an experimental network with fixed unbalanced load. The dashed line represents the examined low voltage local network's voltage unbalance norm (G) without the proposed controller implemented in the inverter unit of the domestic powerplant while the solid line represents the compensated network's value. Note, tat as mentioned in the previous chapter, the geometrical norm is a unit-less value, since it represents the ideal and the real voltage phasor's symmetric difference.

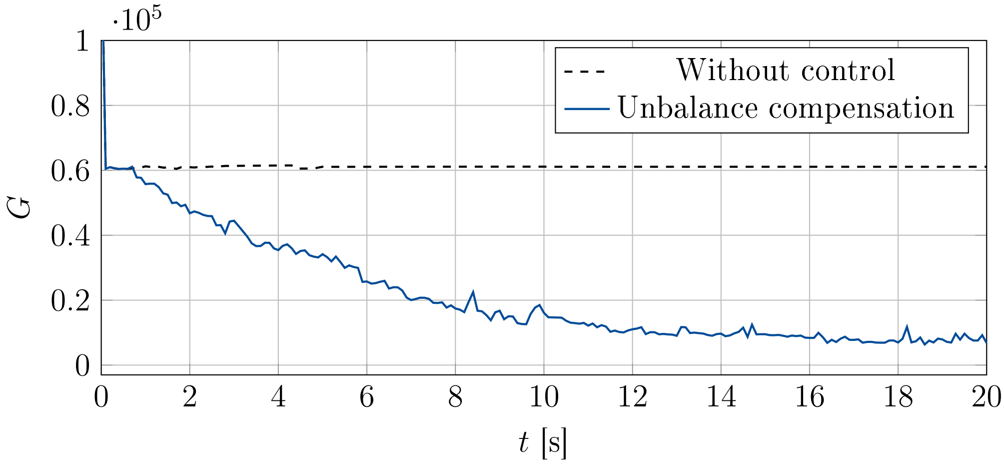

Figure 3.6: Unbalance reduction control's system performance with half charged battery and photovoltaic power source available with an experimental network. The underlying unbalance norm is the geometrical one (G). After starting the controller at $t = 1s$ the unbalance measure G of the network significantly decrease.

Robustness analysis

The robustness of the proposed controller had to be tested via simulation when different types of loads (inductive, capacitive, resistive) had been varied in step changes representing the on/off switching the different types of household appliances (motors, switching mode power supplies, electric heaters, etc.). In the experiment depicted in Figure (3.7), a load change has been introduced to the network in every 15 seconds causing the voltage unbalance to jump to a different value (measured in G). As it can be seen in the figure the controller successfully compensates the unbalance after each transient.

Measurements from a real unbalanced network

In order to expose the method to more realistic circumstances, the simulation model was set up in such a way, that measurement data from a real network with voltage unbalance The measurements took place at the campus building's power electronics laboratory, where a common 400 V connection point was investigated as the behaviour of the network. Afterwards, the measurement data has been used as the input of a micro-grid segment of the Matlab/Simulink model in order to test the controller and inverters structure's performance in quasi-realistic circumstances. Figure (3.8) shows the simulation results with respect to G and VUF. It can be seen, that the optimal

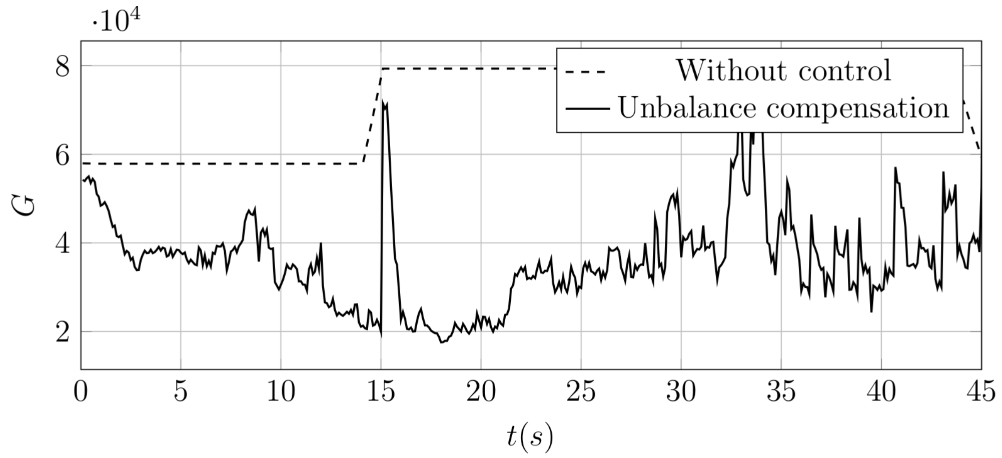

Figure 3.7: Robustness analysis with respect to step type changes in the network load (and voltage unbalance). The unbalance reduction controller successfully compensates the changes in the network voltage unbalance norm (G) value.

compensation that uses G as cost function decreases VUF as well. The compensators performance on the simulated microgrid's network loss reduction can be observed on Figure (3.9a), and Figure (3.9b).

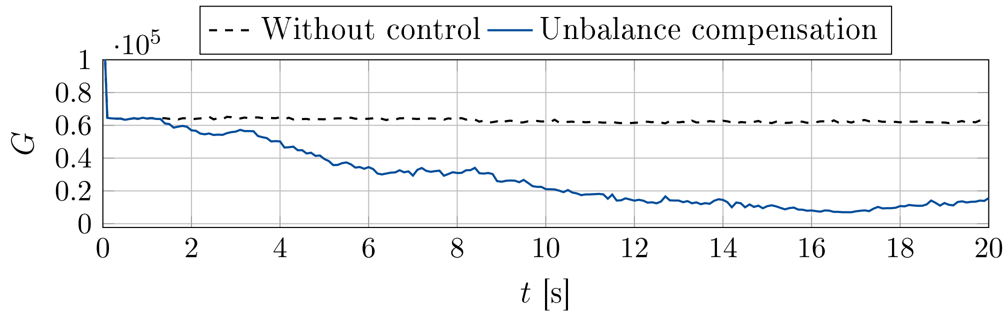

(a) Unbalance reduction control system performance with half charged battery and photovoltaic power source available on a measurement driven network. The underlying unbalance norm is the geometrical one (G) in this experiment. The controller starts at $t = 1s$.

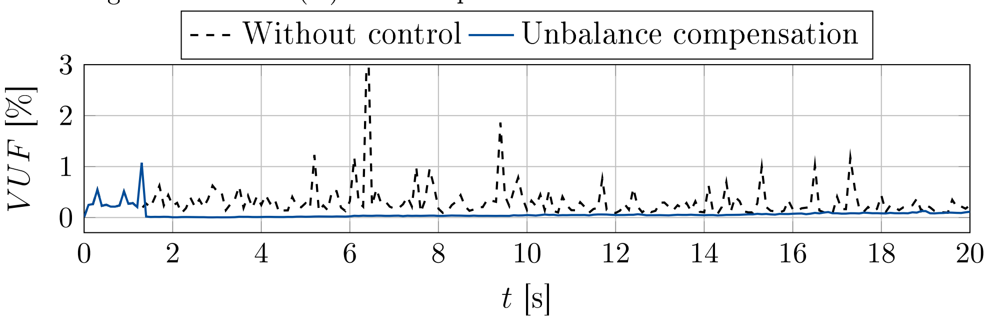

(b) VUFs evolution during control, while the cost function is still G on a measurement driven network. Due to the control action VUF is smoothed.

Figure 3.8: Voltage unbalance compensation with a measurement driven network.

The measurement output is connected to a modeled three phase load and

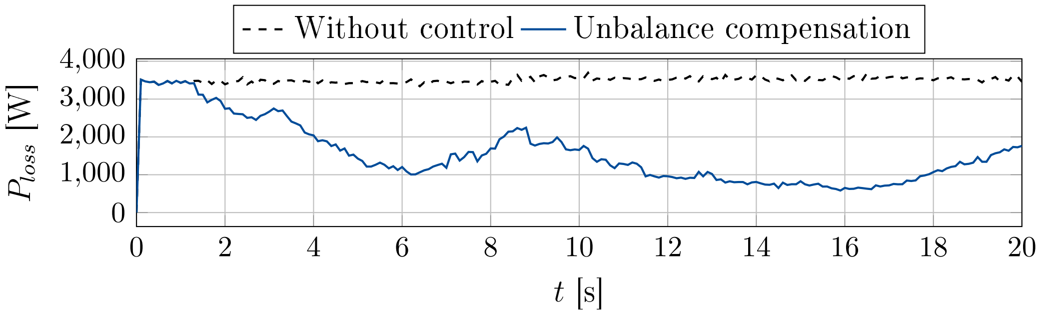

(a) The active power loss (P_{loss}) evolution during control on a measurement driven network. The value is actively decreasing due to the result of unbalance compensation

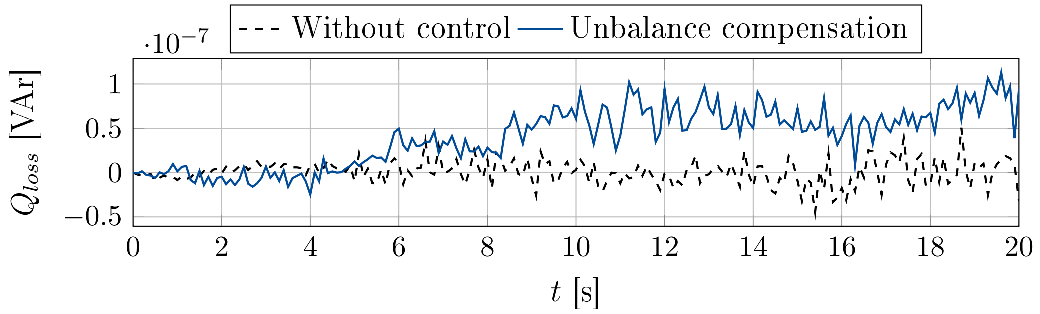

(b) The reactive power loss (Q_{loss}) evolution during control on a measurement driven network. The value, however low, can be uncontrollably affected by the unbalance compensation.

Figure 3.9: Voltage unbalance compensation with a measurement driven network. The measurement was performed at the department's power electronics laboratory.

network system, consisting of symmetrical loads and network segments between them. Further artificial load unbalance is not necessary since the network's unbalance is already present. This structure enables to show that any point the inverter is connected, could restore power quality with a certain degree such unbalance compensation at this case. The future plan is to set up multiple devices on different connection points.

Performance comparison of different unbalance indicators

In this section the chosen unbalance indicators, VUF, and G shall be compared in performance solving the same optimization problem. The only difference between the three compared simulations are the APPS algorithm cost function candidate (VUF, or G), as they are compared to the uncontrolled example. The environment consist of a notable voltage unbalance and an emphasized undervoltage, so the difference of the two approaches would be observable. The simulation's initial stance is visible in Figure (3.10) (same argumentation as with Figure (2.3)), where the triangle in the middle stands for the measured voltage phasor.

It can be observed, that in Figure (3.11) the value of VUF does not deviate much in case of different cost function options. However, observing the trend of G with the same circumstances, the values are showing a different trend

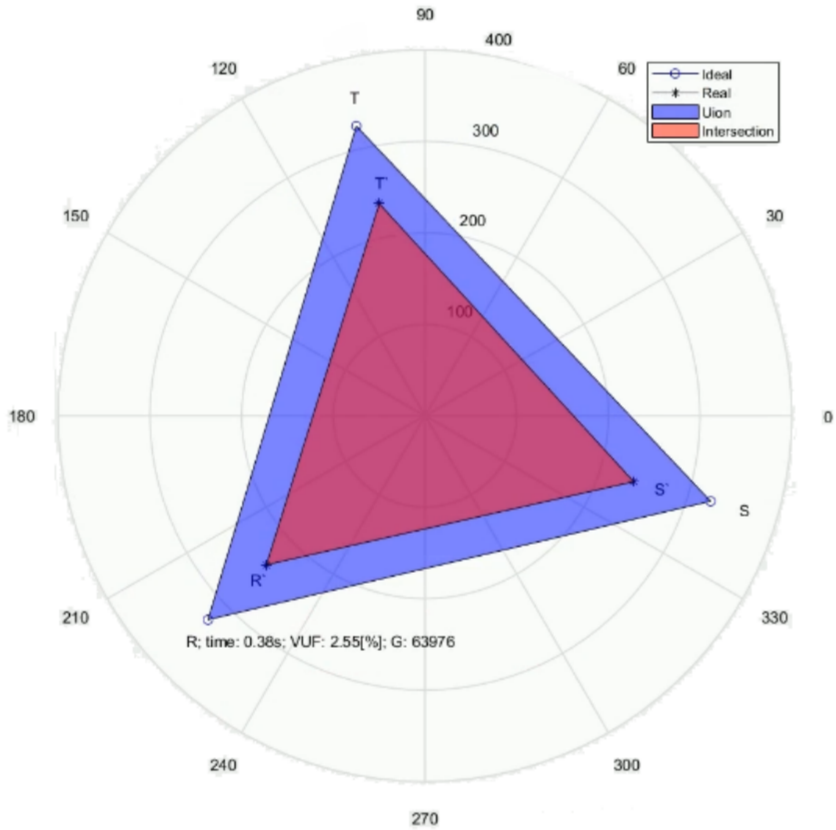

Figure 3.10: The ideal and real voltage phasors at simulation time of 0.38 second. It can be observed, that the voltage is uniformly deviating due to the network load.

with in case of the VUF based approach, the unbalance is slightly above the uncontrolled threshold, and with G a clear reduction is shown. This is due to the case of the initial large undervoltage, which gets compensated, but with VUF it is not recognised.

In terms of network power losses with the previous example observable in Figure (3.12). In case of the active power losses the simulation with G as cost candidate produces clear reduction, but with the VUF a slight increase. However with all approaches the reactive power slowly diverges form zero over time, which is a clear improvement point for the future.

3.5 Summary

A direct optimization based compensation structure applicable for three-phase network is proposed in this chapter. Due to the basic assumptions regarding the network, the optimal input current phasor can be found by any derivative-free optimization method. The cost function for the proposed voltage unbalance optimizer can be any scalar valued VU norm, however, the previously defined geometric norm is suggested here. The geometrical unbalance norm proposed in the previous chapter is applied as a cost function in the asymmetry reducing optimization based control utilizing an asynchronous

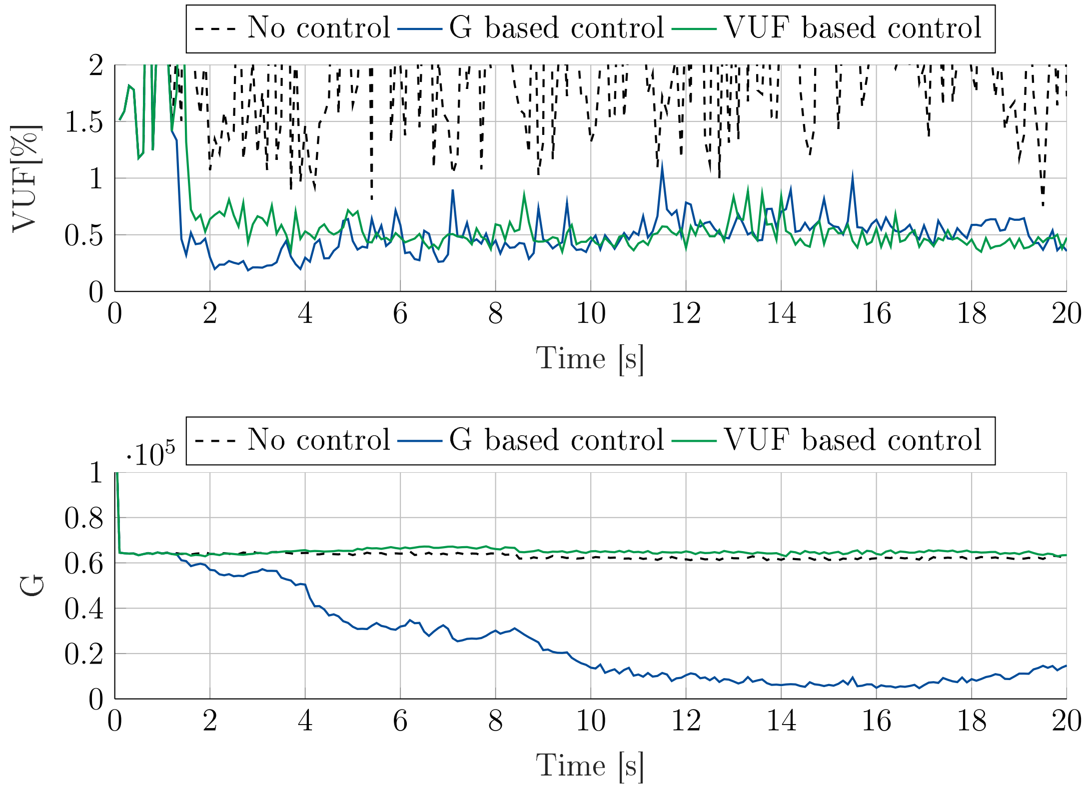

Figure 3.11: Voltage unbalance compensation when employing VUF or G as cost function.

parallel pattern search (APPS) algorithm also presented in the chapter. Simulations, performed in Matlab/Simulink environment show that the geometrical based indicator can serve as a basis of further research. The suggested controller structure enables the residential users owning a grid synchronized domestic power (renewable) plant to reduce voltage unbalance measurable at the connection point. The fundamental element of the system is a modified three phase inverter that is capable of the asymmetric current injection of any current waveforms to the network, via decoupled bi-directional DC-DC converters. The optimization-based control algorithm injects the available energy (as current waveform) in such a way, that the voltage unbalance decreases. This is an optimization problem which is constrained by the available renewable energy supplied by the power plant, or energy storage unit.
The proposed optimal input design based controller has been tested on a low voltage network model in a dynamical simulation environment consisting of the models of the electrical grid, a domestic power plant, an asymmetrical inverter circuit, and different types of loads. Different simulation experiments has been run for each norm and for both the power constrained and unconstrained (zero operation case) case.

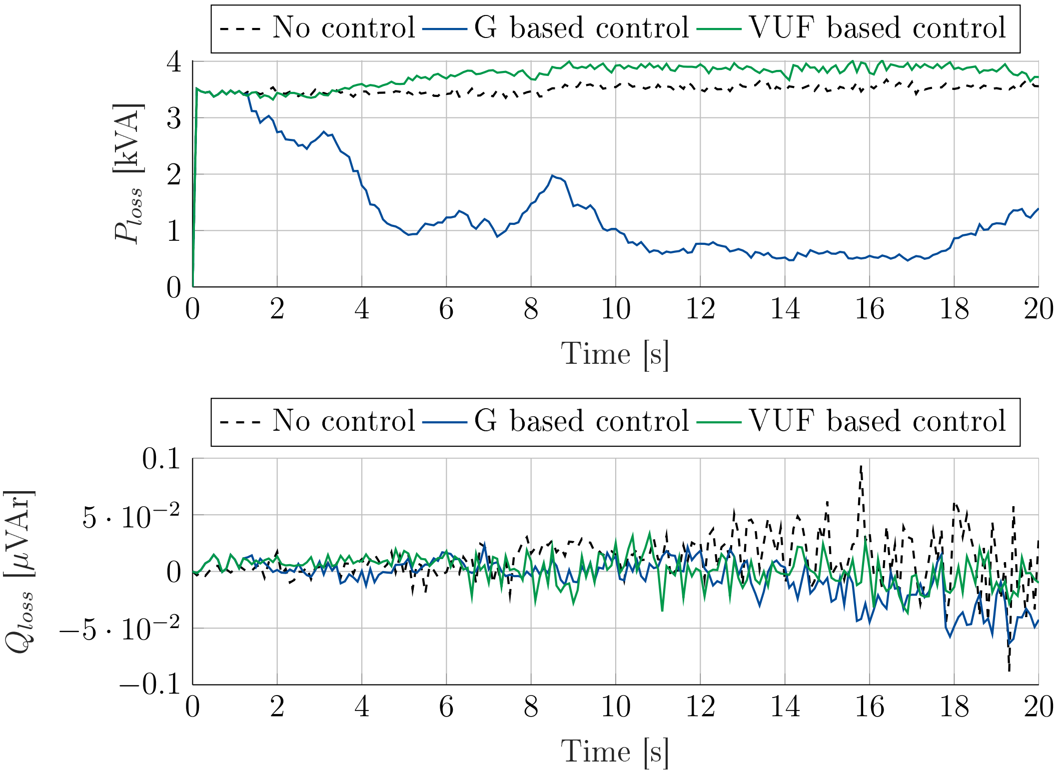

Figure 3.12: The network's active (P_{loss}) and reactive losses Q_{loss} in case of VUF or G as cost function.

3.6 Notations used in the chapter

C_{Batt}	Capacitance of the power storage
C_{inter}	Capacitance of the intermediate buffer
C_{snub}	Capacitance to reduce switching loss and to damp out over-voltage
D_{1+}, D_{2+}	CSI Higher diodes
D_{1+}, D_{2+}	CSI Lower diodes
f_{grid}	Network function at the device's connection point
f_{norm}	Function of voltage unbalance
f_{inter}	Function intermediate voltage controller
$f_{current}$	Function of current injection
$f(\mathbf{x})$	Multivariate function to minimize
G	Geometrical voltage unbalance indicator
h	DC-DC transformer turn ratio
K_D	Intermediate voltage controller's derivative gain
K_I	Intermediate voltage controller's integrator gain
K_P	Intermediate voltage controller's proportional gain
L_+, L_-	CSI current filter inductors
L_a	DC-DC transformer leakage inductance
L_{CSI}	Filter inductance of the current source inverter
L_{Batt}	Filter inductance of the power storage
L_{PV}	Filter inductance of the PV stage
m	Tuning parameter
N	represents the chosen norm's value as the network's
n	Tuning parameter
Q_{hh}	Household load's active power
P_D	DC-DC power transfer under idealized conditions
P_{loss}	Lost power per household due to network unbalance
P_{loss}^{comp}	Assumed network loss with unbalance compensation control
ΔP_{loss}	Saved power with unbalance compensation control

p	APPS process index
q	Discrete time step
V_a, V_b, V_c	Phase-to-line voltages
V_{an}, V_{bn}	Designated point's potential to ground
VUF	Voltage Unbalance Factor
$\mathbf{x}^q$	Local multivariate state at the q^{th} timestep
α	Fortesque operator
Δ	APPS step length control parameter
Δ_q	Step size at q
ω	Angular velocity of output sinusoidal voltage or current
$\triangle_{Ideal}$	Triangle of Ideal voltage vectors
$\triangle_{Real}$	Triangle of real voltage vectors

Chapter 4

Explicit model predictive control of a current source buck-type rectifier

4.1 Motivation and aim of research

The motivation of the research was, that generic three phase rectifiers, employ an equation system that is by default hard to design control to, due to the underlying bilineratiy. Hence a recently popular MPC structure is hard to design for such devices and many authors proposed clever but complicated solutions, like in [61]. The question was tackled by the author of [62] where the results were shown for VSI solution and simple control structure. However, there is no attempt to employ the same principle for devices which are current source (hence there is a general lack of literature on current source devices), as such the question was, if the design simplification simplicities and efficient but complex EMPC design could be merged together in the domain of a current source control, namely by a three phase CSR as it is one of the most basic three phase current source devices, to prove the concept. The hope is that the results listed here could be used in more sophisticated topologies as well. As mentioned in section 4.2 current source rectifiers (CSR) play a major role in industrial instrumentation. They are invaluable, in the fields of direct power control, torque control, or where power injection is required, especially in induction heating and DC traction, so the applicability of the design has promises.

4.2 Literature overview

Current source rectifiers (CSR) are widely used in front-end power electronic converter for the uncontrollable or controllable DC-bus in industrial and commercial applications. They have maintained their position through many applications, with uses such as medium-voltage high-power drives [63], [64] STATCOMs [65] and renewable systems [66], [67]. They have a plain and reliable circuit structure, which makes them attractive for simple control design. The CSRs are traditionally controlled by state feedback, or classic cascaded linear control loops such as PI controllers. These simple control applications are suitable for induction motor control [68], and other electromechanical actuators [69], and unusual topologies [P3]. Also, worth mentioning of self-tuning variants of PI controllers [70].

In the past, the modulation methods used were trapezoidal pulse width modulation techniques (TPWM), or application of pulse patterns calculated offline for selective harmonic elimination (SHE). More recently, current space vector modulation (SVM) has been used for the synthesis of the transistor control signals [71]. Even so, AC-side harmonic elimination could still be an issue at lower switching frequencies where LCL filtering (inductive-capacitive-inductive) would be advised [72].

In terms of the amplitude of the grid and DC-link voltages, CSRs exhibit a step-down conversion. When used as DC voltage source, the rectifier can output a lower DC voltage without the need of a grid-side transformer, as is usually employed in voltage source rectifiers (VSR). Because of their current source behavior, CSRs can easily be paralleled and provide inherent short-circuit protection, representing an excellent potential in DC power supply applications [73], [74].

There are several control strategies in addition to classical PI control for applications in this domain. Self-adapting control methods are on the rise with more sophisticated algorithms, although with varying degree. Filtering the AC side of three-phase current source PWM rectifier is realised with LC filtering, bringing leading power factor and oscillatory current to the set of solvable problems. This means, beside the neccesary power factor correction, by ofsetting the equation set's quadratic component based on further active components and loads, the LC filter acts as a general low pass filter for the high frequency transitions but brings oscillations into the system's dynamics, which need to be compensated. Over sizing this LC filter or the choke inductance (which smoothes the DC current) makes the design not only more expensive to build, but load dynamics could be dampened, making it insufficient for drive control. On top of that, the bilinear nature of PWM rectifier's equation set, makes it difficult for designing control. This means, the sufficient effect could not be obtained with the traditional PID control system under larger disturbance and changes of controlled object, in other words, the general approach suffers from dynamic problems.

The resonance can come either form the PWM process or from the grid voltage distortions, hence results in line current distortion. In [75] state feedback controllers were analysed using different variables in the filtering process. It is shown by [76] that the inductor-voltage feedback or the capacitor-voltage feedback can damp the current oscillations by increasing the damping ratio. The results show that voltage feedback can effectively damp the current oscillations but are unable to suppress the low-order harmonics from low frequency switching. On the other hand, the current feedback can contribute to the sup-

pression of the low-order harmonics but the damping ratio cannot be increased. However, the combined variable feedback controls, can achieve both results.
The author of [77] is proposing the combination traditional PID control with fuzzy control, for a current source rectifier setup based on fuzzy two closed loop control system. The analysis of the differential equations proved, a decoupling is possible for two independent closed loop self-adaptive fuzzy control strategy with disturbance and oscillation compensation. Despite the hardships of tuning a fuzzy controller, good robustness is realized, with of fuzzy controller making the system's interferences to damp and eliminating the time variance.
With model augmentation it is possible to handle increasingly more complicated models and systems with high dynamics and accuracy [78], [79], and even without establishing and validating classical state-space models [80]. The other filed is the sliding mode control, which can achieve good dynamic performance and handle non-linearity. Still, they might also introduce chattering, which can be very undesirable when applied to real-life systems like in [81] and [82]. Additionally in [83] the validity of an MPC-based, digital pulse width modulation control strategy for single-phase voltage source rectifiers is discussed, further confirming the validity of this method in control systems.
A a basic premise a simple predictive control scheme for CSRs is presented in [84], where the control scheme considers the discrete change of switching states at equidistant points with a constant sampling period. The measured output current follows the reference current very closely even under transient conditions,which corroborates the good dynamics provided with the proposal. This makes the model based predictive controller so popular, since control design is much more straightforward and systematic, if the boundary conditions, like linear system design, or perfectly known system model and load can be achieved. However, this is also a requirement of other control schemes based on PID controllers and modulators. As a further step adaptive application was established to tackle parameter estimation problems for better performance in uncertain modeling situations [85].
In the linear domain implicit model predictive control (IMPC or MPC) is the next evolutionary step due its effectiveness because of its configurable cost function and such scalable nature [86], [83]. In this state, variable step size for computation benefits or refined local control dynamics is also an option. In this field also finite-state solutions are present which can be considered also predictive control, where the modulation scheme's defined states serve as optimization potential [87], [88].
Recently, beside implicit, finite-state, and adaptive predictive control, explicit model predictive control has emerged in the field of power electronics [61]. Establishing the MPC cost function can range widely depending on the expected dynamics, degree of noise cancellation, and model complexity. Additionally, embedded state- or input constraints can also be implemented introducing constraints in the control algorithm. This is very beneficial in safety, or automotive applications. However the main advantage, is the the significant reduction of calculation demand, enabling for much higher switching frequencies in applications. This enables the designer to choose lower LC values making the damping

design also easier.

4.3 Three-phase buck-type rectifiers

Three-phase controlled rectifiers have a wide range of applications, from small rectifiers to large high-voltage direct-current transmission systems. They are used e.g. at electrochemical processes, many kinds of motor drives, traction equipment, controlled power supplies, induction furnaces. In this thesis only force commuted rectifiers are examined, which are built with semiconductors (IGBTs in this case) with gate-turn-off capability. The gate-turn-off capability allows full control of the converter, because valves can be switched ON and OFF whenever is required. This allows the commutation of the valves, hundreds of times in one period that is not possible with line-commutated rectifiers, where IGBTs are switched ON and OFF only once a cycle. This has the following advantages:

- The current or voltage can be (pulse width) modulated, generating less harmonic contamination.
- The power factor (ratio of the real and reactive power) can be controlled and even it can be made leading, signifies that the load is capacitive, as the load "supplies" reactive power.
- They can be built as voltage-source or current-source based on the required application.
- The reversal of power in switching rectifiers is by reversal of voltage at the DC link. This allows force commutated rectifiers can be implemented for both, reversal of voltage or reversal of current.

There are two ways to implement force commutated three phase rectifiers, as a current-source rectifier (Fig.(4.1a)), where power reversal is by DC voltage reversal, and as a voltage-source rectifier (Fig.(4.1b)), where power reversal is is solved by current reversal at the DC link.

As general case be a front-end converter power supply (e.g. lighting or telecommunications) shall be designed such that it should have approximately these general characteristics: sinusoidal main currents, unity power factor, high power density and simplicity of the power circuit structure. Two structures are most fitted for the task. First a boost-type input rectifier (e.g., Vienna rectifier, [89]), that typically features two 400 V output voltages with a three-level isolated DC-DC converter or two isolated DC-DC output stage (see Fig. (4.3) in Ch.5.). The second candidate is the buck-type input rectifier (or current source rectifier (CSR)) (conventionally six-switch topologies as proposed in [90], [91]) with only one two-level isolated DC-DC converter output stage. Also the input stage can be realized as a three-switch topology with considerably lower system complexity as compared to the boost-type structure. In

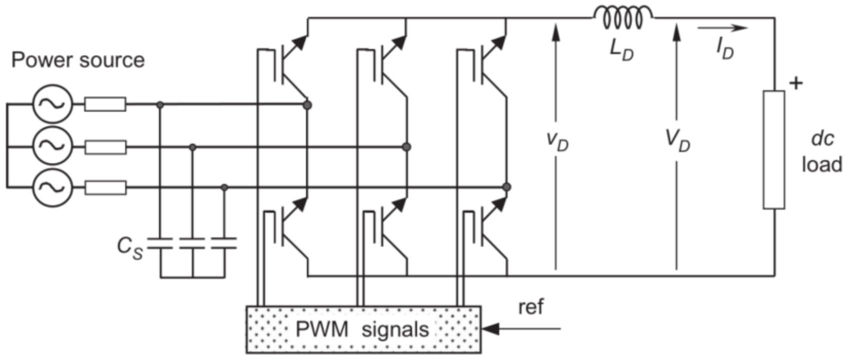

(a) Current source rectifier with capacitive filtering and choke inductance.

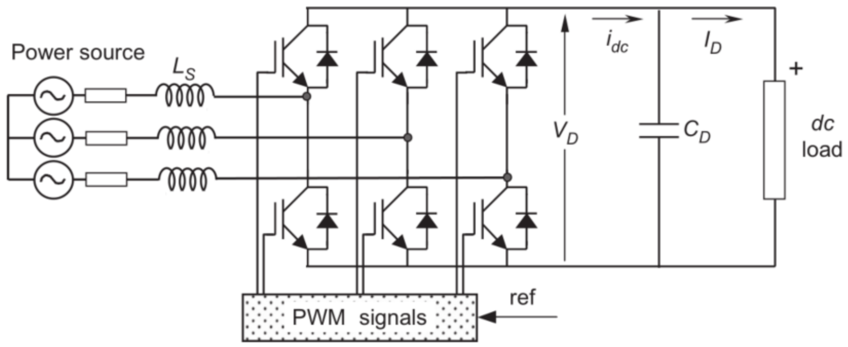

(b) Voltage source rectifier with inductive filtering and DC voltage smoothing capacitance.

Figure 4.1: Basic topologies of force commuted rectifiers.

particular, the number of utilized active and passive components is much lower. Furthermore, there is no middle-point that has to be stabilized, as this is the case for the boost-type structures, making control and active filter design less complex. Further system advantages are the potential of direct start-up and the implicit over current protection in case of an output short circuit. Therefore, these topologies of high interest for many safety critical applications as such future electric aircraft, or automotive applications or as power supplies for process technology [92]. The three-switch buck rectifier topology was first proposed in [93]. In [94] and [95], aspects of the system modulation and control have been treated. The application of the topology used as an active filter is discussed in [96]. The addition of a DC-DC output boost-stage has been proposed in [97] in order to maintain 400 V output voltage for a wide input voltage range and for the case of unbalanced mains as, e.g., the loss of one phase.

Basic operation principles

For the derivation of the relative on-times of the three buck transistors S_i with the following assumptions are made for clarity and facilitation of calculations:

- The AC-side filter capacitor voltages (v_{c_p}, where $p \in \{1, 2, 3\}$) at the input of the CSR are sinusoidal and in phase with the main harmonic component of voltage.

$$\begin{aligned} v_{c_1} &= \widehat{v}_c \cos(\omega t) \\ v_{c_2} &= \widehat{v}_c \cos(\omega t - 2\pi/3) \\ v_{c_3} &= \widehat{v}_c \cos(\omega t + 2\pi/3), \end{aligned} \tag{4.1}$$

where ω is the network voltage's angular velocity.

- The mains currents are assumed to be equal to the fundamental component of the rectifier input currents.

- The current in the DC output inductor L_D is not affected by the high frequency ripple due to the switching operation.

For achieving ohmic mains behavior also in case of unbalanced fundamental harmonics conditions the explained modulation method can still be utilized, however, additionally the control structure presented in [98] has to be employed.
The waveforms of the phase and line-to-line mains voltages are divided into twelve sectors of $\frac{\pi}{6}$ rad wide shown in Fig.(4.2). The following calculations are based on the analysis of the first sector which is characterized by the voltage harmonic phase relation. For the remaining sectors the calculations can be accomplished in an similar manner [92].

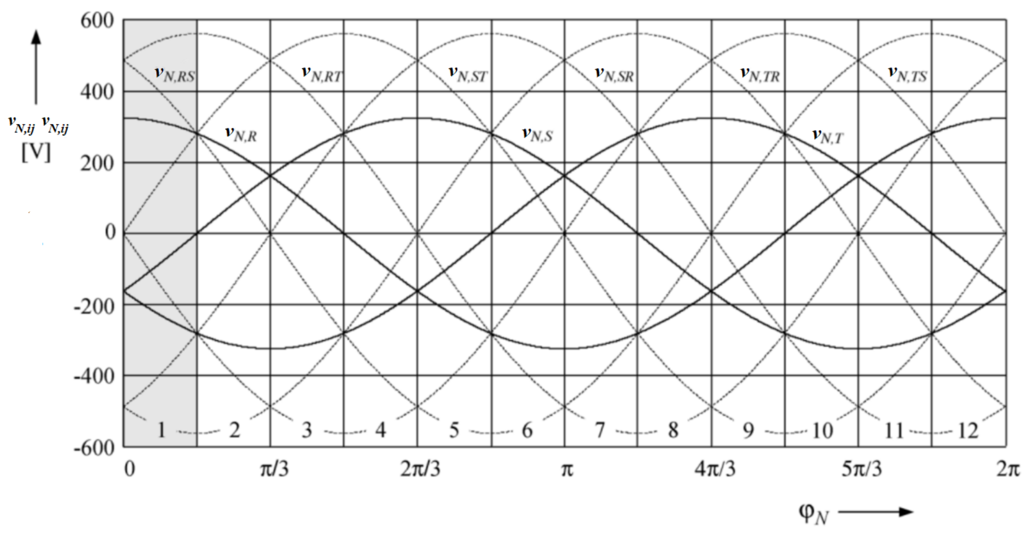

Figure 4.2: Phase voltages v_i, where line-to-line voltages $v_{N,ij} = v_{N,i} - v_{N,j}$, $(i, j) \in \{R, S, T\}$ and sectors 1 to 12 being defined by the different relations of the instantaneous values of the mains phase voltages for $v = 400V$

Accordingly, on AC side, if conditions are favorable, inductor current can appear in an instant of time either in two out of three phases or in none. In this modulation technique, the switches in each converter leg can conduct only one at the time (aside from zero states, where both upper and lower switches are conducting). When the upper leg is conducting it is indicated by '1', when the lower '−1' and when neither '0'. As such the choice whether upper or lower switch of the leg conducts current depends of the reference current vector's sector location. According to the actual switch combination the DC link current shaped by the choke inductance, and distributed to two of the input phases or the freewheeling diode. With this, the input current space vectors can be calculated for each of the before-mentioned switching states. Generally the space vector of three-phase quantities (e.g., for the rectifier input current) are described as:

$$\vec{i} \;=\; \tfrac{2}{3}\left(\vec{i}_a + \vec{i}_b e^{\frac{j\pi}{3}} + \vec{i}_b c^{\frac{4j\pi}{3}}\right). \tag{4.2}$$

Based on (4.2) the corresponding active space vectors in the first sector can be obtained as:

$$\begin{aligned} \vec{i}_{(1,0,-1)} = \vec{i}_1 &= 2i_{dc}e^{j\pi/6}/\sqrt{3} \\ \vec{i}_{(0,1,-1)} = \vec{i}_2 &= 2i_{dc}e^{j\pi/2}/\sqrt{3} \\ \vec{i}_{(-1,1,0)} = \vec{i}_3 &= 2i_{dc}e^{j5\pi/6}/\sqrt{3} \end{aligned} \tag{4.3}$$

The resulting discrete space vectors can be used to synthesize desired current space vector $\vec{i}_{ref}$.

The modulation methods were evaluated in and chosen for this paper based on [99], which ensures minimum switching-losses, minimum ripple values of the input capacitor voltages and of the output inductor current. According to this modulation, each pulse interval comprises two active states and a freewheeling state, arranged symmetrically about the middle of the pulse interval (see Table (4.3)). For more in depth functional description see section (4.4.4).

4.3.1 Coordinate transformations

In section (4.4.2) the three phase current source rectifier's (CSR) equations are converted to different coordinate spaces.

Clarke transformation

In electrical engineering, Clarke transformation is a mathematical transformation employed to simplify the analysis of three-phase circuits. Conceptually it is similar to the Park transformation. One very useful application is the generation of the reference signal used for space vector modulation control of three-phase inverters. The transformation follows:

$$\mathbf{i}_{\alpha\beta\gamma}(t) \;=\; T_{Clarke}\mathbf{i}_{abc}(t) \begin{bmatrix} 1 & -\frac{1}{2} & -\frac{1}{2} \\ 0 & \frac{\sqrt{3}}{2} & -\frac{\sqrt{3}}{2} \\ \frac{1}{2} & \frac{1}{2} & \frac{1}{2} \end{bmatrix} \begin{bmatrix} i_a(t) \\ i_b(t) \\ i_c(t) \end{bmatrix}, \tag{4.4}$$

where $\mathbf{i}_{abc}$ is the generic three phase current sequence, and $\mathbf{i}_{\alpha\beta\gamma}$ is given by the transformation.

Park transformation

The Park transformation is a tensor that rotates the reference frame of a three-element vector or a three-by-three element matrix in an effort to simplify analysis. The transform can be used to rotate the reference frames of AC waveforms such that they become DC signals. Simplified calculations can then be carried out on these dc quantities before performing the inverse transform to recover the actual three-phase ac results. As an example, the Park transform is often used in order to simplify the analysis of three-phase synchronous machines or to simplify calculations for the control of three-phase inverters. In analysis of three-phase synchronous machines the transformation transfers three-phase stator and rotor quantities into a single rotating reference frame to eliminate the effect of time-varying inductances. The transformation follows:

$$\mathbf{i}_{dq0}(t) \;=\; T_{Park}\mathbf{i}_{abc}(t)\sqrt{\frac{2}{3}}\begin{bmatrix} \cos(\theta) & \cos(\theta-\frac{2\pi}{3}) & \cos(\theta+\frac{2\pi}{3}) \\ -\sin(\theta) & -\sin(\theta-\frac{2\pi}{3}) & -\sin(\theta+\frac{2\pi}{3}) \\ \frac{\sqrt{2}}{2} & \frac{\sqrt{2}}{2} & \frac{\sqrt{2}}{2} \end{bmatrix}\begin{bmatrix} i_a(t) \\ i_b(t) \\ i_c(t) \end{bmatrix}, \tag{4.5}$$

where θ is instantaneous angular position of an arbitrary frequency.

4.4 Constrained, explicit predictive control for current source buck-type rectifiers

4.4.1 Overview

In this section, I propose an explicit model based predictive control scheme realised on a classic CSR (or buck-type rectifier) control structure. The device as the name suggests utilizes three phase alternating current waveform, obtained from domestic three phase source, to create a steady direct current on the output poles. This structure was described in section 4.3, where the topology and waveform formulation is written in detail. Also worth mention that the modelled devices's equations (described in section 4.4.2) are not entirely in the linear domain.

The employed control structure (section 4.4.3) is unique in a sense, since classic model based predictive control was not part of the power electronic domain recently. The high frequency switching periods and dynamical demand renders classic MPCs ineffective due to they massive calculation demand. However, if the control space is mapped and an effective search pattern is utilized, the feasibility could be guarantied. Also since the control structure relies on physical parameters the structure of choice supports embedded constraint handling(described in section 5.7.1) which is essential in electric power conversion realisations.

The aim of the proposed control structure is two fold. On one hand the goal is to reach the steady state current reference, with minimal overshoot, at the output poles as fast as possible with a resistive load assumed. On the other, the reactive power and process noise on the network's side shall be also minimized.

4.4.2 Modeling

Understandably, model based controllers require the system's model the ought to control, or supervise. In this case the most common structure of a CSR is chosen, with inductive and capacitive filtering on both ends. The differential equations are constructed based on Kirchoff's law and then presented as a state space model for further examination.

Mathematical modeling of the CSR

The structure of the classical three phase buck-type current source rectifier (CSR) is presented in (4.3). The purpose of such a device is provide a continuous direct current at the output (i_{dc}) but instead of the widely used boost type counterparts, the voltage can be consideraby lower, making ideal for high current operations like induction heating. The device's detailed contexture can be observed in section 4.3. Basically, a finite configuration of switching states with high enough frequency consists a continuous current flow of direct- at the output poles and alternating current at the input poles. This is reached via filtering the high dynamic ripples with low pass filtering realised with LC components. In continuous current mode, the differential equations corresponding to the CRS's inductor currents and capacitor voltages (obtained straightforwardly via Kirchoff's law.) are the following:

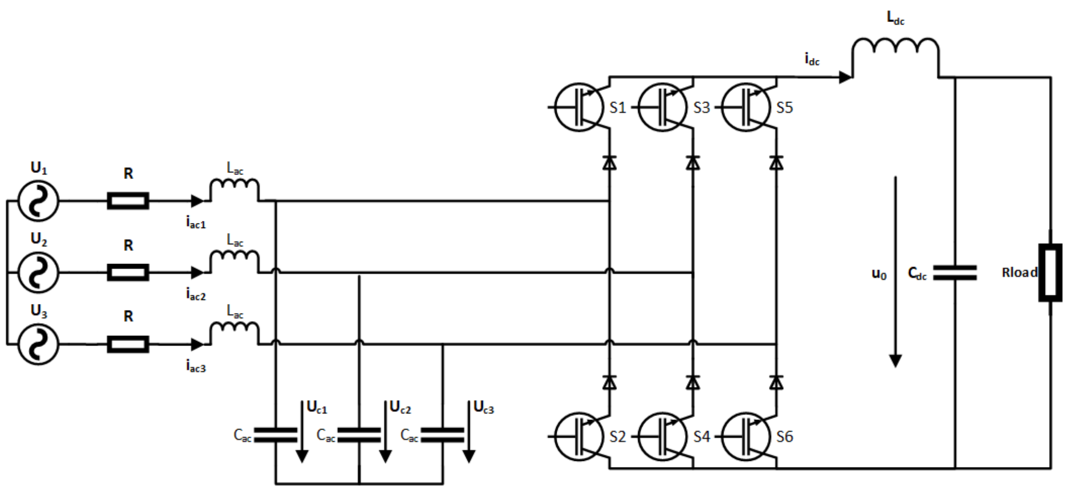

Figure 4.3: Circuit diagram of the three-phase buck-type rectifier with insulated gate bipolar transistors (IGBTs).

$$
\begin{aligned}
L_{ac}\dot{i}_{ac_p} &= u_p - u_{c_p} - R i_{ac_p} \\
C_{ac}\dot{u}_{c_p} &= i_{ac_p} - \delta_p i_{dc} \\
L_{dc}\dot{i}_{dc} &= (\textstyle\sum_{p=1}^{3} \delta_p u_{c_p}) - u_0 \\
C_{dc}\dot{u}_0 &= i_{dc} - \frac{u_0}{R_{load}}
\end{aligned}
\tag{4.6}
$$

where $p \in \{1, 2, 3\}$ is the index of three phases and δ_p describes the conduction state of the rectifier leg p (4.7).

$$\delta_p = \begin{Bmatrix} \text{1 if the upper transitor is ON} \\ \text{-1 if the lower transistor is ON} \\ \text{0 if both are ON or OFF} \end{Bmatrix} \tag{4.7}$$

Converting the components in the stationary (Clarke) frame (displayed in section 4.3.1) of the space phasors of the three-phase quantities, from (4.6) it results:

$$\begin{aligned} L_{ac}\dot{i_{ac_\alpha}} &= u_\alpha - u_{c_\alpha} - Ri_{ac_\alpha} \\ L_{ac}\dot{i_{ac_\beta}} &= u_\beta - u_{c_\beta} - Ri_{ac_\beta} \\ C_{ac}\dot{u_{c_\alpha}} &= i_{ac_\alpha} - \delta_\alpha i_{dc} \\ C_{ac}\dot{u_{c_\beta}} &= i_{ac_\beta} - \delta_\beta i_{dc} \\ L_{dc}\dot{i_{dc}} &= 1.5(\delta_\alpha u_{c_\alpha} + \delta_\beta u_{c_\beta}) - u_0 \\ C_{dc}\dot{u_0} &= i_{dc} - \frac{u_0}{R_{load}} \end{aligned} \tag{4.8}$$

Equation (4.8) is transformed to the synchronous reference (Park) frame (displayed in section 4.3.1) rotating with the u_{c_d} capacitor voltage space vector. The resulting mathematical model is thus:

$$\begin{aligned} L_{ac}\dot{i_{ac_d}} &= u_d - u_{c_d} - Ri_{ac_d} + \omega_s L_{ac} i_{ac_q} \\ L_{ac}\dot{i_{ac_q}} &= u_d - u_{c_q} - Ri_{ac_q} - \omega_s L_{ac} i_{ac_d} \\ C_{ac}\dot{u_{c_d}} &= i_{ac_d} - \delta_d i_{dc} + \omega_s C_{ac} u_{c_q} \\ C_{ac}\dot{u_{c_q}} &= i_{ac_q} - \delta_q i_{dc} - \omega_s C_{ac} u_{c_d} \\ L_{dc}\dot{i_{dc}} &= 1.5(\delta_d u_{c_d} + \delta_q u_{c_q}) - u_0 \\ C_{dc}\dot{u_0} &= i_{dc} - \frac{u_0}{R_{load}} \end{aligned} \tag{4.9}$$

where ω_s represents the network voltage vector's angular velocity.

Model simplification

Notice, that the sixth-order ODE model (4.9) is bilinear in its states and inputs because of the product terms (e.g.: $\delta_d i_{dc}$). As such, using design methods for linear systems is not straightforward. The high complexity given by the system's order is another problem to tackle. For designing classic MPC, linear, low-order equation systems are favorable. Hence simplification of the model would bring noteworthy benefits, making the MPC design more straightforward, when a linear system resulted. Since the three phase alternating current (AC) and the direct current (DC) side's time constants differ significantly (as in the AC: $\omega_{ac} = \frac{1}{\sqrt{L_{ac}C_{ac}}} \cong 5.7{\cdot}10^3$ rad/s, and on the DC: $\omega_{dc} = \frac{1}{\sqrt{L_d c C_d c}} \cong 2.8{\cdot}10^2$ rad/s, see Table (4.1). for reference). Thus, the differential equations can be separated into two sets, and the control of the AC and DC sides can be decoupled as described in [83]. The AC side model results as follows:

$$\begin{bmatrix} \dot{i}_{ac_d} \\ \dot{i}_{ac_q} \\ \dot{u}_{c_d} \\ \dot{u}_{c_q} \end{bmatrix} = \begin{bmatrix} -\frac{R}{L_{ac}} & \omega & -\frac{1}{L_{ac}} & 0 \\ -\omega & -\frac{R}{L_{ac}} & 0 & -\frac{1}{L_{ac}} \\ \frac{1}{C_{ac}} & 0 & 0 & \omega \\ 0 & \frac{1}{C_{ac}} & -\omega & 0 \end{bmatrix} \begin{bmatrix} i_{ac_d} \\ i_{ac_q} \\ u_{c_d} \\ u_{c_q} \end{bmatrix} + \begin{bmatrix} \frac{u_d}{L_{ac}} \\ \frac{u_q}{L_{ac}} \\ -\frac{\delta_d i_{dc}}{C_{ac}} \\ -\frac{\delta_q i_{dc}}{C_{ac}} \end{bmatrix} \tag{4.10}$$

Looking at the state matrix it can be further stated that there are only weak couplings between the d and q synchronous reference frame components. This allows to handle them separately, and later to design separate control for each. The equation system describing the DC side dynamics is the following:

$$\begin{bmatrix} \dot{i}_{dc} \\ \dot{u}_0 \end{bmatrix} = \begin{bmatrix} 0 & -\frac{1}{L_{dc}} \\ \frac{1}{C_{dc}} & -\frac{1}{R_{load}C_{dc}} \end{bmatrix} \begin{bmatrix} i_{dc} \\ u_0 \end{bmatrix} + \begin{bmatrix} \frac{1.5}{L_{dc}}(\delta_d u_{c_d} + \delta_q u_{c_q}) \\ 0 \end{bmatrix} \tag{4.11}$$

It can be noticed that, with the AC and DC model separation, bilinearity disappears, since the binding coefficients are present only in the input ($\mathbf{u}$) of the DC state space model (4.11). Consequently, all equations are linear and with a considerably lower order, making control design much easier and allowing for the application of linear design methods. For the DC side dynamics, the linear time invariant differential equation system's matrices can be identified for predictive control design purposes:

$$\begin{aligned} \mathbf{x} &= \begin{bmatrix} i_{dc} \\ u_0 \end{bmatrix}, \\ \mathbf{u} &= (\delta_d u_{c_d} + \delta_q u_{c_d}), \\ \mathbf{y} &= u_0, \\ \mathbf{A} &= \begin{bmatrix} 0 & -\frac{1}{L_{dc}} \\ \frac{1}{C_{dc}} & -\frac{1}{R_{load}C_{dc}} \end{bmatrix}, \\ \mathbf{B} &= \begin{bmatrix} i_{dc} \\ u_0 \end{bmatrix}, \\ \mathbf{C} &= \begin{bmatrix} 0 & 1 \end{bmatrix}. \end{aligned} \tag{4.12}$$

where $\mathbf{x}$, $\mathbf{u}$ and $\mathbf{y}$ are the state, input and output vectors of the DC-side system, and $\mathbf{A}$, $\mathbf{B}$ and $\mathbf{C}$ are the state, input and output matrices. The circuit parameters used for the implementation of the control structure based on this model are presented in Table (4.1).

Control structure

The described structure of the CSR naturally can only be interpreted in a power electric context. As such the control requirements of the system is shifted respectfully in such a direction that those requirements are met within physical constrains also, within the dissertation's scope. As mentioned in the previous chapter, the modeling of the CSR enables to handle the control goal from two somewhat disjunct perspective. With this in mind, the control requirements can be placed on three categories. With (4.12) in mind these are the following:

Table 4.1: The applied parameters in model and controller design

Parameter	Value
R	0.3 Ω
Rload	10 Ω
Lac	1 mH
Ldc	30 mH
Cac	30 μF
Cdc	400 μF
f	50 Hz
fpwm	20 kHz
Un	400 V

- **AC side:** Minimize current ripple and reactive power from the network's measurement point (at the voltage sources on the topology). In this scenario the domestic network is assumed ideal, aka. the voltage source is an ideal three phase sinusoidal waveform with $50Hz$ network frequency. The disturbance is coming exclusively form the LC filter's oscillation, and from the PWM switching behaviour.

- **DC side:** Reach the reference of u_0^* the fastest possible with minimal overshoot, and steady state error on the resistive load's poles. The fewer number of critical regions, and less horizon length of the EMPC shall be chosen, since these are correlating between the calculation requirements of possible experimental setup.

- **Modulation:** The modulation shall transform the reference current into the optimal switching state, which was permitted by the modulation table. Also, the desired switching sequence shall be conducted with minimum amount of switching used.

Using the separation of the AC side and DC side controllers, the control structure depicted in Fig. (4.4). is proposed.

The controllers operate in the synchronous frame of the AC filter capacitor voltages $u_{c_{(1,2,3)}}$, and the rectifier input currents $i_{r_{(1,2,3)}}$ are in phase with the capacitor voltages. The current reference $i^*_{\alpha\beta}$ supplied to the space vector modulation unit in the stationary frame, is obtained by coordinate transformation $[D(-\Theta)]$ (or Park to Clarke transformation) of the current reference (4.13) delivered by the current controllers in the synchronous frame.

$$\begin{Bmatrix} i^*_{r_d} = i_{rcontrol_d} + i_{rHF_d} \\ i^*_{r_q} = 0 \end{Bmatrix} \tag{4.13}$$

In (4.13), $i_{rcontrol_d}$ represents the output of the DC voltage controller, while i_{rHF_d} represents the damping current, proportional with the high frequency component of the filter capacitor voltage (the fundamental component of the capacitor voltage in the stationary frame becomes a DC component in the synchronous frame). The DC and AC side control units are explained in more

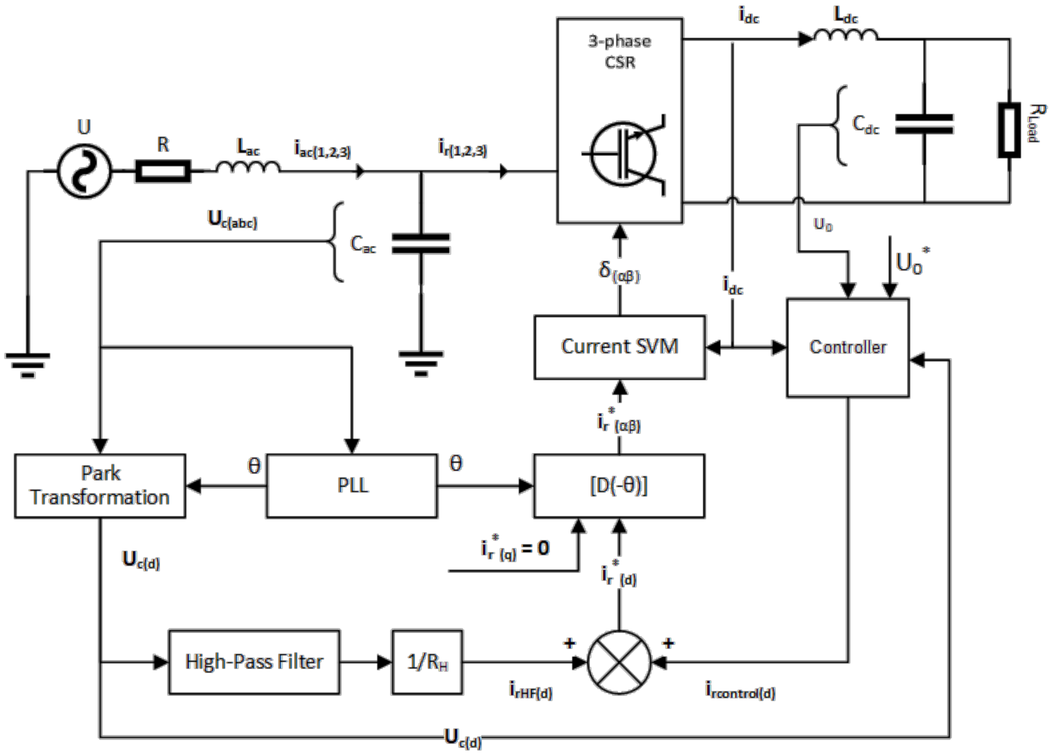

Figure 4.4: Block diagram of the control structure.

detail in the following sections, and the performance of the control structure is evaluated.

4.4.3 Control

In this section the model based control algorithm is explained, used on the DC side, followed by a simpler AC side active damping.

DC-side explicit model predictive control

Model predictive control (MPC) is an efficient and systematic method for solving complex multi-variable constrained optimal control problems [63]. The basic notions of MPC is explained in section 5.7.1, where the MPC control law is explained, namely, is based on the "receding horizon formulation", where the model's assumed behavior is calculated for a number of N steps, where N stands for the horizon's length. Only the first step of the computed optimal input is applied in each iteration. The remaining steps of the optimal control input are discarded and a new optimal control problem (explained in section 5.7.1) is solved at the next sample time. Using this approach, the receding horizon policy provides the controller with the desired feedback characteristics, although with high order systems the computational effort is considerably demanding since all the steps should be taken in to account on the specified horizon in every iteration.
With Explicit MPC (EMPC), the discrete time constrained optimal control

problem is reformulated as multi-parametric linear or quadratic programming. As explained in section 5.7.1, the optimization problem can be solved off-line, making it much more feasible from the perspective of the optimal control task. The optimal control law is a piecewise affine function of the states, and the resulting solution is stored in a pre-calculated lookup table. The parameter space, or the state-space is partitioned into critical regions. The real-time implementation consists in searching for the active critical region, where the measured state variables lie, and in applying the corresponding piecewise affine control law to achieve the desired dynamics. In order to introduce the MPC implementation, let us consider a linear discrete time system (4.14) derived with the discretisation of system (4.11) with zero-order hold method, where control inputs are assumed piecewise constant over the simulation sample time $T_s = \frac{1}{f_s}$:

$$\begin{aligned} \mathbf{x}(t+1) &= \mathbf{A}_d\mathbf{x}(t) + \mathbf{B}_d\mathbf{u}(t) \\ \mathbf{y}(t) &= \mathbf{C}_d\mathbf{x}(t) \end{aligned} \tag{4.14}$$

where $\mathbf{A}_d$, $\mathbf{B}_d$, $\mathbf{C}_d$ are the matrices of the discretised system derived from (4.12). With system (4.14) is linear and time invariant, MPC design can be followed. The following constraints have to be satisfied:

$$\begin{aligned} \mathbf{y}_{min} \leq \mathbf{y}(t) \leq \mathbf{y}_{max}, \\ \mathbf{u}_{min} \leq \mathbf{u}(t) \leq \mathbf{u}_{max} \end{aligned} \tag{4.15}$$

where $t > 0$, $\mathbf{x} \in \mathbb{R}^n$, $\mathbf{u} \in \mathbb{R}^m$, $\mathbf{y} \in \mathbb{R}^p$. The MPC solves the following constrained optimization problem [87]:

$$\min_{U=\{u_t \dots u_t+N_u-1\}} J(\mathbf{u}, \mathbf{x}(t)) = \sum_{k=0}^{N_y-1}(\mathbf{x}^T_{t+N_y|t}\mathbf{Q}\mathbf{x}_{t+N_y|t} + \mathbf{u}^T_{t+k}\mathbf{R}\mathbf{u}_{t+k}) \tag{4.16}$$

subject to:

$$\begin{aligned} &\mathbf{x}_{min} \leq \mathbf{x}_{t+k|t} \leq \mathbf{x}_{max},\ k = 1, \dots, N_c - 1 \\ &\mathbf{u}_{min} \leq \mathbf{u}_{t+k|t} \leq \mathbf{u}_{max},\ k = 1, \dots, N_c - 1 \\ &\mathbf{x}_{t|t} = \mathbf{x}(t),\ \mathbf{u}_{t|t} = \mathbf{u}(t) \\ &\mathbf{x}_{t+k+1|t} = \mathbf{A}_d\mathbf{x}_{t+k|t} + \mathbf{B}_d\mathbf{u}_{t+k|t} \\ &\mathbf{y}_{t+k|t} = \mathbf{C}_d\mathbf{x}_{t+k|t} \\ &\mathbf{u}_{t+k|t} = -K\mathbf{x}_{t+k|t},\ k \geq N\mathbf{u} \end{aligned} \tag{4.17}$$

There the formulation of such problem is described in detail in chapter (5.7.1). This problem is solved at each time instant t, where $\mathbf{x}_{t+k|t}$ denotes the state vector predicted at time $t+k$, obtained by applying the input sequence $\mathbf{u}_{t|t}...\mathbf{u}_{t|t+1}$ to model (4.20), starting from the state $\mathbf{x}_{t|t}$. Further, it is assumed that Q and R, are symmetric positive semidefinite ($\mathbf{Q}_w = \mathbf{Q}_w^T \geq 0$, $\mathbf{R}_w = \mathbf{R}_w^T > 0$) and K is a feedback gain. Further, N_y, N_u, N_c are the output, input and constraint horizons, respectively. Using the model for predicting the future behavior of the system and with some appropriate substitution and variable manipulation which basic notions showed in section 5.7.1, the problem (4.16),(4.17) can be transformed to the standard multi parametric quadratic programming form, as described in [87]:

$$J^*(\mathbf{x}(t)) = \min_{\mathbf{z}} J(\mathbf{x},\mathbf{z}) = \tfrac{1}{2}\mathbf{z}'\mathbf{H}\mathbf{z} \tag{4.18}$$

where subject to:

$$\mathbf{G}\mathbf{z} \leq \mathbf{w} + \mathbf{S}\mathbf{x}(t) \tag{4.19}$$

where the matrices **H**, **G**, **w**, **S** result directly from the coordinate transformations described in (5.7.1). The solution of the quadratic optimization problem for each critical region has the form:

$$\mathbf{u}^* = \mathbf{F}_i\mathbf{x} + \mathbf{g}_i \tag{4.20}$$

and the critical region is described by:

$$\mathcal{C}_{reg_i} = \{\mathbf{x} \in \mathbb{R}^n | \mathbf{H}_i\mathbf{x} \leq \mathbf{K}_i\} \tag{4.21}$$

Thus, the explicit MPC controller is completely characterized by the set of parameters:

$$\{\mathbf{F}_i, \mathbf{g}_i, \mathbf{H}_i, \mathbf{K}_i | i = 1 \dots N\} \tag{4.22}$$

In case of the discrete time system resulting from (4.12), for sampling time equal with the switching period $T_s = 5 \cdot 10^{-5}$ s, the problem defined to be solved by MPC is the minimization of the quadratic cost function (4.14) for:

$$\mathbf{R}_w = \begin{bmatrix}1\end{bmatrix}, \mathbf{Q}_w = \begin{bmatrix} 5 \cdot 10^{-5} & 0 \\ 0 & 5 \cdot 10^{-5} \end{bmatrix}, N_y = N_u = N_c = 4. \tag{4.23}$$

Since N_y, N_u, N_c take the same value, they will be substituted by N. The constraints defined based on the rated power of the CSR $P_n = 2500$ W, are:

$$\begin{array}{ccc} 0 \leq & i_{dc} & \leq 50A \\ 0 \leq & u_0 & \leq 500V. \end{array} \tag{4.24}$$

The state space partition resulting from this problem has 10 critical regions, which can be observed in Fig. (4.5).

From the basis of the discretised model (4.14), the given constraints (4.24), and horizon (4.24) the cost function (4.16) is established via the MPT toolbox [100] and uaastrom2013computeraastrom2013computerzhang2015simplifiedsed in the generated controller for the EMPC design [29], [31]. The controller is created as a compliable S-function in the Matlab/Simulink environment and its place in the control structure can be observed in Fig. (4.6). as the EMPC controller. The output of the MPC controller is the control variable obtained via solving (4.17) and $u_{MPC} = (\delta_d u_{c_d} + \delta_q u_{c_q})$, from which the current reference can be calculated using (4.24). The quadrature component u_{c_q} is zero in the synchronous frame of the filter capacitor voltage.

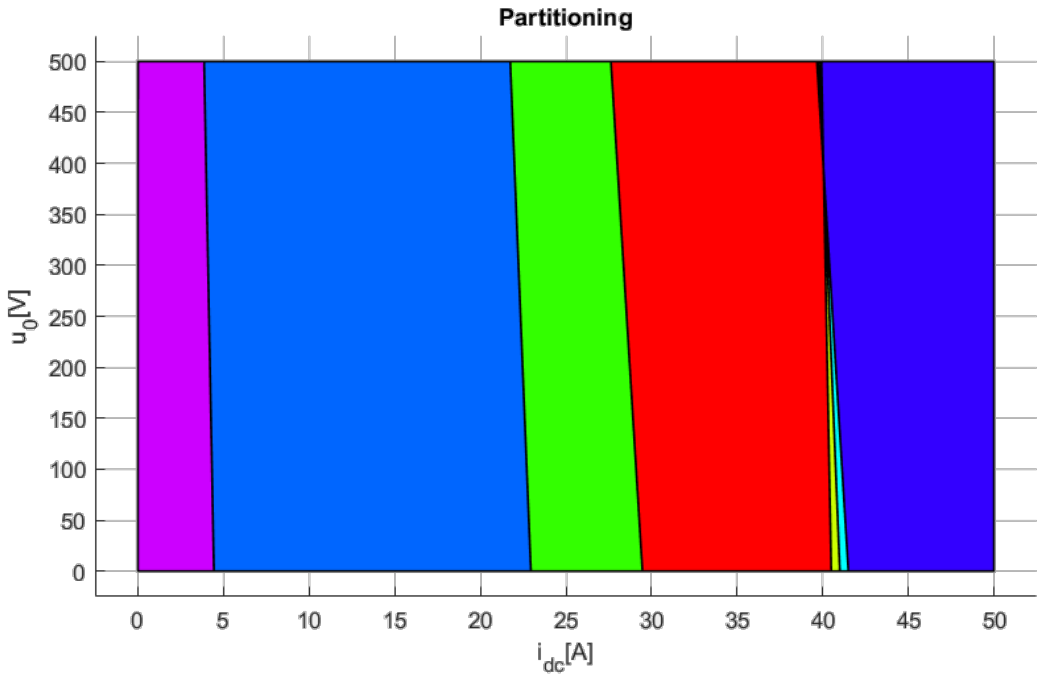

Figure 4.5: State space partitioning over the determined constraints.

$$i_{rMPC_d} = \frac{u_{MPC}}{u_{c_d}} \cdot i_{dc} \tag{4.25}$$

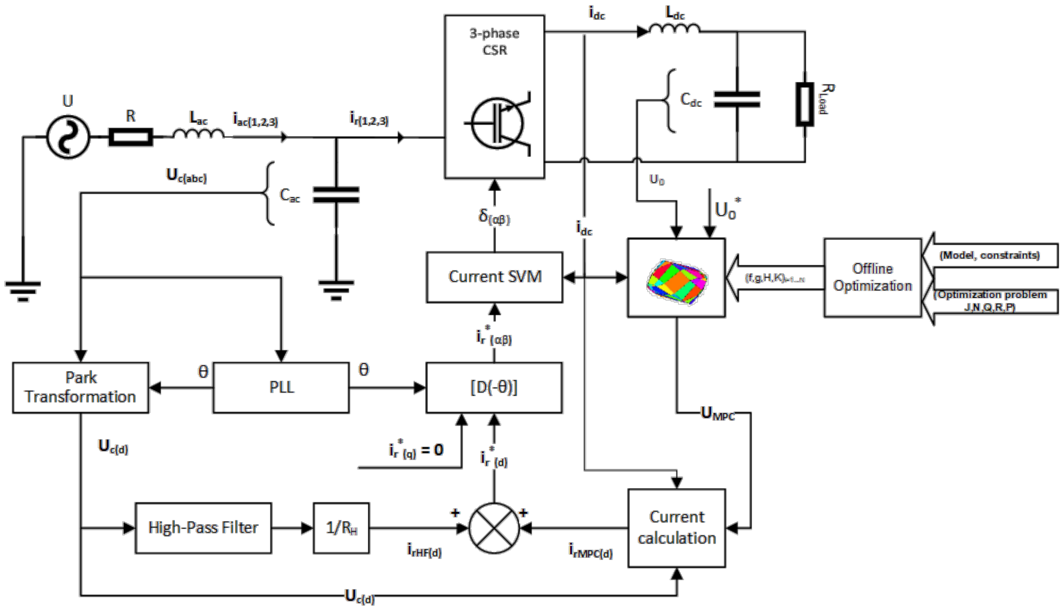

Figure 4.6: The control structure of the CSR, with MPC controller on the DC side.

Active AC-side damping

The CSR requires a voltage supply on the AC side. Taking the inductive character of the mains into consideration, the presence of a three-phase capacitor bank at the input of the CSR is a must. The most convenient is to use three-phase LC filtering with inductors on the lines and star connected capacitors resembling those in Fig. (4.3), although the resonance phenomena between these components can still cause difficult problems.
Let us consider the AC side differential equation of the CSR from (4.10):

$$\begin{bmatrix} \dot{i_{ac_d}} \\ \dot{i_{ac_q}} \\ \dot{u_{c_d}} \\ \dot{u_{c_q}} \end{bmatrix} = \begin{bmatrix} -\frac{R}{L_{ac}} & \omega & -\frac{1}{L_{ac}} & 0 \\ -\omega & -\frac{R}{L_{ac}} & 0 & -\frac{1}{L_{ac}} \\ \frac{1}{C_{ac}} & 0 & 0 & \omega \\ 0 & \frac{1}{C_{ac}} & -\omega & 0 \end{bmatrix} \begin{bmatrix} i_{ac_d} \\ i_{ac_q} \\ u_{c_d} \\ u_{c_q} \end{bmatrix} + \begin{bmatrix} \frac{u_d}{L_{ac}} \\ \frac{u_q}{L_{ac}} \\ -\frac{\delta_d i_{dc}}{C_{ac}} \\ -\frac{\delta_q i_{dc}}{C_{ac}} \end{bmatrix}.$$

The above equation set is representing the AC dynamics well, however, since the physical system is compliant to some boundaries, further simplification can be obtained as displayed by [62]. The capacitor's voltage's d-axis can be aligned with the q-axis, as:

$$u_{c_q} = 0 \tag{4.26}$$

Since the time constant difference between AC and DC side, described in 4.4.2, and the large difference between L_{ac} and L_{dc}, displayed in Table (4.1). Also i_{dc} can be approximated as an I_{dc} constant (modulated by δ_d), and neglecting small couplings such ωL_{ac}, and ωC_{ac}, the AC side model looks like this:

$$\begin{aligned} L_{ac}\dot{i_{ac_d}} &= u_d - u_{c_d} \\ L_{ac}\dot{i_{ac_q}} &= u_q \\ C_{ac}\dot{u_{c_d}} &= i_d - \delta_d I_{dc} \\ 0 &= i_q - \delta_q I_{dc}, \end{aligned} \tag{4.27}$$

Such as in (4.27) the equation along the q-axis is first order and has good stability, in addition, the d-axis can be extended in frequency domain as:

$$u_{c_d} = \frac{u_d}{s^2 L_{ac} C_{ac} + 1} - \frac{s L_{ac} I_{dc} \delta_d}{s^2 L_{ac} C_{ac} + 1}, \tag{4.28}$$

where u_d carries potential disturbance due resonance of the LC filter. Hence, equation (4.30) is a second order linear system without any damping, therefore active damping (or resonance suppressing control) can be implemented.
The simplest way to dampen the resonance would be to add further damping resistor across the capacitor [81], to dampen the oscillation. Because these resistors result in high losses, active damping method can be utilised as displayed in [101], which emulate damping resistors by control. The circuit and control schematics of the AC damping can be observed on Fig. (4.7). This makes the CSR bridge produce an additional high frequency current i_{rHF}, equivalent to

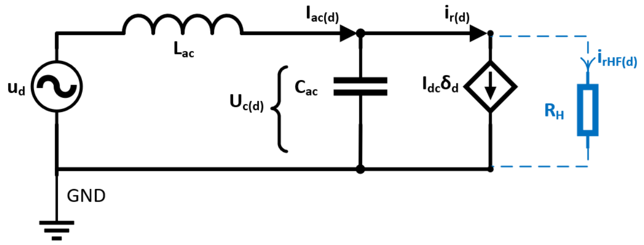

(a) Circuit schematics of AC damping.

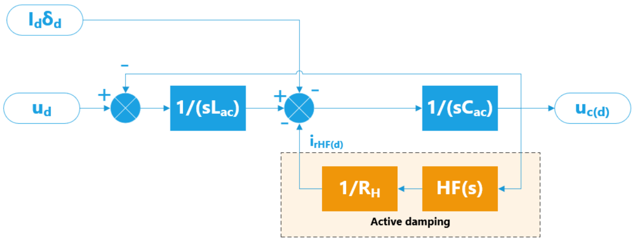

(b) Control schematics of AC damping.

Figure 4.7: Circuit, and control schematics of AC damping via virtual damping resistance R_H, and high pass filter $HF(s)$.

the presence of virtual damping resistor R_H connected in parallel with the AC capacitors.

The resonance of the AC side LC filter produces harmonics in the capacitor voltage with frequency close to $\omega_{ac} = \frac{1}{\sqrt{L_{ac}C_{ac}}}$, which appears as $\omega_{ac} - \omega$ component in u_{c_d}, where $\omega = 2\pi f$. The fundamental component of the capacitor voltage represents a DC component in the synchronous reference frame. Therefore, a high-pass filter (HF) is applied to filter out this DC component, with the transfer function:

$$HF(s) = \frac{s}{s+0.1\cdot(\omega_{ac}-\omega)}. \tag{4.29}$$

Adding the HF's transfer function and the virtual resistance, the damped dynamics follows:

$$u_{c_d} = \frac{u_d}{s^2 L_{ac}C_{ac}+1} - \frac{sL_{ac}I_{dc}\delta_d}{s^2 L_{ac}C_{ac}+1} - \frac{HF(s)}{sC_{ac}R_H}, \tag{4.30}$$

A virtual damping resistance R_H has been defined for calculation of the damping current component i_{rHF} from the HF component of the capacitor voltage, which can be observed in Fig. (4.4), as well as in Fig. (4.6).

4.4.4 Modulation

Modulation is required to govern the CSR device's switching states to realize the control displayed at (4.4). In other words the reference current in Clarke frame $i_{r_{\alpha\beta}}$ needs to be translated into interpretable switching states for the device. In this work this is realised via space vector modulation (SVM), meaning that the current reference is converted to the superposition of the finite set of switching states the converter could realize without malfunction

(some states are prohibited e.g. breaking the choke inductor's current flow.) Of course there are other modulation schools for example SHE (mentioned in section 4.2) but they can not translate the control action so easily as SVM. As such they are not in the scope of the thesis.
The chosen modulation strategy is developed in the "$\alpha\beta$" stationary reference frame, where $i_{r_{\alpha\beta}} = \vec{i}_{ref}$. Based on the notions already mentioned in section 4.3. The structure requires simultaneous conduction of the upper and lower transistors of the bridge, since the current of the L_{dc} choke must not be interrupted. Additionally, the switching devices are considered as ideal.

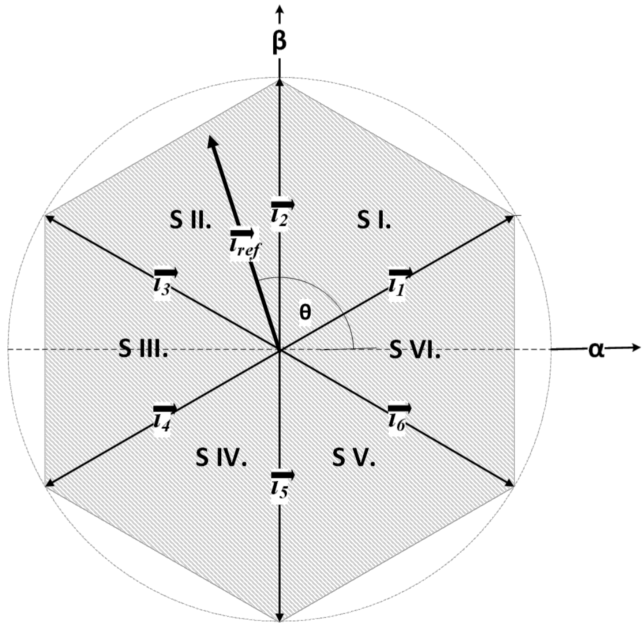

Figure 4.8: The fundamental input current vectors corresponding to the active switching states of the CSR.

According to this, one of the upper and one of the lower switches must be closed at all times. This allows nine states, six of which are active. There are three "zero" vectors, corresponding to the switching states, when both devices of one of the bridge legs are in conduction. These current vectors are shown in Table (4.2).

The neighboring space phasors can be formulated as:

$$\begin{aligned} \vec{i}_n &= \frac{2}{\sqrt{3}} i_{dc} e^{j(\frac{n\pi}{3}-\frac{\pi}{6})} \\ \vec{i}_{n+1} &= \frac{2}{\sqrt{3}} i_{dc} e^{j(\frac{n\pi}{3}+\frac{\pi}{6})} \\ n &= 1, 2, \ldots, 6, \end{aligned} \tag{4.31}$$

which can be observed in Figure (4.9).

The reference current vector is sampled with fixed sampling period T_s. The sampled value of $\overrightarrow{i_{ref}}$ is synthesized as the time average of two neighbouring space phasors adjacent to the reference current:

$$T_n \vec{i}_n + T_{n+1} \vec{i}_{n+1} = T_s \vec{i}_{ref} \tag{4.32}$$

Table 4.2: The fundamental input current vectors corresponding to the active switching states of the CSR.

Name	Switching State						Phase currents			Vector representation
	1	2	3	4	5	6	ia	ib	ic	
$\vec{i}_1$	1	0	0	0	0	1	i_{dc}	0	-i_{dc}	$2i_{dc}e^{j\pi/6}/\sqrt{3}$
$\vec{i}_2$	0	0	1	0	0	1	0	i_{dc}	-i_{dc}	$2i_{dc}e^{j\pi/2}/\sqrt{3}$
$\vec{i}_3$	0	1	1	0	0	0	-i_{dc}	i_{dc}	0	$2i_{dc}e^{j5\pi/6}/\sqrt{3}$
$\vec{i}_4$	0	1	0	0	1	0	-i_{dc}	0	i_{dc}	$2i_{dc}e^{j7\pi/6}/\sqrt{3}$
$\vec{i}_5$	0	0	0	1	1	0	0	-i_{dc}	i_{dc}	$2i_{dc}e^{j3\pi/2}/\sqrt{3}$
$\vec{i}_6$	1	0	0	1	0	0	i_{dc}	-i_{dc}	0	$2i_{dc}e^{j11\pi/6}/\sqrt{3}$
$\vec{i}_7$	1	1	0	0	0	0	0	0	0	0
$\vec{i}_8$	0	0	1	1	0	0	0	0	0	0
$\vec{i}_9$	0	0	0	0	1	1	0	0	0	0

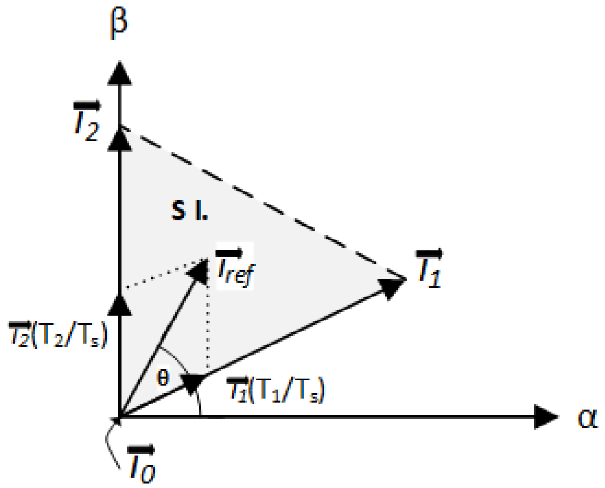

Figure 4.9: Synthesis of $\overrightarrow{i_{ref}}$ by $\vec{i_1}$, $\vec{i_2}$, and $\vec{i_0}$

T_n and T_{n+1} represent the individual durations of the switching states corresponding to the neighboring vectors. For example, in case of a current reference vector situated in the first sector, T_1, T_2 and T_0 can be calculated using (4.33).

$$\begin{aligned} T_1 &= T_s \frac{i_{ref\alpha}}{i_{dc}} \\ T_2 &= T_s \frac{\sqrt{3}}{2i_{dc}}(i_{ref\beta} - \frac{i_{ref\alpha}}{\sqrt{3}}) \\ t_0 &= T_s - T_n - T_{n-1} = T_{7,8,9} \end{aligned} \tag{4.33}$$

The complex plane is naturally divided by the fundamental space vectors into six areas, named "sectors".

$$\begin{aligned} & x\frac{\pi}{6} + \frac{(n-1)\pi}{3} \leq \theta_n \leq \frac{\pi}{6} + \frac{n\pi}{3} \\ & n = 1, 2, \ldots, 6 \end{aligned} \tag{4.34}$$

The non-zero space vectors are selected based on the phase angle θ between

$\overrightarrow{i_{ref}}$ and the real axis. Table (4.3) presents an example of switching pattern in case of a current reference vector situated in Sector I.
The switching scheme represented in Table (4.2). is aimed at reducing the number of commutations in a switching cycle, resulting in the reduction of the switching losses [99].

Table 4.3: Representation of switching sequences for SECTOR I.

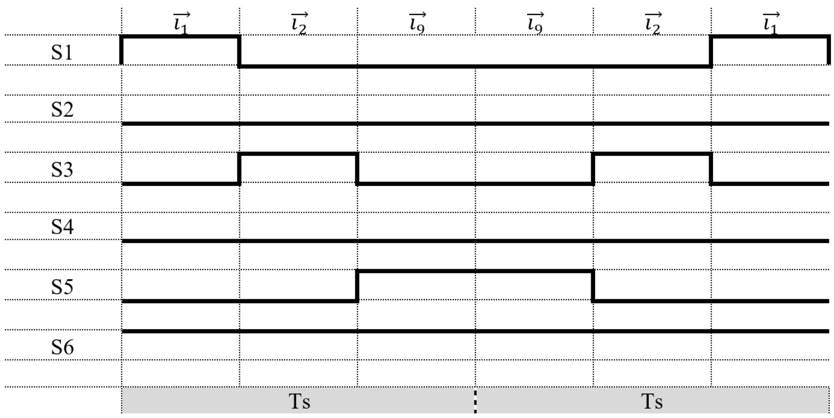

Additionally, the implemented modulation logic prevents the reference from applying currents outside the modulation circle of (4.8). This is realised in ((4.35)) resulting from the available magnitudes of the current vectors, is applied to the current reference, on top of the controller constraints in (4.24).

$$0 \leq |i_{ref}| \leq \frac{\sqrt{6} i_{dc}}{cos\theta + \sqrt{3} sin\theta} \tag{4.35}$$

The modulation formulation is only meant to apply on the control action in the above mentioned ways (realizing and constraining the reference) since the switching frequency $fpwm$ is chosen so high that the controller dynamics match with the SVM state switching frequency. As such no lag or under-sampling is assumed, and the system dynamics are already implicit in the controller design.

4.4.5 Discussion

From the continuous AC (4.10), and DC (4.11) model equations described in Ch.X., the controller is formulated form discretised system (4.14), and it is described via the cost function and control problem of (4.16), and (4.17) in Ch.X+1. The evaluated model and control structure are shown on Fig.4. In the following section said EMPC's computational requirements are evaluated, and the Matlab/Simulink simulation results are compared to a classic state feedback controller's dynamic performance.

Lyapunov stability

The systematic finding of Lyapunov functions is described in detail in section 5.7.1 as well as in [102]. The explicit receding horizon control law formulated in section 4.4.3 is mapped according to (4.22), resulting the partitioning of the constrained state space displayed on Fig. (4.5). Considering system (4.14) with the given constraints of (4.24) and RHC law (4.16), the assumption is that a maximal positive-, and control invariant set $\mathcal{X}_f$ can be obtained for the closed loop system, for every defined critical region. For finding and $\mathcal{X}_f$ and the feasibility of constructing the critical region specific Lyapunov function an implemented verification method is available from [100], by searching $\mathcal{X}_f$ for the closed loop autonomous PWA system. Then piece-wise quadratic (PWQ) Lyapunov function can be constructed displayed on Fig (4.10).

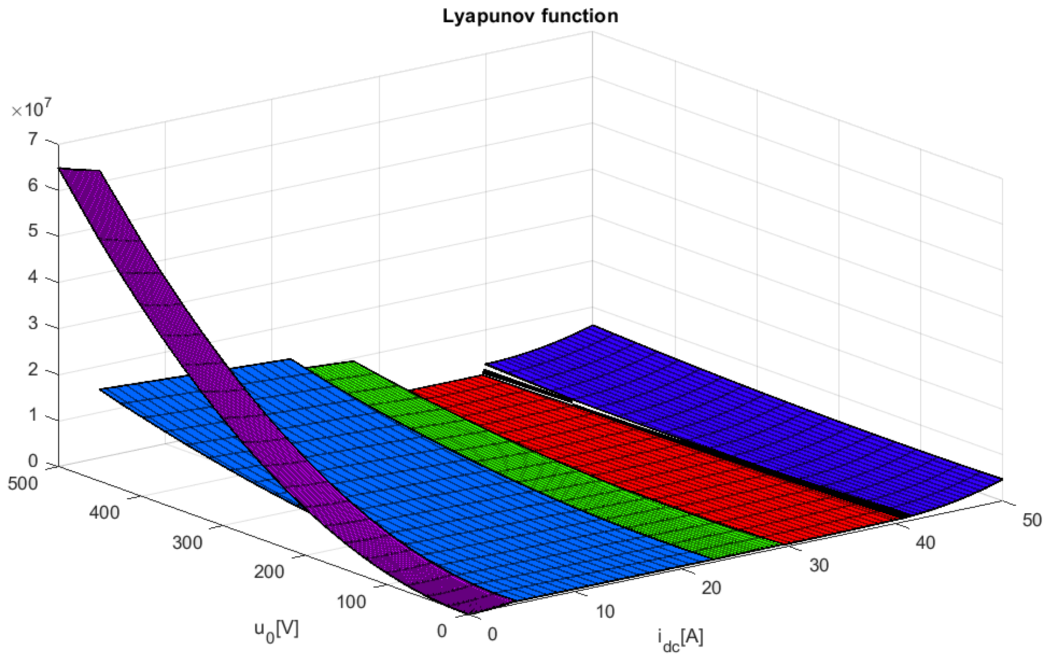

Figure 4.10: Lyapunov function for EMPC every partition.

Computational effort

The binary search tree generated for the control problem presented in Fig. (4.11). The search method and formulation of the tree is described in chapter (5.8.1). The depth of the search tree is 5 and it has a total number of 29 nodes. It is utilized with the MPT toolbox [100], and it can be used for the computationally optimal real-time implementation of the proposed algorithm on low-cost hardware.

The search for an active critical region starts from the first level and represents the evaluation in each adjacent node of an inequality of the form: $x \leq K$. Thus, in this case a maximum number of 3 inequalities have to be evaluated to reach the active critical region. Implementing the presented algorithm is

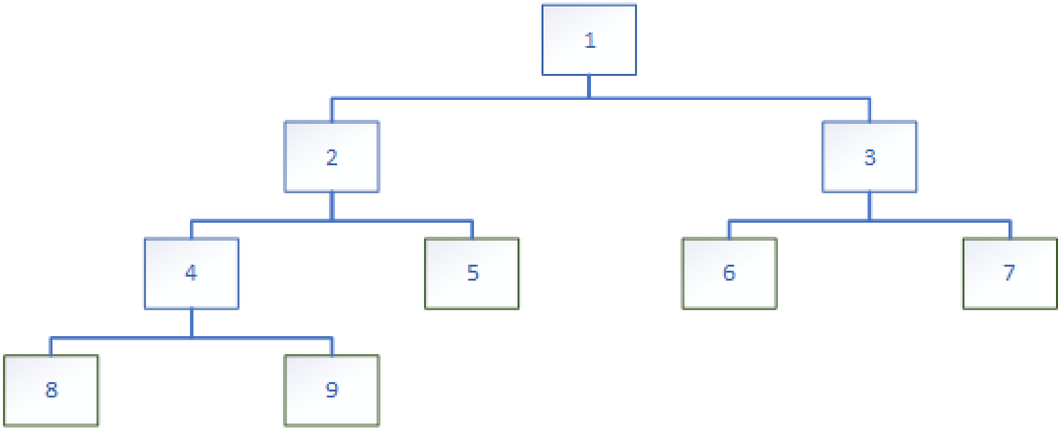

Figure 4.11: Binary search tree of the controller for a horizon of $N = 4$. The leaf nodes are depicted with filled squares. The depth of the tree is 4.

straightforward on a DSP processor, for instance from the dsPIC33 family by Microchip. Using the MAC (multiply and accumulate) instruction the inequality is evaluated for each node using 4 instructions (two multiply, one add and one compare), thus in 80 ns on a 50 MIPS processor (Fig. (4.12)). The active critical region can be reached in a maximum of $80 \cdot 3 = 240$ ns. Compared to the typical sample rate of 10 us in the case of a CSR, the real-time implementation on a DSP processor is possible. More information about storing critical regions can be found in 5.8.1.

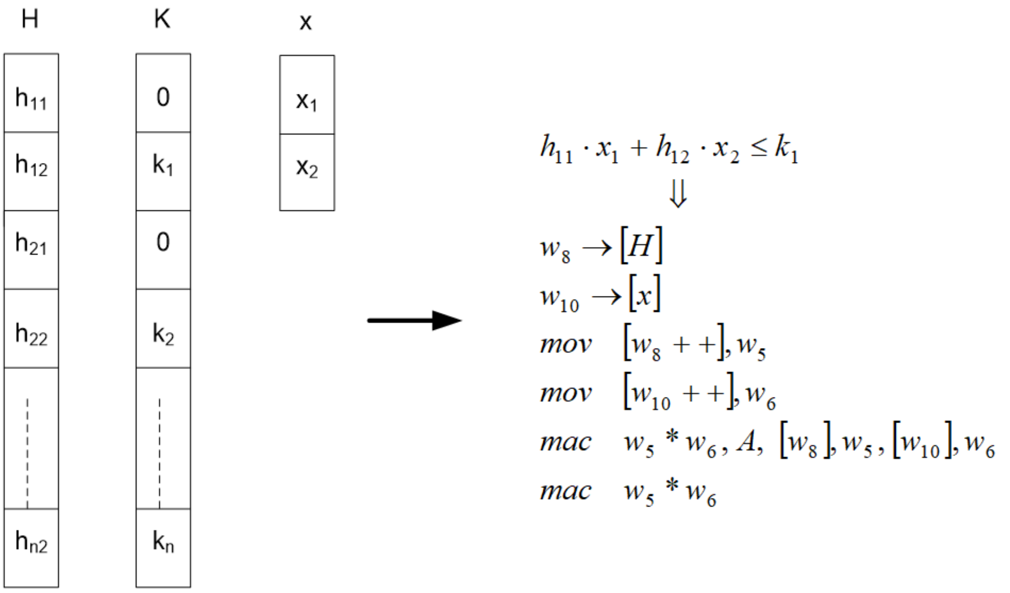

Figure 4.12: Data organization in the data memory of a single core DSP and the evaluation of a 2-dimensional inequality

More information about storing critical regions can be found in 5.8.1.

Horizon performance

With the cost function (4.16) employed using (4.36), changing the length of the horizon N affects the system's complexity illustrated by the partition in the state space shown in Fig. (4.5), and Fig. (4.13) presents the step response of the controlled system for different lengths of the horizon. It shows, that the response is heavily affected by the horizon length at the first three iterations, rendering the one step choice useless, whilst by increasing the horizon, the steady state error of the algorithm decreases.

Unfortunately, the steady state error is is still present after the computational boundary of **XY** ns regardless of increasing the horizon. As such an additional integrator component is advised to embed into the model equations of (4.11), aka. augment the model. The results can be observed in the next section and on Fig. (4.14).

Simulation results

The simulation results are produced with Matlab/Simulik. The discrete model's (4.14) simulation frequency was 1 MHz, with the model parameters represented in Table (4.1). As mentioned the base control structure has considerable steady state error, which can be mitigated, by increasing the control horizon, but the computation cost is NP-heavy. The solution is to augment the model with an additional integrator. As such, with some re-parametrisation with the const function weights:

$$\mathbf{R}_w = \begin{bmatrix} 1 \cdot 10^{-6} \end{bmatrix}, \mathbf{Q}_w = \begin{bmatrix} 1 & 0 \\ 0 & 1 \end{bmatrix}, N = 4, \tag{4.36}$$

the partition space grows to 49 regions but the steady state error lessens significantly. The comparison of the EMPC performances is shown on Fig. (4.14).

More details about the Matlab simulation are presented in [103].

Comparison with a state feedback control

On the DC side, not only the output voltage u_0 but also the inductor current i_{dc} needs to be controlled. Described in [62], a state feedback control with optimal parameters can be used as a reference based on the model properties listed in Table (4.1), with output voltage u_0 and DC bus current i_{dc} chosen as the state variables. Since u_0 is a DC quantity in steady state, an integrator signal is introduced to diminish the steady-state error. The structure of the controller is represented in Fig. (4.15).

The tuning constants applied and calculated according to [88] are:

$$k1 = \frac{\omega_n^3}{1.5 U_n \omega_{dc}^2}, \; k2 = \frac{2.2\omega_n^2}{1.5 U_n (\omega_{dc}^2 - 1)}, k3 = \frac{1.9\omega_n L_{dc}}{1.5 U_n}, \tag{4.37}$$

where $\omega_n = 1.1$, $\omega_{ac} = \frac{1}{\sqrt{L_{ac} C_{ac}}}$, $\omega_{dc} = \frac{1}{\sqrt{L_{dc} C_{dc}}}$. The state feedback controllers block on the diagram is taking the controller's place, shown on Fig.

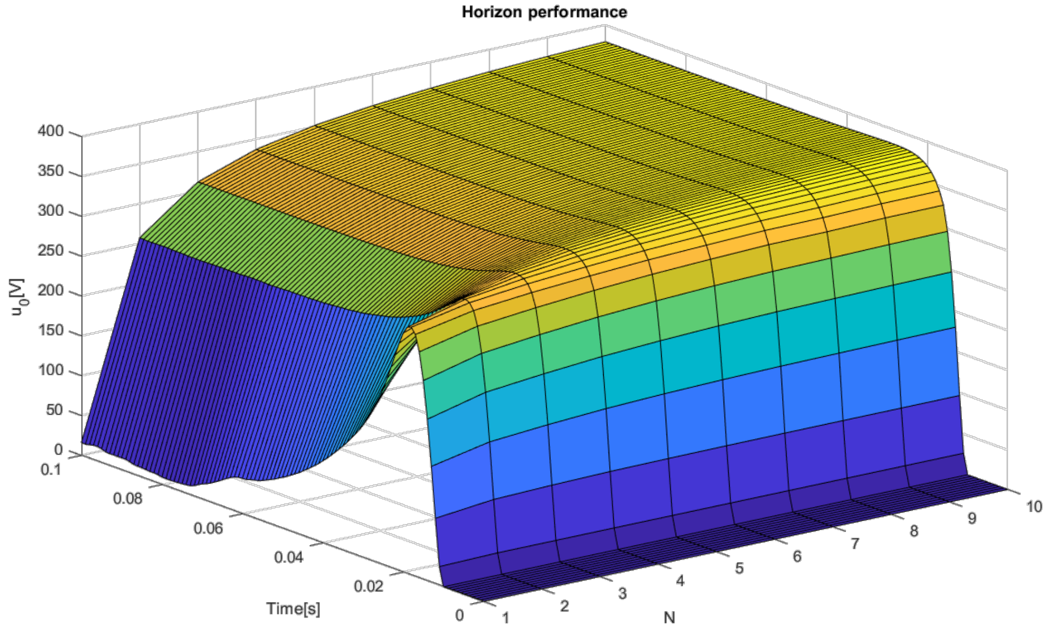

(a) Overall performance of the EMPC, with different control horizons.

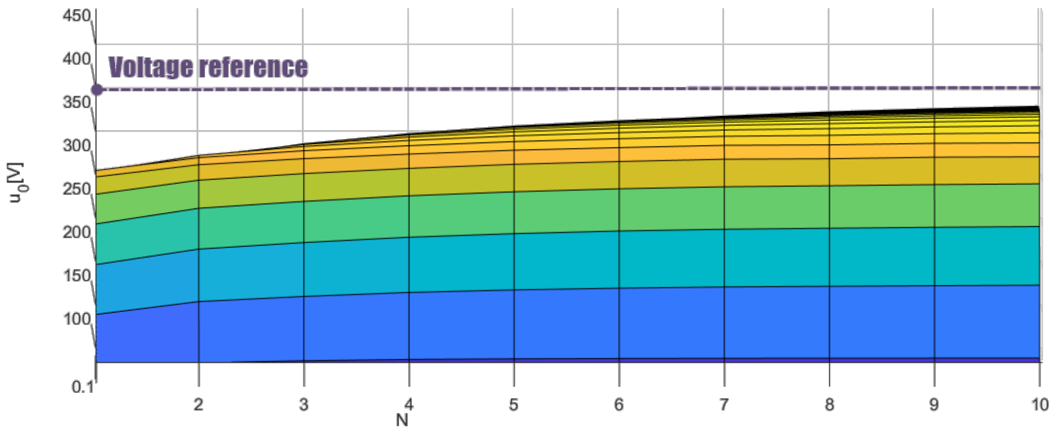

(b) The projection on the time axis indicates the decrease of steady state error with the horizon length.

Figure 4.13: Step response of the system as a function of the horizon length N.

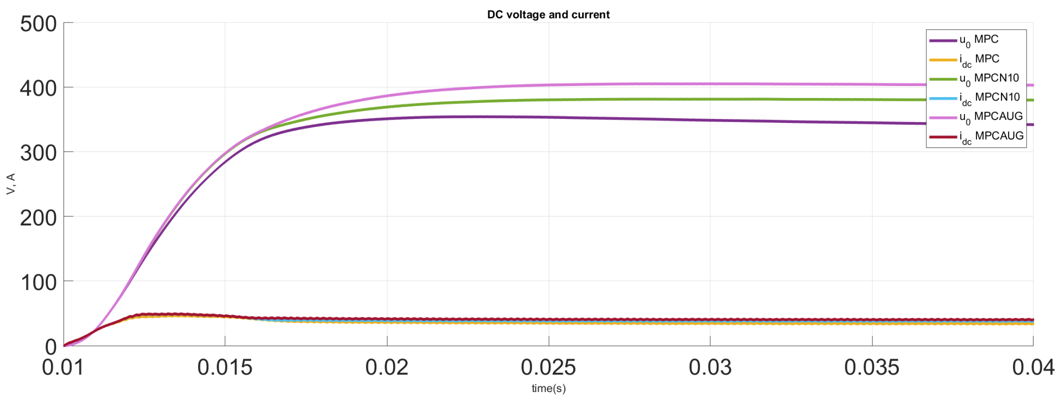

Figure 4.14: Resulting current and voltage trajectories of the CSR with (EMPC).

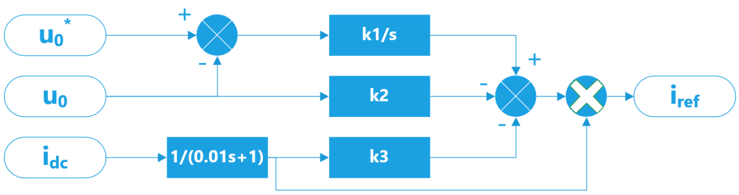

Figure 4.15: Simple DC side state feedback control structure.

(4.4). The independent outputs are the high pass filter's output $i_{rHF(d)}$ and the controller's output $i_{ref} = i_{rcontrol(d)}$. The sum of the independent current values is converted to Clarke frame to be able to govern the switching states of the IGBT's. This can be done because $i_{rHF(d)}$ has only high frequency components and $i_{rcontrol(d)}$ has low frequency components due to the differences in LC time constants, as discussed in the second section. Then the control signal governing the switches is applied in the same manner, described at the start of section 4.4.4. The state feedback control's performance in comparison with the EMPC is shown in Fig. (4.16).

4.5 Conclusion

The constrained, model-based optimal control of a current source rectifier has been presented in this dissertation. The dynamic model of a three-phase current source rectifier has been developed in Park frame. The proposed model has been examined from the design and implementation points of view with the purpose of explicit model-based predictive control. It proved to be the case that the regular set of differential equations of the CSR appears to be too complex, and contains non-linearity for such a design approach. To address this issue the usage of separated AC and DC equation sets was suggested to avoid linearization and complexity reduction. This solution eliminates bilinearity

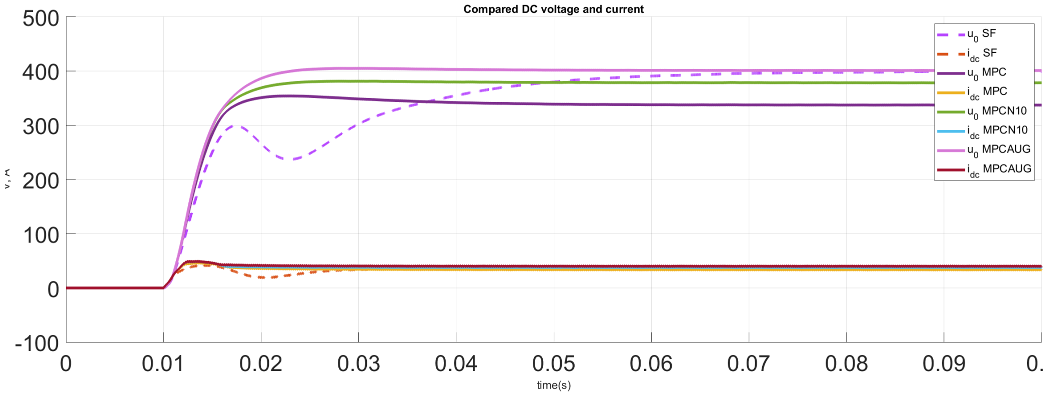

Figure 4.16: Resulting current and voltage trajectories of the CSR with explicit model predictive control (MPC) compared to the $N = 10$ case (MPCN10), the augemnted model (MPCAUG), and the state feedback control (SF).

and enables the application of linear control design techniques. Current-based SVPWM of the three-phase converter has been used with an emphasis on the reduction of switching losses. Throughout the chapter the explicit model predictive control method is described and the method's effectiveness compared to conventional state feedback control is show. The implementation and simulation experiments have been performed in Matlab/Simulink environment. Moreover, the proper implementation of the system in a modern DSP chip will result in real-time operation.

4.6 Notations used in the chapter

$\mathbf{A}$	State matrix of the DC side system
$\mathbf{B}$	Input matrix of the DC side system
$\mathbf{B\_d}$	Discretised input matrix of the DC side system
C_{ac}	AC side inductance
C_{dc}	DC side inductance
$\mathbf{C}$	Output matrix of the DC side system
$\mathbf{C\_d}$	Discretised output matrix of the DC side system
C_{reg_i}	Critical region
$D(-\Theta)$	Inverse Clarke transformation
$\mathbf{F}$	State coefficient matrix for calculating the optimal input
f	Network voltage frequeny
$fpwm$	Rectifier switching frequency
f_s	Simulation frequency
f_i	Function of state at the i^th step
$\mathbf{G}$	Unified constraint input matrix
g_i	Function of input at the i^th step
H	Supplementary quadratic optimizer matrix
$HPF(s)$	High pass filter transfer function
i_{abc}	Generic three phase current
$i_{ac_{1,2,3}}$	AC side inductance current
$i_{ac_{\alpha,\beta}}$	AC side inductance current in Clarke frame
$i_{ac_{d,q}}$	AC side inductance current in Park frame
i_{HPF}	AC side damping current
$i_{r_{1,2,3}}$	Rectifier current
i_{rMPC_d}	Direct component of the output of the EMPC controller
$i^*_{r_{1,2,3}}$	Rectifier reference current
$i^*_{r_{\alpha,\beta}}$	Rectifier reference current in Clarke frame
$i_{rcontrol_d}$	Direct component of the output of the DC voltage controller
i_{rHF_d}	Direct component of the damping current of AC noise
i_{dc}	DC side inductance current
$i_{ref_{\alpha,\beta,\gamma}}$	α, β, or γ component of the reference current vector respecively
i_{dq0}	Three phase current converted to Park frame
$\vec{i}_{0,\ldots,9}$	Current vector of the phasor
$\vec{i}_{ref}$	Reference current vector
J	Quadratic EMPC cost function
J^*	Optimal cost value
J_0	Cost function to optimize at the initial state
J^*_0	Optimal cost function at the initial state
K	Feedback gain of EMPC controller
$k_{1,2,3}$	State feedback controller's coefficients
L_{ac}	AC side inductance
L_{dc}	DC side inductance
L_S	Input filter inductance of the three phase alternating current in VSR
L_D	Inductor for filtering the output current of the CSR (Choke)
N	Control horizon
N_y, N_u, N_c	Output, input and constraint horizons
n	Current phasor sector indicator
P_n	Nominal power of the CRS
$\mathbf{Q}$	State weight matrix of quadratic MPC cost function
R	Phase resistance
R_H	Virtual damping resistance
R_{load}	Load resistance
$\mathbf{R}$	Input weight matrix of quadratic MPC cost function
$\mathbb{R}$	Set of real numbers
S	Current phasor sector
T_s	Switching period
$T_{0,\ldots,9}$	Dwell time in the corresponding sector
t	Discrete timestep
U	Set of MPC inputs
Un	Network line-to-line voltage
$\mathbf{U}^*_0$	Optimal vector of future inputs starting from the initial state
$\widehat{u}$	Peak value of AC-side capacitor voltage
$\mathbf{u}$	Output vector of the DC side system
$u_{1,2,3}$	AC side phase voltage
$u_{\alpha,\beta}$	AC side phase voltage in Clarke frame
$u_{d,q}$	AC side phase voltage in Park frame

$u_{c_{1,2,3}}$	AC side capacitance voltage
$u_{c_{\alpha,\beta}}$	AC side capacitance voltage in Clarke frame
$u_{c_{d,q}}$	AC side capacitance voltage in Park frame
u_0	DC side voltage on load
u_0^*	DC side voltage reference
u_{MPC}	MPC control variable
$\mathbf{u}^*$	Optimal input vector
v_D	Output voltage before the choke inductor L_D
$v_{i,j}$	Three phase phase-to-neutral voltage $i, j \in \{R, S, T\}$
$v_{N,RS}$	Three phase line-to-line voltage of R and S
v_{c_p}	AC-side capacitor voltage, where $p \in \{1, 2, 3\}$
$\hat{v}$	Voltage peak
$\mathbf{x}$	State vector of a linear time invariant model
$\mathbf{x}(0)$	Initial state
$\mathbf{y}$	Input vector of the DC side system
$\delta_{1,2,3}$	Conduction state leg
$\delta_{\alpha,\beta}$	Conduction state leg in Clarke frame
$\delta_{d,q}$	Conduction state leg in Park frame
θ	Network voltage vector's angular displacement
$\epsilon, \varphi, \chi, \psi$	Constant sets
Ω	Closed and bounded set of states containing the origin
ω	Network voltage vector's angular velocity
ω_{ac}	Ac side LC filter angular velocity
ω_n	Damping angular velocity

Chapter 5

Thesis and Summary

5.1 Summary

The topic of this PhD. dissertation is optimal current control. The aim of the research was to apply and simulate high frequency controllers with optimization purpose of cost functions with the presence of constraints and circumstances, on controlled switch based power electronic devices.
In chapter 3, a current controlled inverter structure was presented, connected to a small, domestic grid, representing the connection of a household with possible renewable (or other) generators, to balance consumption. The examined grid, the phenomena of voltage unbalance was assumed to be present, as the main problem, of which this device was ought to not only handle, but mitigate within the limit of its physical capabilities. For this reason, first an indicator was established, based on a proposed geometrical operation, as a voltage unbalance norm candidate (section 2.4). This norm was calculated from the symmetrical difference between the convex hull of voltage phasor vectors, always present on a three phase network. The idea was, that any deviation from the ideal phasor, (which first vector assumed in phase with the ideal one) introduces sub-optimal behavior, or fault of appliances connected. This way the already present indicators of voltage unbalance was examined (section 2.5). Afterwards found that not only, they vary in result, but ignore phase differences, or the zero-sequence component (based on the Fortescue method), or its ponderous to serve as a cost function need to be minimize. The proposed geometrical norm however considers all of the above, with the addition that since it calculates area, instead of vector length differences, the result is a square-like function, serves as an excellent candidate. The downside is the yet unresolved computational overload, that is method introduces.
In the next phase, the network's unbalance was attempted to be mitigated by applying a power electronic converter for a household, which utilizes an external power source (a photo voltaic source in this case) for counter balance (section 3.4). Using the basic optimization structure proposed in chapter 3, a derivative-free optimization method (APPS) has been used along with the geometric norm as cost function to decrease the voltage unbalance in a simulated three-phase low voltage grid. The results were tested in Matlab/Simulink envi-

ronment with simulating the actual device via Simscape, and the unbalanced network, also with experimental measurements. The result was, that the controller could reduce the network's voltage unbalance, based on the network's robustness (how large is the impedance, which created the unbalance), how much control reserve is present as energy source, and physical boundaries (the device can not supply infinite current). Based on this the household's normal operation can withheld even in with unbalanced loads.
Lastly in chapter 4.4 in-depth modeling and predictive control task has been performed, on one power electric component, namely on a buck-type rectifier. This rectifier uses current source operation to supply the load it is connected to. The main goal was to create on the Kirchhoff's law based differential equations a model based predictive controller, suited to reach the reference point with the best dynamics. It was also taken in mind, that an implicit MPC would not be up to the task, sice every control rule was to be re-calculated from scratch, implying a very expensive CPU. This gap could be bridged by reaching out for the explicit MPC method, by partitioning the state space, on a pre-defined rule set. This way the control demand could be reduced significantly, however, this is not suited for high rank systems. As such the system's bi-linearity was eliminated by applying on the premise that two dynamics which have highly different fundamental frequencies can operate in superposition. This way the problem was simplified, and explicit MPC could be implemented in DC-side, whilst active damping at the AC-side. The method's efficiency was tested in Matlab/Simulink environment against a conventional state-feedback controller, with good results. Additionally the computational demand was evaluated, with assumed binary search algorithm.

5.2 New scientific results

I. Thesis:

I extended the currently used measures of voltage unbalance with a new norm candidate. I found out that it is more demanding from the computational point of view, but has a new feature namely it checks electrical asymmetry, i.e. the norm of a ± 120 degree rotated version of the ideal three phase phasor is zero in the geometrical sense. I compared my geometrical approach to the standard wide-spread use of voltage unbalance factor (VUF) and found out it carries additional information, whilst retaining it's original purpose. As such I derived the following thesis:

The three-phase voltage unbalance of three phase networks can be quantified by the symmetrical difference between the ideal and actual voltage phasors, defined as follows:

$$G = \text{Area of } (\triangle_{Ideal} \cup \triangle_{Real} - \triangle_{Ideal} \cap \triangle_{Real}), \tag{5.1}$$

It has been shown, that the proposed geometric norm (Figure (5.1))

is a powerful VU indicator by means of amplitude and phase deviation and also balanced three phase under-voltage.

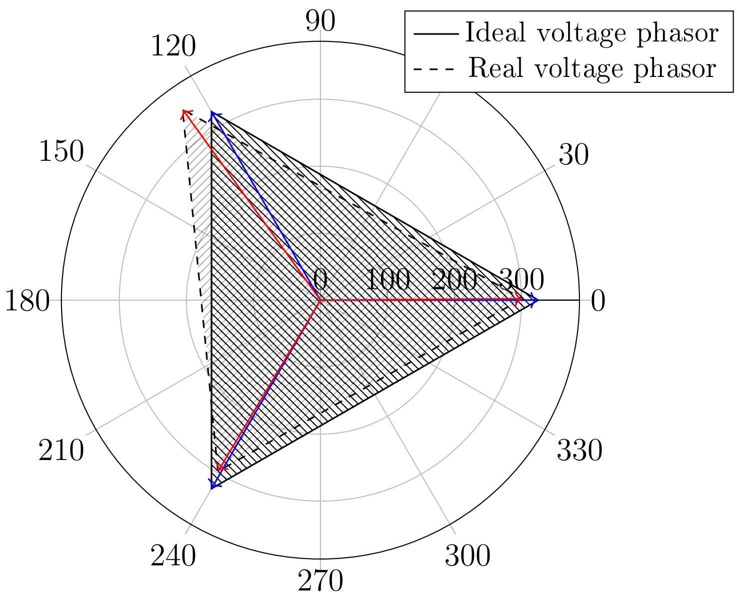

Figure 5.1: Proposed geometrical representation of three phase voltage unbalance.

Related publications: [P2], [P1].

II. Thesis:

In case of connecting to an unknown network, where current measurements are infeasible, I found out that the regular current controlling applications would not fit to the purpose for reducing voltage unbalance if they only relying on the voltage measurement. I have suggested an direct optimization based structure that can be used for such networks. The method uses a derivative-free optimization algorithm and a voltage unbalance norm to decrease the VU of the network. As such I employed an asynchronous parallel pattern search (APPS) optimizer, in Matlab/Simulink environment, and I applied the geometrical norm (as well as VUF to serve as comparison) as cost of the optimization. I showed with validating simulations, that the geometrical based unbalance indicator can serve as a basis of further research. As such I derived the following thesis:

The voltage unbalance of three-voltage electrical networks with unknown network model or topology can be decreased by the direct optimization based compensator structure of Figure (5.2), where the unbalance indicator can be any suitable scalar-valued voltage unbalance norm. Also the optimizer can be any suitable derivative-free optimization method. It has been shown based on simulation experiments, that for three-phase low voltage networks, using asynchronous parallel pattern search optimizer, the geometric norm proposed in Thesis 1 performs better than VUF by means of unbalance compensation and active power loss.

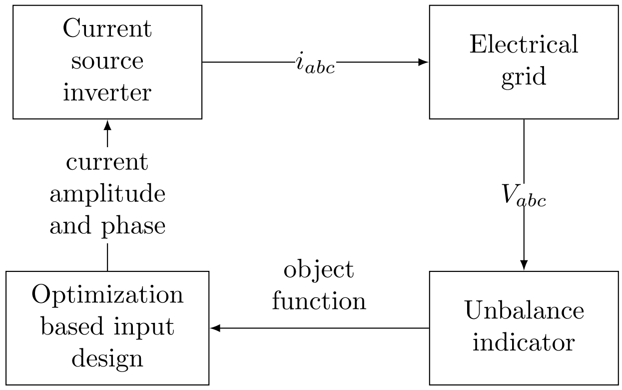

Figure 5.2: Block scheme of the voltage unbalance compensation, where i_{abc} is the injected current, and V_{abc} is the measured voltage at the three phase connection point.

Related publications: [P1], [P4], [P3].

III. Thesis:

I proposed a simplified CSR model, which was derived from the well known CSR structure and was examined from design and implementation points of view with the purpose of explicit model-based predictive control. The regular set of differential equations of the CSR appeared to be too complex for my a design approach, for applying explicit predictive control.
I adressed this issue with the separation AC and DC equation sets was of the CSR to decrease complexity and easy controller design. With this solution I eliminated bi-linearity and enabled the application of linear control design techniques. I used current-based SVPWM the modulation, what has been used with an emphasis on the reduction of switching losses.
For DC side control I implemented explicit model predictive control (EMPC) and I compared this method's effectiveness to conventional state feedback control. I implemented the CSR structure and the proposed controller with EMPC on DC and active damping on the AC side in Matlab/Simulink environment and tested by simulation. Additionally, I tested the proper implementation's computational requirements in a modern DSP chip, which would serve in real-time operation. As such I derived the following thesis:

The generic three phase current source rectifier's differential equation set is not applicable for basic MPC (model predictive control) design, due to the underlying bilinearty, and the MPC design's computational demand. However, the AC and the DC side can be seen as two systems in superposition due to the twentyfold (exacly 20.357) difference between the two side's time constants, enabling linear predictive design. Moreover this design enables a current SVM (space vector modulation) based explicit MPC design solving the optimization problem offline with state-space partitioning, as it can be observed in Figure (5.3).

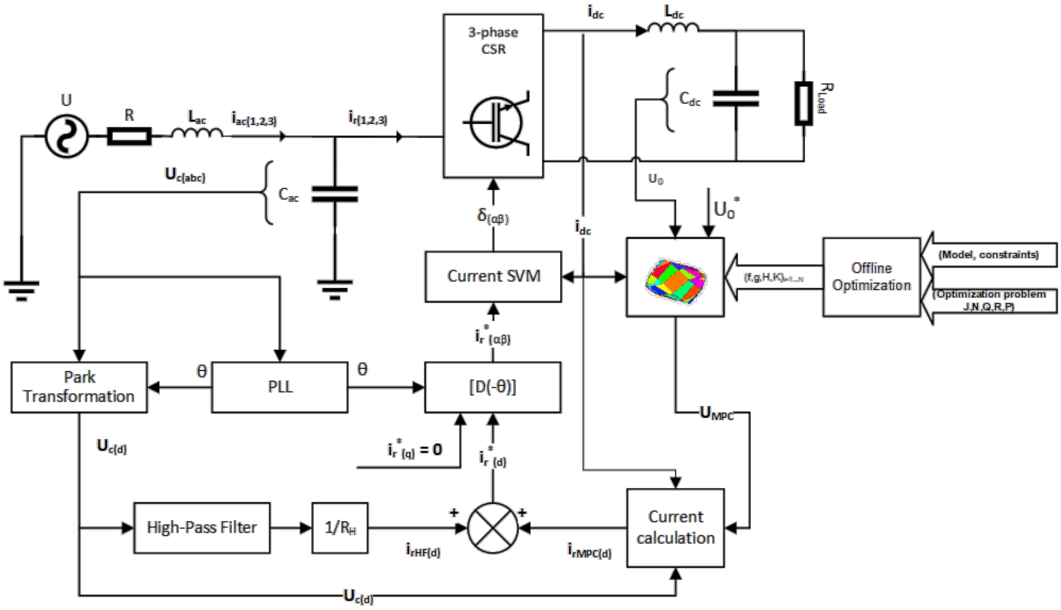

Figure 5.3: Superimposed AC and DC control structure of a CSR, with explicit MPC controller on the DC side.

Related publications: [P5].

5.3 Applications and future work

In this section the possible applications shall be described based on my thesis. These are not yet scope of current research activities, but can serve as a potential direction and evolution for these results.

5.3.1 Geometrical voltage unbalance norm

As mentioned the geometrical norm's largest weakness is the computational demand. The required areas, computed from the voltage phasors realized with the corresponding Matlab functions, which are not designed for continuous calculation, especially not for time constants for power electronic devices. This can be resolved, via replacing the calculation of the symmetrical difference (difference between the two polygon's union and intersection) with finite-element method, with scalability, where the segmentation's resolution would be adjustable and based on the corresponding simulation's (or system's) time constant and the simulator machine's calculation capabilities. After this, the calculation method shall be phrased in an traditional equation form, using the toolset of set theory, and linear algebra. This way, the norm's calculation could be further reduced, and could be implemented on a cheaper embedded system.

The geometrical norm's usefulness was already proven compared o the regular VUF method. However the robustness of the method seems implicitly proven, is shall be tested on real conditions, even in extreme (faulty) situations, and with such hard constrains could be defined, where the algorithm outlives its usefulness. This way, instead of just a resulting number, a full formulation of an optimization problem could be utilized, presented in section (5.7.1), with model based predictive capabilities. This can be further enhanced, with recognizing different scenarios, form general inefficiency, to fault prediction, or handling (like graceful degradation).

5.3.2 Voltage unbalance reducing inverter structure

The inverter structure employ a variety of subsystems, which shall work together in harmony. A global optimum shall be defined (with weighting the various factors) based on external circumstances, and the customers needs. This way, the individual Kirchhoff equations based differential equations shall be established, and controller designed.
The APPS method, however fulfills its optimizing responsibilities very well in such an environment, where changes are expected to be highly stochastic, based on network knowledge, a network- and/or device model based optimal control shall be established, where various current and voltage inertias can be taken into account, giving a leverage for prediction.
The setup of the subsidiary network is is using a very basic network setup. The controller needs to be tested on real world low voltage network models with multiple topologies, and circumstances, established by other research groups and companies, to have a good representation of the system's capabilities.
The total harmonic distortion (THD) was not in the scope of the research, as such, there was no counter measure implemented in the control cycle, to prevent increasing the system's THD. In an experimental setup this needs to be addressed.
The controller is not handling reactive power well, means the reactive power evolution was not in the scope of the research, as such due to the unpredictable nature of the network, the injected reactive power could be an issue.
This way the system's physical properties shall be scalable (based on a household's needs and its energy producing and storing capabilities), as in designing a real power electric system for implementation. Next actual implementation shall be proceeded, with prototype realization on a test bench, with a simulated domestic network connection. Further step to test the presence of multiple of such devices on the network, and how they could mitigate unbalance in synchronous or asynchronous operation.

5.3.3 Explicit model predictive control for buck-type rectifier

From mathematical perspective it is an alternative possibility to take the harder route and take the inherent bilinearity into account. This way, the devices equations should not be partitioned, and a hybrid design can be commenced. This has been performed in the literature, but seldom on three phase systems, for complexity reasons.
The topology could be altered, by removing (or greatly decreasing) some of the device's filtering capabilities, in inductive or capacitive terms (some inductors, like the choke L_{dc} are non-removable), and try to outsource this problems to the controller itself to some degree.
Try the cost function from Euclidean norm to an infinity norm, and also give stricter constrains. The optimum could be power throughput based instead of a specified current. The types of loads can be extended, and merged with the current equation system. This enables to expand the research on electric machinery, where starting/ breaking dynamics can be tested. On the other side, the effects on the supplying network can be taken into consideration, further reducing harmonics, and test conditions in the presence of unbalance. Lastly, experimental results shall be performed on a device, further validating its usefulness, and implement the used S-function from Simulink to an embedded system.

Appendix

5.4 Network substitute model

For the voltage unbalance compensation setup, a substitute network model was used, to be able to recreate said phenomena. The network is a very simplified version of a low voltage residual area with two symmetric loads, a symmetric ohmic load, and one asymmetrical load, for decreasing the voltage quality. See Figure (5.4), (5.5) for details.

The network has the following components:

- **Voltage measurement:** Either could be an ideal three phase sine wave or the measured voltage at the university laboratory. See section 3.4.2 for further details. The voltage values V_a, V_b, and V_c are representing the measurable network voltage, and $R_s = 0.4\Omega$ is representing the source resistance.

- Line multiplexer: substitutes the three phase four wire connection with one representative line between the actors.

- Network segment: Influences the network topology, and represents the line between actors. The network segment is modelled with 0.4Ω wire resistance on each of the four lines. The network's power loss is measured in these line segments.

- Symmetric Ohmic load: Symmetrical resistive component at the end of the main branch, with 50Ω on each phase.

- Three phase parallel RLC load: Represents an unbalance-neutral actor, with balanced RLC loads on each phase in star connection, where the load's active power is $\frac{10000}{3}W$, inductive reactive power is $\frac{2000}{3}VAr$, and the capacitive reactive power is $0VAr$.

- Asymmetrical load: The load mainly responsible for the network unbalance. There loads connected to the phases are:

  - Active power: $5kW$, Inductive reactive power: $1kVAr$, Capacitive reactive power: $0.5kVAr$.
  - Active power: $5kW$, Inductive reactive power: $0.555kVAr$, Capacitive reactive power: $0.111kVAr$.

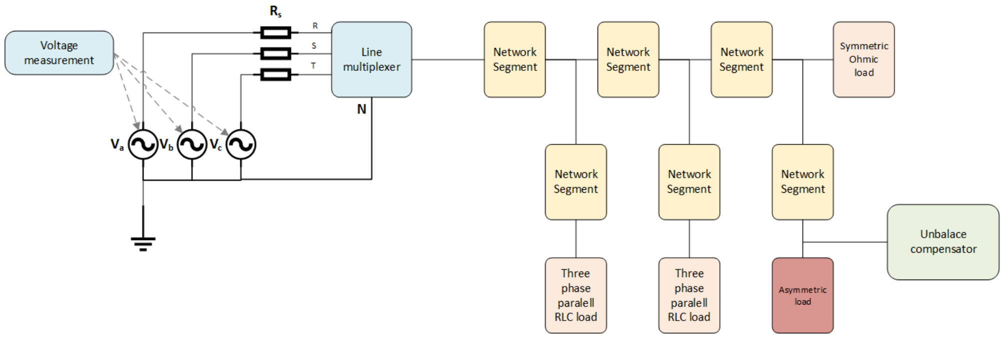

(a) Schematic of network model, for creating an environment for voltage unbalance compensation setup.

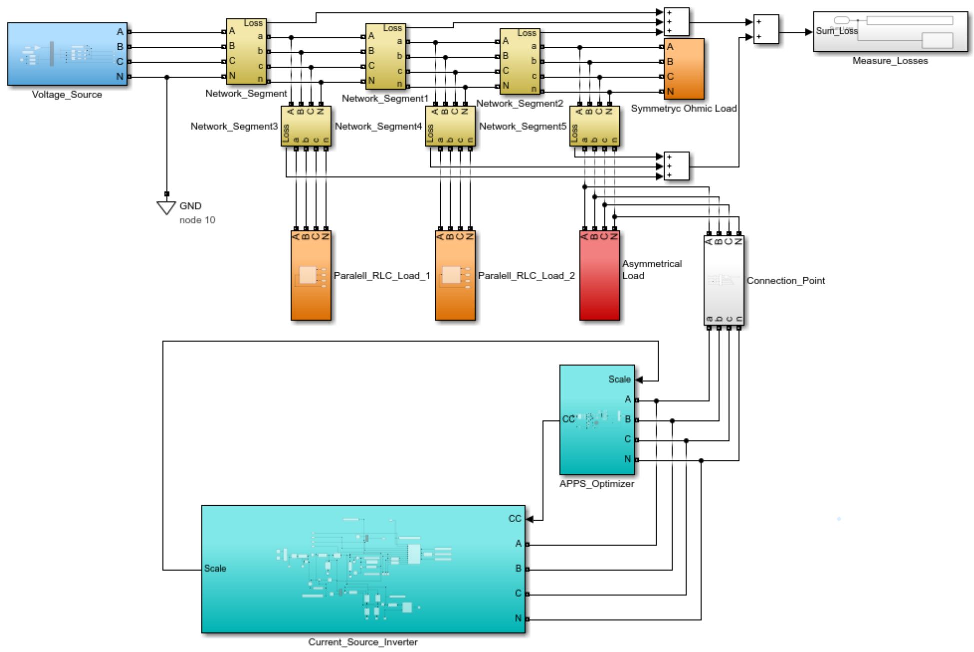

(b) Equivalent Simulink model environment.

Figure 5.4: Schematic of network and equivalent Simulink implementation.

  – Active power: $5kW$, Inductive reactive power: $0.277kVAr$, Capacitive reactive power: $0.055kVAr$.

- Unbalance compensator: The device responsible for decreasing the network unbalance. Setup and function was detailed in chapter 3.4.

5.5 Power electronic components for current control

As the introduction suggest the main topic of the thesis is optimal current control. As such for reaching the desired optimum, the necessary actuators are needed for the task. For this, power electric converters are used, all of them based on a simple principle, namely they use controllable switches to set the

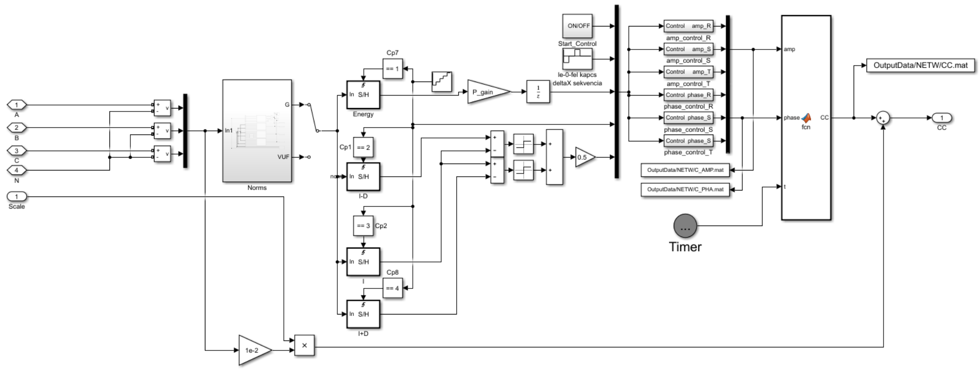

(a) Simulink model of the APPS optimizer.

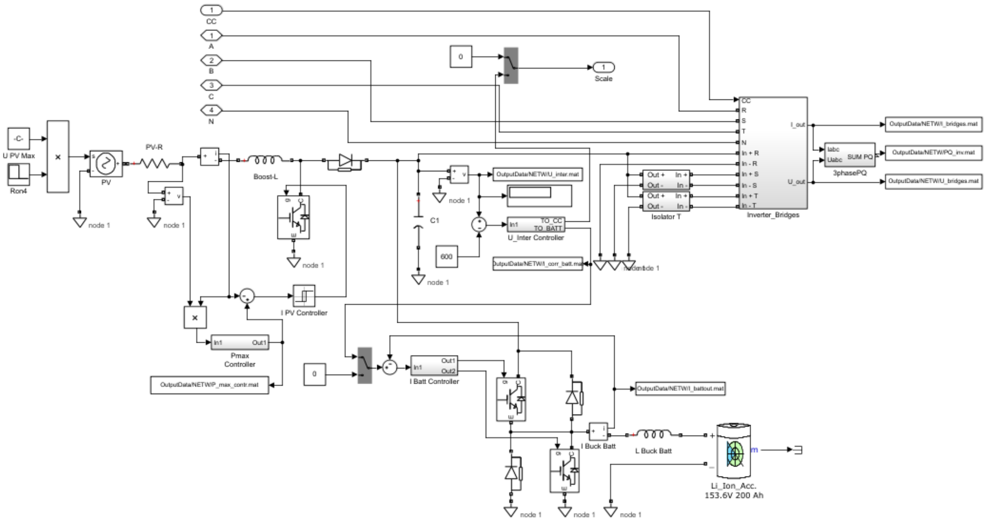

(b) Simulink model of the asymmetric current source inverter.

Figure 5.5: Notable Simulink subsystems.

required voltage level or the conducting current value, required on the load's end.

5.5.1 Galvanic decoupled bi-directional DC-DC converters

In this section a basic galvanic decoupled voltage source DC-DC converter shall be presented. In many DC power supplies, a galvanic isolation between the DC or AC input and the DC output is required for safety and reliability. An economical mean of achieving such an isolation is to employ a transformer version of a DC-DC converter. High-frequency transformers are of small size and weight and provide high efficiency. Their turns ratio can be used to additionally adjust the output voltage level. Generally, electric power generated by renewable energy sources is unstable in nature, thus producing an unwanted effect on the utility grid. This fact motivates research on energy storage and quality systems to smooth out active-power flow.
On the converter Fig.(5.6) has two symmetrical single-phase voltage-source

full-bridge converters, allowing a bi-directional power flow. Thanks to advancement in power device technology over the last decade the DC-DC devices are able to operate at an efficiency as high as $\approx 97\%$ by using the latest trench-gate IGBTs. Therefore this topology has become a promising candidate as a power electronic interface for an energy storage and renewable system [104] [105].

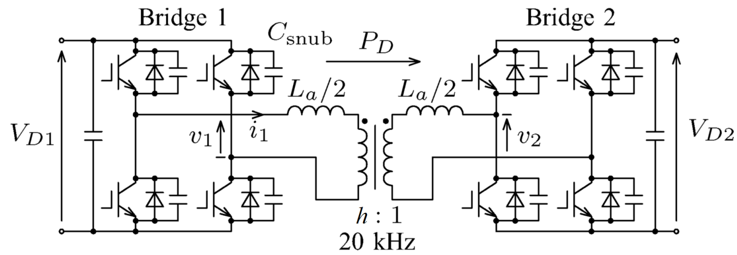

Figure 5.6: Bidirectional isolated DC-DC converter, where V_{D1}, and V_{D2} are the two end's voltage (in- and output depends on the power flow), v_1 and v_2 are the transformer voltages, C_{snub} are to reduce switching loss and to damp out over-voltage, and h is the transformer turn ratio.

The principle of operation of the DC-DC converter is very simple. Two active bridges are interfaced through a transformer and are phase shifted from each other to control the amount of power flow from one DC voltage source to the other. This allows a fixed frequency, square-wave mode of operation and utilization of the leakage inductance of the transformer as the main energy transfer element. The power transfer under idealized conditions is defined as:

$$P_D = \frac{V_{D1}V_{D2}}{\omega L_a}\left(\delta - \frac{\delta^2}{\pi}\right) \tag{5.2}$$

where $\omega = 2\pi f$ is the switching angular frequency of the two single phase full bridge controllers, L_a is the sum of the transformer leakage inductance.

5.5.2 Current source inverters

Single-phase inverter's operating principles are different in each converter. The main features of the different approaches are reviewed and presented in the following. Although these converters cover the low-power range, they are widely used in power supplies or single-phase supplies. For this thesis a domestic current source inverter is considered, which fits into this category.
A current source inverter is composed of capacitors, switches, and diodes, where an array of two switches is called inverter leg shown in Fig.(5.7). The capacitors required to provide a neutral point, such that each capacitor maintains a constant voltage.

The inductors required are large, such that the inductors maintain a constant current i_i. Current-source topologies feature a low switching voltage gradient and reliable over-current or short-circuit protection. In order to operate properly the current-source inverter, we need to adhere to the following rules:

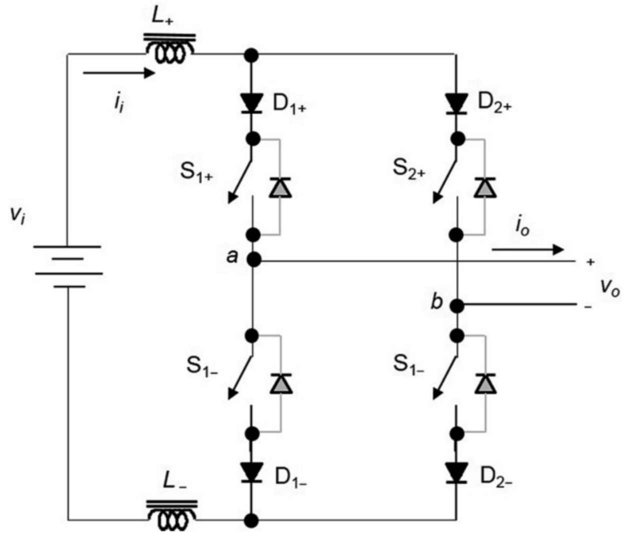

Figure 5.7: Topology of a singly phase current source inverter, where V_i, and V_o are the input and output voltages, i_i, and i_o are the input and output currents respectively. L_+ and L_- are current filter inductances, S_{1+}, S_{2+}, D_{1+}, and D_{2+} are the higher switches (controlled IGBTs for instance) and diodes, and S_{1-}, S_{2-}, D_{1-}, and D_{2-} are the lower switches and diodes respectively.

- Top or bottom switches of the different legs cannot be off simultaneously, because no current path is provided to the input inductors.

- Diode must be placed in series with each switch, because a short circuit across the output voltage V_o would be produced. If the commercial switch does not include anti- parallel diodes, then the circuit is already complete.

- In practical implementation, an overlapping time must be considered in the control signals of the top or bottom switches of the different legs.

According to the previous rules, it should be noticed that all switches of the inverter leg can be turned on at the same time. This is not possible in voltage source inverters. There are four (1^{st} to 4^{th}) defined states of the switches and one not permitted switching state (5^{th} state) as shown in Table (5.1). The modulating technique should always ensure that at any instant, at least one of the top and bottom switch of the inverter legs is on, otherwise the inverter will be damaged.

The ideal waveforms are shown in Fig.(5.8).

The states for the switches are defined by the modulating technique, which in this case is a carrier-based PWM, but unipolar output is considered. For the CSIs, different output filters may be employed, in order to provide the fundamental component of the output waveform. Depending on the application, it would be desirable to provide a voltage or current output.

Table 5.1: Switching states of the current source inverter, where V_{an}, V_{bn} are the a and b point's potential to ground.

Components conducting				State	Output voltages		
S_{1+}	S_{2+}	S_{1-}	S_{2-}		V_{an}	V_{bn}	V_o
1	0	0	1	1	$V_i/2$	-$V_i/2$	V_i
0	1	1	0	2	-$V_i/2$	$V_i/2$	-V_i
1	1	0	0	3	$V_i/2$	$V_i/2$	0
0	0	1	1	4	-$V_i/2$	-$V_i/2$	0
0	-	0	-	5	Not permitted		
-	0	-	0				

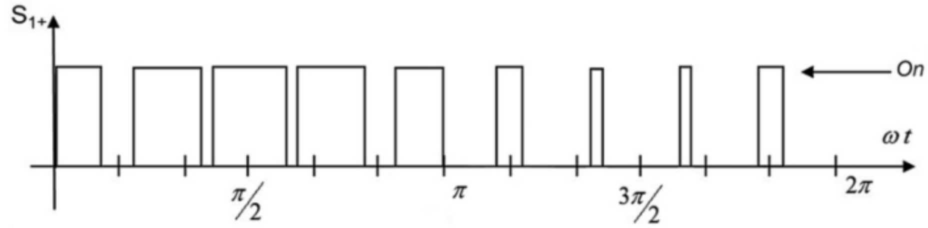

(a) The state of switch S_{1+}.

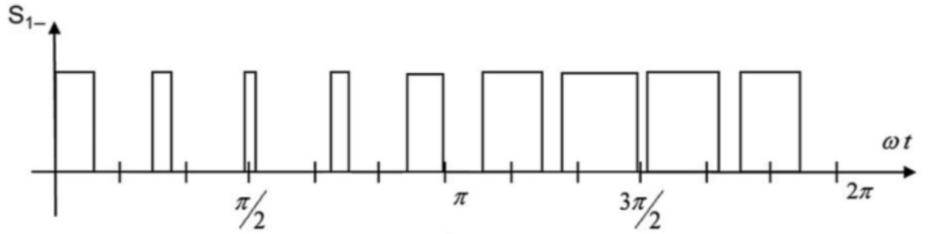

(b) The state of switch S_{2+}..

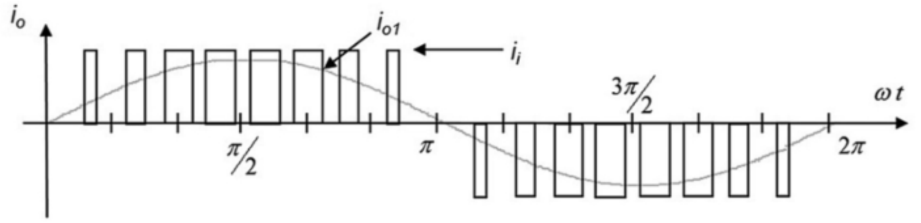

(c) AC output current.

Figure 5.8: The CSI, ideal waveforms as the result of the modulation.

5.5.3 Implemented asymmetrical inverter topology

The applied structure based on a full bridge IGBT structure used in single phase current injection. Three different IGBT full bridge were connected at the output point, thus our structure has three phase and neutral connection too, to carry out any current form. The disadvantage of this structure is that it needs 12 IGBTs in the output stage as opposed to the 6 IGBTs needed for a classical full bridge structure and needs three galvanically isolated direct current (DC) voltage source for feeding.

The other standard elements, that the inverter design consists:

- PV source, with standard maximum power point tracking (MPPT) input stage, to inject the maximum available power from the renewable source to the intermediate voltage capacitor with a simple controlled boost converter.
- A battery, with half bridge current controller to charge or deploy the battery pack connected to the complex energetic system for energy storage and energy unbalance compensation.
- Intermediate buffer for balancing the device's energy usage.
- Universal three phase output stage with 3 single phase full bridge CSIs and 2 high current DC-DC converter

This is suitable to inject any necessary current shape to the low voltage three phase grid even DC currents too.

Of course there is a possibility that there is no renewable power available for a longer period of time and the battery completely looses its charge. In this case the system should work merely with the power of the connection point but with zero energy balance. This states to operate two controller with semi-opposite control goals. The optimization based controller requires current injection while the intermediate voltage controller (Figure (5.9)) keeps the inverters energy balance. Although for this operation some of the control's performance should be sacrificed, unbalance compensation could be achieved even without external renewable power, and energy storage at a minimum power requirement. The individual physical values of the CSI can be observed in Table (5.2).

In the following paragraphs the sub-stages of the VU compensating device shall be explained in detail, and they role in solving the control problem.

PV energy source

The PV plant is the renewable power source of the device, modelled as a controlled voltage source with the value of V_{PV}, and with serial resistance R_{PV}, and filtering inductance of L_{PV}. The voltage source was modelled with periodic pattern, as PV panels give variable power output as well. For continuous operation a maximum power point tracker (MPPT) was implemented as this is the state of the art handling of uncertain PV sources. The MPPT controls a single IGBT of which emitter leg is connected to the ground.

Energy storage

A Li-ion battery with 153.6 V and 200 Ah, with series choke inductance of L_{Batt} is providing energy storage capability, when the PV source is not present, or the required mitigation is too low to dissipate all the energy to the

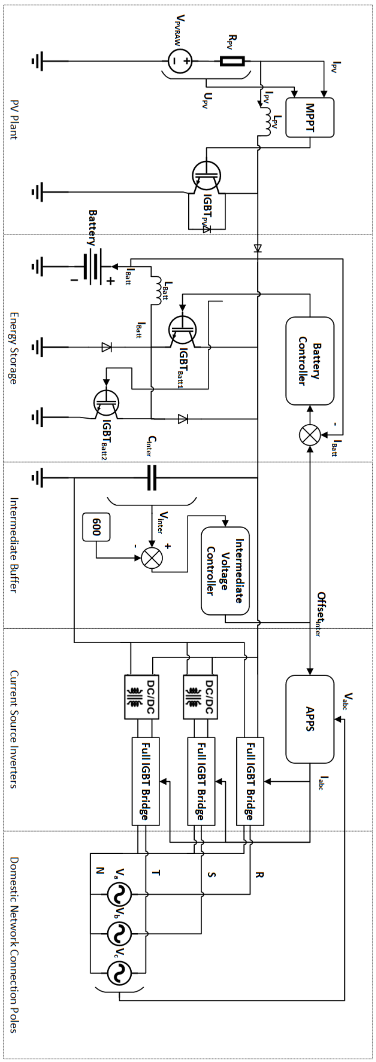

Figure 5.9: Full topology of the VU compensator. The device is segmented into PV plant as a renewable energy source with added MPPT unit, power storage with a Li-ion battery extended with charger/discharge half bridge, buffer capacitance with intermediate voltage controller, three separated CSI with DC-DC isolators, and the network substituting voltage sources.

network. For controlling the power flow, a classic half-bridge structure was employed, with a simple windowed control with 10 kHz switching frequency. The reference signal is set by the battery's current I_{Batt} subtracted from the intermediate voltage controller's reference $Offset_{inter}$.

Intermediate buffer

The in intermediate buffer capacitance was placed between the energy storage stage and the CSI actuators. This stage is responsible for the whole device's energy management, via an intermediate voltage control scheme. The intermediate voltage controller's flowchart can be observed on Fig.(5.10), where K_P, K_I, and K_D are the controller gains, and p_{inter} is the filter's gain. Further-

Table 5.2: The applied parameters and physical values in the VU compensator design

Parameter	Value
R_{PV}	5 Ω
R_{line}	0.4 Ω
L_{PV}	100 mH
L_{Batt}	100 mH
L_{CSI}	2 mH
C_{inter}	10 mF
V_{Batt}	153.6 V
$\widehat{V}_{PV}$	30 V
C_{Batt}	200 Ah
P_{hh}	$10^3/3$ W
Q_{Lhh}	2000/3 VAR
Q_{Chh}	0 VAR
K_P	1
K_I	0.4
K_D	0.6
p_{inter}	200

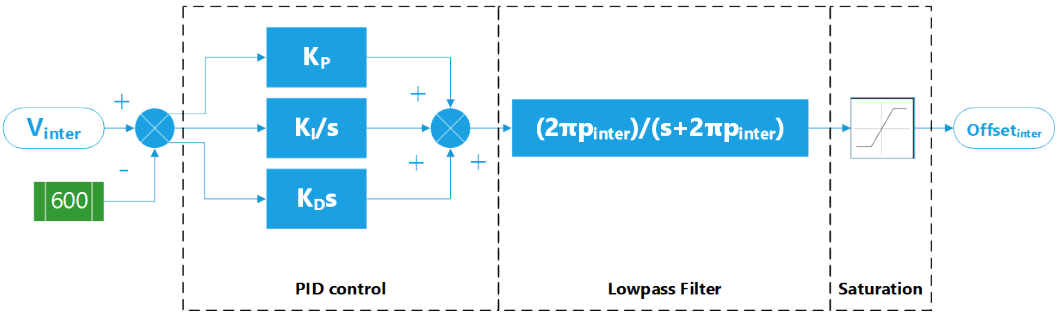

Figure 5.10: A general PID scheme and low pass filter of the intermediate voltage controller.

more, to direct the power flow from the battery into the intermediate buffer capacitance, via the battery controller's reference signal.

5.6 Asynchronous parallel pattern search

In the following section, the applied optimization structure, namely the APPS algorithm shall be discussed in detail. They commonality in this work, is that all of them are designed to search for the optimal control input for a current governing system, should it be voltage unbalance reduction with no applicable network model (due the actors unpredictability), or reaching the fastest reference value with explicit predictive control with the converter's equation's considered, which shall be discussed in section (5.7.1).
The APPS can rather be described as a linear search program, distributed in a

multi-dimensional plane, where the it is only a black box model available [56]. These variants of pattern search can solve nonlinear unconstrained problems of the form of:

$$\min_{x \in \mathbb{R}^n} f(x), \tag{5.3}$$

where $f : \mathbb{R}^n \longrightarrow \mathbb{R}$. We assume that the evaluation of f is computationally expensive, hence our interest in using either distributed or parallel computing environments to solve the problem. It needs to be concentrated on the parallelization of the search strategy, rather than on the evaluation of f, though the techniques we discuss here can be adapted to handle problems for which the computation of f also can be distributed. Additionally is is assumed that f is continuously differentiable. It can be assumed that the gradient ∇f is unavailable, but the method is applicable as presented in section 3.4.1, where the gradient determines the direction of the next step, further increasing its efficiency. For such problems, pattern search methods are one possible solution technique since they neither require nor explicitly estimate derivatives.

Parallel pattern search

Lets adopt an infinite sequence of iterations $\rho = 0, 1, 2, \ldots,$ with the last iteration noted as $\rho - 1$ and initialization at 0. It is assumed that the process knows the best point so far as $x^{\rho-1}$, where $f(x^{\rho-1})$ is the global minima of f. Associated with $x^{\rho-1}$ there is a step-length control parameter namely $\Delta^{\rho-1}$. Each $i \in \mathcal{P}$, where $\mathcal{P} = \{1, \ldots, p\}$ process ends iteration at $\rho - 1$ by constructing it's trial point and initiating an evaluation of $f(x_i^{\rho-1} + \Delta_i^{\rho-1} d_i)$, where $\mathcal{D} = \{d_1, \ldots, d_p\}$ is the finite set of directions applied by each individual process. The simultaneous start of the function evaluations at the trial points on each of the p processes signals the start of iteration ρ. When all of the participating processes are finished with their evaluation of f, they communicate these values to each other and determine the new values of x^ρ, and Δ^ρ. If there exists an $i \in \mathcal{P}$, such that $f(x_i^{\rho-1} + \Delta_i^{\rho-1} d_i) < f(x^{\rho-1})$, then $\rho \in \mathcal{S}$, where $\mathcal{S}$ denotes the successful iterations.

Adding asynchronicity

With said above, the general strategy for asynchronous parallel pattern search, from the perspective of a single process $i \in \mathcal{P}$ can be outlined:

1. Evaluate $f(x_i^{best} + \Delta_i^{best} d_i)$.

2. If $f(x_i^{best} + \Delta_i^{best} d_i) < f(x_i^{best})$, then broadcast result to all other processes.

3. Update local values x_i^{best} and Δ_i^{best} based on the current local information.

4. Repeat.

The price payed is that each process has its own notion of the best known point seen so far, as well as its own value for Δ^i. Any success on one process is communicated to all other processes participating in the search, but the successful process carries on from its new best point without waiting for a response from the other processes. By adding a few mild conditions, the global convergence of the search can be still ensured [56]. Instead of indexing based on a notion of iterations, we switch from ρ to indexing based on discrete time instance, letting the set $\mathcal{Q} = \{1, 2, \ldots, q\}$ denote the index of steps. Thus x_i^q s used for the best point known to process i at time step q, and similarly, Δ_i^q. So if process i starts a function evaluation at time step q, the trial point at which the function evaluation will be made at $x_i^q + \Delta_i^q d_i$. Further worth mention, that time steps are assumed to be of fine enough resolution so that at most one function evaluation finishes per process per time step.
Lets define two sets that satisfy $\mathcal{Q} = \mathcal{S}_i \cup \mathcal{U}_i$, , and $\mathcal{S}_i = \mathcal{I}_i \cup \mathcal{E}_i$, where $\mathcal{S}_i$ is the set of all time successful steps on process i, $\mathcal{I}_i$ is the set if internal successes, $\mathcal{E}_i$ is the set of external successes, and $\mathcal{U}_i$ consists the unsuccessful steps respectfully. An internal success, where the process finds itself the minima, the external success is where the process is updated externally by the minima. Further $\mathcal{C}_i \in \mathcal{U}_i$ is defined as the set of time steps where Δ_i^t is reduced. All the above cases $(\mathcal{U}_i \backslash \mathcal{C}_i)$ no action is performed.
The updating functions allow us to give the following general definitions for x_i^q and Δ_i^q. For every $q \in \mathcal{Q}$, $q > 0$, the best point for the i^{th} process defined to be:

$$x_i^q = \left\{ \begin{matrix} x_{\omega_i(q)}^{\tau_i(q)} + \Delta_{\omega_i(q)}^{\tau_i(q)} d_{\omega_i(q)}, & \text{if } q \in \mathcal{S}_i \\ x_i^{q-1}, & \text{otherwise} \end{matrix} \right\}, \tag{5.4}$$

with the initialisation $x_i^0 = x^0$, where $\omega_i(q)$ is the generating process index for the update time at step q on process i, and $\tau_i(q)$ is the time index for initialization of the function evaluation, that produced the update at time q on process i. For every q the step length control parameter Δ_i^q defined to be:

$$\Delta_i^q = \left\{ \begin{matrix} \lambda_{\omega_i(q)}^{\nu_i(q)} \Delta_{\omega_i(q)}^{\tau_i(q)}, & \text{if } q \in \mathcal{S}_i \\ \theta_i^q \Delta_{\omega_i(q)}^{\tau_i(q)}, & \text{if } q \in \mathcal{C}_i \\ \Delta_i^{q-1}, & \text{otherwise} \end{matrix} \right\}, \tag{5.5}$$

with the initialization $\Delta_i^0 = \Delta^0$, where $\nu_i(q)$ is time index for the completion of the function evaluation that produced the update at time step q on process i, and θ_i^q and λ_i^q are chosen. With the following pattern followed, the local minima of f shall eventually be reached in an undetermined number of steps.

5.7 Model based predictive control

5.7.1 Quadratic optimization and predictive control

Philosophically MPC reflects human behavior whereby we select control actions which we think will lead to the best predicted outcome (or output) over some limited horizon. To make this selection we use an internal model of the process in question, and constantly update our decisions as new observations become available. Hence a predictive control law has the following components:

- The control law depends on predicted behavior.
- The output predictions are computed using a process model.
- The current input is determined by optimizing some measure of predicted performance.
- The receding horizon: the control input is updated at every sampling instant.

Most control laws, say PID (proportional, integral and derivative) control, does not explicitly consider the future implication of current control actions. To some extent this is only accounted by the expected closed-loop dynamics. MPC on the other hand implicitly (or explicitly) computes the predicted behavior over some horizon. One can therefore restrict the choice of the proposed input trajectories to those that do not lead to difficulties in the future.
In order to predict the future behavior of a process, we must have a model of how the process behaves. In particular, this model must show the dependence of the output on the current measured variable and the current/future inputs. This does not have to be linear (e.g. transfer function, state-space) and in fact can be just about anything. A precise model is not always required to get tight control, because the decisions are updated regularly. This will deal with some model uncertainty in a fairly fast time scale. The decision on the best control is thus continually updated using information from this comparison [106].
This way, model based predictive control methods are optimal regulators, with a defined cost function on a defined and encompassed prediction horizon with restrictions [107], [108], [109], [110]. The control signal is calculated over a defined horizon, but from the sequence of applicable control signals only the first one is used in the next sample. This procedure is repeated according to the principle of the moving horizon, using new iterations, as such provides the reaction in each sample. The method was developed for systems with physical restrictions, in the first stage for the control of chemical processes in the oil industry, then it was applied to various rapid processes from automotive or power electronics industry [111] , [112]. By default the optimization problem can be solved, for each sample, or explicitly using the multi-parameter programming techniques (mp-LP, mp-QP).

Linear quadratic optimal control

In practice most MPC algorithms use linear models because the dependence of the predictions on future control choices is then linear and this facilitates optimization as well as off-line analysis of expected closed-loop behavior. However, nonlinear models can be used where the implied computational burden is not a problem and linear approximations are not accurate enough. It is also important to note here the comment fit for purpose. In predictive control, the model is used solely to compute system output predictions, so the model is fit for purpose if it gives accurate enough predictions. The effort and detail put into modeling stage should reflect this. Let the us assume that the system is linear and time-invariant (LTI):

$$\mathbf{x}(q+1) \quad = \quad \mathbf{A}\mathbf{x}(q) + \mathbf{B}\mathbf{u}(q), \tag{5.6}$$

where $\mathbf{x}(q) \in \mathbb{R}^n$ and $\mathbf{u}(q) \in \mathbb{R}^m$ are the state and input vectors respectively. We define a quadratic cost function over a finite horizon of N steps:

$$J_0(\mathbf{U}_0, x(0)) \quad = \quad \mathbf{x}_N'\mathbf{P}\mathbf{x}_N + \textstyle\sum_{k=0}^{N-1} \mathbf{x}_k'\mathbf{Q}\mathbf{x}_k + \mathbf{u}_k'\mathbf{R}\mathbf{u}_k \tag{5.7}$$

where $U_0 = [\mathbf{u}_0', \ldots, \mathbf{u}_{N-1}'] \in \mathbb{R}^s$, $s = m \cdot N$ is the decision vector (with m dimensional input vector) constraining all future inputs, also $\mathbf{P} = \mathbf{P}' \succeq 0$, $\mathbf{Q} = \mathbf{Q}' \succeq 0$, $\mathbf{R} = \mathbf{R}' \succeq 0$, and $\mathbf{x}_k$ denotes the state vector at time k obtained form $\mathbf{x}_0 = \mathbf{x}(0)$. We also apply the system model based on (5.6):

$$\mathbf{x}_{k+1} \quad = \quad \mathbf{A}\mathbf{x}_k + \mathbf{B}\mathbf{u}_k, \tag{5.8}$$

From the above a finite optimal control problem can be considered:

$$\begin{array}{rcl} J_0^*(\mathbf{x}(0)) & = & \min_{\mathbf{U}_0} J_0(\mathbf{U}_0, x(0)) \\ & \text{subj. to} & \mathbf{x}_{k+1} = \mathbf{A}\mathbf{x}_k + \mathbf{B}\mathbf{u}_k \\ & & \mathbf{x}_0 = \mathbf{x}(0) \\ & & k = 0, 1, \ldots, N-1 \end{array} \tag{5.9}$$

The first step is to write the equality constraints to express all future states and inputs from the initial state $\mathbf{x}_0$ until the and of horizon N:

$$\underbrace{\begin{bmatrix} \mathbf{x}(0) \\ \mathbf{x}_1 \\ \vdots \\ \vdots \\ \mathbf{x}_N \end{bmatrix}}_{\mathcal{X}^x} = \underbrace{\begin{bmatrix} \mathbf{I}_0 \\ \mathbf{A}_1 \\ \vdots \\ \vdots \\ \mathbf{A}^N \end{bmatrix}}_{\mathcal{S}^x} \mathbf{x}(0) + \underbrace{\begin{bmatrix} 0 & \ldots & \ldots & 0 \\ \mathbf{B} & 0 & \ldots & 0 \\ \mathbf{A}\mathbf{B} & \ddots & \ddots & \vdots \\ \vdots & \ddots & \ddots & \vdots \\ \mathbf{A}^{N-1}\mathbf{B} & \ddots & \ddots & \mathbf{B} \end{bmatrix}}_{\mathcal{S}^u} \begin{bmatrix} \mathbf{u}_0 \\ \vdots \\ \vdots \\ \mathbf{u}_N \end{bmatrix}. \tag{5.10}$$

Here all future states are explicit functions of the state $\mathbf{x}(0)$ and the future inputs of $\mathbf{u}_0, \mathbf{u}_1\cdot$ only. By defining appropriate quantities, we can rewrite (5.10) in a compact form:

$$\mathcal{X}^x \quad = \quad \mathcal{S}^x(0) + \mathcal{S}^u\mathbf{U}_0. \tag{5.11}$$

Using the same notation the object function can be rewritten as:

$$J(\mathbf{x}_0, \mathbf{U}_0) \quad = \quad \mathcal{X}'\bar{\mathbf{Q}}\mathcal{X} + \mathbf{U}_0\bar{\mathbf{Q}}\mathbf{U}_0', \tag{5.12}$$

where $\bar{\mathbf{Q}} = diag\{\mathbf{Q}, \ldots, \mathbf{Q}, \mathbf{P}\}$, and $\bar{\mathbf{R}} = diag\{\mathbf{R}, \ldots, \mathbf{R}\}$. Substituting (5.11) into the objective function (5.12) yields:

$$
\begin{aligned}
J(\mathbf{x}_0, \mathbf{U}_0) &= (\mathcal{S}^x(0) + \mathcal{S}^u\mathbf{U}_0)'\bar{\mathbf{Q}}(\mathcal{S}^x(0) + \mathcal{S}^u\mathbf{U}_0) + \mathbf{U}_0'\bar{\mathbf{R}}\mathbf{U}_0 \\
&= \mathbf{U}_0' \underbrace{(\mathcal{S}^{u'}\bar{\mathbf{Q}}\mathcal{S}^u + \bar{\mathbf{R}})}_{\mathbf{H}} \mathbf{U}_0 + \\
&+ \; 2\mathbf{x}'(0) \underbrace{(\mathcal{S}^{x'}\bar{\mathbf{Q}}\mathcal{S}^u)}_{\mathbf{F}} \mathbf{U}_0 + \\
&+ \; \mathbf{x}'(0) \underbrace{(\mathcal{S}^{x'}\bar{\mathbf{Q}}\mathcal{S}^x)}_{\mathbf{Y}} \mathbf{x}(0) \\
&= \mathbf{U}_0'\mathbf{H}\mathbf{U}_0 + 2\mathbf{x}'(0)\mathbf{F}\mathbf{U}_0 + \mathbf{x}'(0)\mathbf{Y}\mathbf{x}(0).
\end{aligned} \tag{5.13}
$$

Because $\bar{\mathbf{R}} \succ 0$, and $\mathbf{H} \succ 0$, thus $J(\mathbf{x}_0, \mathbf{U}_0)$ is a positive definite quadratic function of $\mathbf{U}_0$, therefore its minimum can be found by computing its gradient and setting it to zero, which yields the optimal vector of future inputs:

$$
\begin{aligned}
\mathbf{U}_0^*(\mathbf{x}(0)) &= -\mathbf{H}^{-1}\mathbf{F}'x(0) \\
&= -(\mathcal{S}^{u'}\bar{\mathbf{Q}}\mathcal{S}^u + \bar{\mathbf{R}})^{-1}\mathcal{S}^{u'}\bar{\mathbf{Q}}\mathcal{S}^x\mathbf{x}(0).
\end{aligned} \tag{5.14}
$$

With (5.14) applied and calculated $\mathbf{U}_0$ the cost is the optimal following:

$$
\begin{aligned}
\mathbf{J}_0^*(\mathbf{x}(0)) &= -\mathbf{x}(0)'\mathbf{F}\mathbf{H}^{-1}F'x(0) \\
&= \mathbf{x}(0)' \left[\mathcal{S}^{x'}\bar{\mathbf{Q}}\mathcal{S}^x - \mathcal{S}^{x'}\bar{\mathbf{Q}}\mathcal{S}^u(\mathcal{S}^{u'}\bar{\mathbf{Q}}\mathcal{S}^u + \bar{\mathbf{R}})^{-1}\mathcal{S}^{u'}\bar{\mathbf{Q}}\mathcal{S}^x\right] \mathbf{x}(0).
\end{aligned} \tag{5.15}
$$

Note that the optimal vector of future inputs $\mathbf{U}_0^*(\mathbf{x}(0))$ is a linear function of (5.14) of the initial state $\mathbf{x}(0)$ and the optimal cost $J_0^*(x(0))$ is a quadratic function (5.15) of the initial state $\mathbf{x}(0)$.
Alternatively the formulation can be done in a recursive manner. The optimal cost can be defined as $J_j^*(\mathbf{x}_j)$ fot the j^{th} for the $N-j$ step problem starting from state $\mathbf{x}_j$ as:

$$
J_j^*(\mathbf{x}_j) = \min_{\mathbf{u}_j,\ldots,\mathbf{u}_{N-1}} \mathbf{x}_N'\mathbf{P}\mathbf{x}_N + \textstyle\sum_{k=0}^{N-1} \mathbf{x}_k'\mathbf{Q}\mathbf{x}_k + \mathbf{u}_k'\mathbf{R}\mathbf{u}_k. \tag{5.16}
$$

The optimal "one step cost to go" can be obtained as:

$$
\begin{aligned}
J_{N-1}^*(\mathbf{x}_{N-1}) \quad &= \quad \min_{\mathbf{u}_{N-1}} \mathbf{x}_N'\mathbf{P}_N\mathbf{x}_N + \mathbf{x}_{N-1}'\mathbf{Q}\mathbf{x}_{N-1} + \mathbf{u}_{N-1}'\mathbf{R}\mathbf{u}_{N-1}. \\
\text{subj. to} \quad & \mathbf{x}_N = \mathbf{A}\mathbf{x}_{N-1} + \mathbf{B}\mathbf{u}_{N-1} \\
& \mathbf{P}_N = \mathbf{P},
\end{aligned} \tag{5.17}
$$

where $J_{N-1}^*(\mathbf{x}_{N-1})$ is a positive quadratic function of the decision variable $\mathbf{u}_{N-1}$. Writing (5.17) as the objective function:

$$
\begin{aligned}
J_{N-1}^*(\mathbf{x}_{N-1}) &= \min_{\mathbf{u}_{N-1}} \{\mathbf{x}_{N-1}'(\mathbf{A}'\mathbf{P}_N\mathbf{A} + \mathbf{Q})\mathbf{x}_{N-1} + \\
&+ \; 2\mathbf{x}_{N-1}'\mathbf{A}'\mathbf{P}_N\mathbf{B}\mathbf{u}_{N-1} + \\
&+ \; \mathbf{u}_{N-1}'(\mathbf{B}'\mathbf{P}_N\mathbf{B} + \mathbf{R})\mathbf{x}_{N-1}\}.
\end{aligned} \tag{5.18}
$$

The optimal input can be found by setting the gradient to zero:

$$\mathbf{u}^*_{N-1} = \underbrace{-(\mathbf{B}'\mathbf{P}_N\mathbf{B} + \mathbf{R})^{-1}\mathbf{B}'\mathbf{P}_N\mathbf{A}}_{\mathbf{F}_{N-1}}\mathbf{x}_{N-1}, \tag{5.19}$$

and the optimal one step optimal cost:

$$J^*_{N-1}(\mathbf{x}_{N-1}) \quad = \quad \mathbf{x}'_{N-1}\mathbf{P}_{N-1}\mathbf{x}_{N-1}, \tag{5.20}$$

where $\mathbf{P}_{N-1}$ can be defined recursively as:

$$\mathbf{P}_{N-1} = \mathbf{A}'\mathbf{P}_N\mathbf{A} + \mathbf{Q} - \mathbf{A}'\mathbf{P}_N\mathbf{B}(\mathbf{B}'\mathbf{P}_N\mathbf{B} + \mathbf{R})^{-1}\mathbf{B}'\mathbf{P}_N\mathbf{A}. \tag{5.21}$$

The next stage is to write down the "two step" problem based on (5.17):

$$\begin{array}{rcl} J^*_{N-2}(\mathbf{x}_{N-2}) & = & \min_{\mathbf{u}_{N-2}} \mathbf{x}'_{N-1}\mathbf{P}_{N-1}\mathbf{x}_{N-1} + \mathbf{x}'_{N-2}\mathbf{Q}\mathbf{x}_{N-2} + \mathbf{u}'_{N-2}\mathbf{R}\mathbf{u}_{N-2}. \\ & \text{subj. to} & \mathbf{x}_{N-1} = \mathbf{A}\mathbf{x}_{N-2} + \mathbf{B}\mathbf{u}_{N-2} \end{array} \tag{5.22}$$

We since (5.22) has the same form as (5.17) we can apply the same solution seen at (5.19):

$$\mathbf{u}^*_{N-2} = \underbrace{-(\mathbf{B}'\mathbf{P}_{N-1}\mathbf{B} + \mathbf{R})^{-1}\mathbf{B}'\mathbf{P}_{N-1}\mathbf{A}}_{\mathbf{F}_{N-2}}\mathbf{x}_{N-2}, \tag{5.23}$$

where the "two step" cost:

$$J^*_{N-2}(\mathbf{x}_{N-2}) \quad = \quad \mathbf{x}'_{N-2}\mathbf{P}_{N-2}\mathbf{x}_{N-2}, \tag{5.24}$$

where $\mathbf{P}_{N-2}$ can be defined recursively as:

$$\mathbf{P}_{N-2} = \mathbf{A}'\mathbf{P}_{N-1}\mathbf{A} + \mathbf{Q} - \mathbf{A}'\mathbf{P}_{N-1}\mathbf{B}(\mathbf{B}'\mathbf{P}_{N-1}\mathbf{B} + \mathbf{R})^{-1}\mathbf{B}'\mathbf{P}_{N-1}\mathbf{A}. \tag{5.25}$$

Continuing in this manner at some arbitrary time k the optimal control action is:

$$\mathbf{u}^*(k) = \underbrace{-(\mathbf{B}'\mathbf{P}_{k+1}\mathbf{B} + \mathbf{R})^{-1}\mathbf{B}'\mathbf{P}_{k+1}\mathbf{A}}_{\mathbf{F}_k}\mathbf{x}_k, \tag{5.26}$$

where $k = 0, 1, \ldots, N-1$ and:

$$\mathbf{P}_k = \mathbf{A}'\mathbf{P}_{k+1}\mathbf{A} + \mathbf{Q} - \mathbf{A}'\mathbf{P}_{k+1}\mathbf{B}(\mathbf{B}'\mathbf{P}_{k+1}\mathbf{B} + \mathbf{R})^{-1}\mathbf{B}'\mathbf{P}_{k+1}\mathbf{A}. \tag{5.27}$$

and the optimal starting cost starting from the measured state:

$$J^*_k(\mathbf{x}(k)) \quad = \quad \mathbf{x}'(k)\mathbf{P}_k\mathbf{x}(k). \tag{5.28}$$

Equation (5.27) is called the discrete Ricatti equation [102], or Ricatti difference equation, which is initialised with $\mathbf{P}_n = \mathbf{P}$ and solves backwards. It is worth noting that from (5.26) the optimal control action $\mathbf{u}^*(k)$ is obtained in the form of feedback law as linear function of the measured state $\mathbf{x}(k)$ at time instance k, and the optimal cost is (5.28).

Constrained optimal control

In constrained optimal control for any input action with a given initial state the control action can be computed with quadratic programming but with respect to pre described constraints. As displayed, the linear quadratic approach requires a numerical definition so that a precise calculation can be made, that is, which optimal input trajectory gives the lowest numerical value to the cost. The main requirement is that the cost depends on the batch or recursive input sequence and that low values of cost imply good closed-loop performance good being defined for the process. Of course the choice of the cost affects the complexity of the implied optimization and this is also a consideration.
With considering an LTI system such as (5.6), let us assume that it is subject to constraints:

$$\mathbf{x}(q) \in \mathcal{X}^x, \quad \mathbf{u}(q) \in \mathcal{U}^u, \quad \forall t \geq 0, \tag{5.29}$$

where the set of inputs $\mathcal{U}^u \subseteq \mathbb{R}^m$ and states $\mathcal{X}^x \subseteq \mathbb{R}^n$ are polyhedra. when Eucledian norm is used with the cost as (5.7) with $\mathbf{P} \succeq 0$, $\mathbf{Q} \succeq 0$, and $\mathbf{R} \succ 0$ we define the constrained optimal control problem as:

$$\begin{array}{rcl} J_0^*(\mathbf{x}(0)) & = & \min_{\mathbf{U}_0} J_0(\mathbf{x}(0), \mathbf{U}_0) \\ & \text{subj. to} & \mathbf{x}_{k+1} = \mathbf{A}\mathbf{x}_k + \mathbf{B}\mathbf{u}_k, k = 0, 1, \ldots, N-1 \\ & & \mathbf{x}_N \in \mathcal{X}_f, \mathbf{x}_k \in \mathcal{X}^x, \mathbf{u}_k \in \mathcal{U}^u \\ & & \mathbf{x}_0 = \mathbf{x}(0), \end{array} \tag{5.30}$$

where $\mathbf{x}_N \subseteq \mathbb{R}^n$ is the terminal polyhedral region, and $\mathbf{U}_0 = [\mathbf{u}_0', \ldots, \mathbf{u}_{N-1}']' \in \mathbb{R}^s$ with $s = m \cdot N$ is the optimization vector. We denote $\mathcal{X}_0 \subset \mathcal{X}^x$ as the set of initial states $\mathbf{x}(0)$ for which the optimal control problem is feasible such as:

$$\begin{array}{rcl} \mathcal{X}_0 & = & \{\mathbf{x}_0 \in \mathbb{R}^n : \exists \mathbf{U}_0, \\ & & s.t. : \mathbf{x}_k \in \mathcal{X}^x, \mathbf{u}_k \in \mathcal{U}^u, \mathbf{x}_N \in \mathcal{X}_f, \\ & & where\, \mathbf{x}_{k+1} = \mathbf{A}\mathbf{x}_k + \mathbf{B}\mathbf{u}_k, k = 0, \ldots, N-1\}. \end{array} \tag{5.31}$$

We denote $\mathcal{X}_i$ as the set of states $\mathbf{x}_i$ at time $i = 0, 1, \ldots, N$ which is feasible for (5.30). The sets $\mathcal{X}_i$ are independent of the cost function as long as it guaranties the exsistence of a minima and the algorithm used to compute the solution. There are also ways to define an compute $\mathcal{X}_i$. With the batch approach is as follows:

$$\begin{array}{rcl} \mathcal{X}_i & = & \{\mathbf{x}_i \in \mathbb{R}^n : \exists \mathbf{U}_i, \\ & & s.t. : \mathbf{x}_k \in \mathcal{X}^x, \mathbf{u}_k \in \mathcal{U}^u, \mathbf{x}_N \in \mathcal{X}_f, \\ & & where\, \mathbf{x}_{k+1} = \mathbf{A}\mathbf{x}_k + \mathbf{B}\mathbf{u}_k, k = 0, \ldots, N-1\}. \end{array} \tag{5.32}$$

This definition requires, that for any initial $\mathbf{x}_i \in \mathcal{X}_i$ state there exsists a feasible $\mathbf{U}_i = [\mathbf{u}_i, \ldots, \mathbf{u}_{N-1}]$ which keeps the state evolution in the feasible set $\mathcal{X}^x$ at future time instants k and forces $\mathbf{x}_N$ into $\mathcal{X}_f$ at $k = N$.
Next we show how to compute $\mathcal{X}_i$ for $i = 0, \ldots, N-1$. It is stated that the state

$\mathcal{X}^x$, $\mathcal{X}_f$ and input $\mathcal{U}^u$ sets are $\mathcal{H}$-polyhedra [102], and $\mathbf{A}_x \leq \mathbf{x}\mathbf{b}_x$, $\mathbf{A}_f\mathbf{x}_N \leq \mathbf{b}_f$, are the set of equality and inequality constraints for the states and the terminal state and $\mathbf{A}_u\mathbf{u} \leq \mathbf{b}_u$ are the set of of equality and inequality constraints on inputs respectively. We define the set of constraints as polyhedron $\mathcal{P}_i^c$ at time instance i as:

$$\mathcal{P}_i^c \quad = \quad \{(\mathbf{U}_i, \mathbf{x}_i) \in \mathbb{R}^{m\cdot(N-i)+n}, s.t. : \mathbf{G}_u\mathbf{U}_i - \mathbf{E}_i\mathbf{x}_i \leq \mathbf{w}_i\}, \tag{5.33}$$

where $\mathbf{G}_i$, $\mathbf{E}_i$, and $\mathbf{w}_i$ as the matrices of inequality and equality constraints are defined as:

$$\mathbf{G}_i = \begin{bmatrix} \mathbf{A}_u & 0 & \cdots & 0 \\ 0 & \mathbf{A}_u & \cdots & 0 \\ \vdots & \vdots & \ddots & \vdots \\ 0 & 0 & \cdots & \mathbf{A}_u \\ 0 & 0 & \cdots & 0 \\ \mathbf{A}_x\mathbf{B} & 0 & \cdots & 0 \\ \mathbf{A}_x\mathbf{A}\mathbf{B} & \mathbf{A}_x\mathbf{B} & \cdots & 0 \\ \vdots & \vdots & \ddots & \vdots \\ \mathbf{A}_f\mathbf{A}^{N-i-1}\mathbf{B} & \mathbf{A}_f\mathbf{A}^{N-i-2}\mathbf{B} & \cdots & \mathbf{A}_f\mathbf{B} \end{bmatrix} \mathbf{E}_i = \begin{bmatrix} 0 \\ 0 \\ \vdots \\ 0 \\ -\mathbf{A}_x \\ -\mathbf{A}_x\mathbf{A} \\ -\mathbf{A}_x\mathbf{A}^2 \\ \vdots \\ -\mathbf{A}_f\mathbf{A}^{N-i} \end{bmatrix} \mathbf{w}_i = \begin{bmatrix} \mathbf{b}_u \\ \mathbf{b}_u \\ \vdots \\ \mathbf{b}_u \\ \mathbf{b}_x \\ \mathbf{b}_x \\ \mathbf{b}_x \\ \vdots \\ \mathbf{b}_f \end{bmatrix}. \tag{5.34}$$

Also, the set $\mathcal{X}_i$ is a polyhedron serves as the projection of $\mathcal{P}_i^c$ in (5.33) and in (5.34).
Next the previously mentioned terms are implemented with using the Euclidian norm case. For this we start with the constrained control problem (5.30) with the assumption of $\mathbf{Q} = \mathbf{Q}' \succeq 0$, $\mathbf{R} = \mathbf{R}' \succ 0$, and $\mathbf{R} = \mathbf{R}' \succeq 0$. As such the constrained control problem with euclidian norm:

$$\begin{array}{rcl} J_0^*(\mathbf{x}(0)) & = & \min_{\mathbf{U}_0} J_0(\mathbf{x}(0), \mathbf{U}_0) = \mathbf{x}_N'\mathbf{P}\mathbf{x}_N + \sum_{k=0}^{N-1} \mathbf{x}_k'\mathbf{Q}\mathbf{x}_k + \mathbf{u}_k'\mathbf{R}\mathbf{u}_k \\ & \text{subj. to} & \mathbf{x}_{k+1} = \mathbf{A}\mathbf{x}_k + \mathbf{B}\mathbf{u}_k, k = 0, 1, \ldots, N-1 \\ & & \mathbf{x}_N \in \mathcal{X}_f, \mathbf{x}_k \in \mathcal{X}^x, \mathbf{u}_k \in \mathcal{U}^u \\ & & \mathbf{x}_0 = \mathbf{x}(0). \end{array} \tag{5.35}$$

As shown in the unconstrained case (5.35) can be rewritten as:

$$\begin{array}{rcl} \min_{\mathbf{U}_0} J_0(\mathbf{x}(0), \mathbf{U}_0) & = & \mathbf{U}_0'\mathbf{H}\mathbf{U}_0 + 2\mathbf{x}(0)\mathbf{F}\mathbf{U}_0 + \mathbf{x}(0)\mathbf{Y}\mathbf{x}(0) \\ & = & [\mathbf{U}_0'\mathbf{x}'(0)] \begin{bmatrix} \mathbf{H} & \mathbf{F}' \\ \mathbf{F} & \mathbf{Y} \end{bmatrix} [\mathbf{U}_0'\mathbf{x}'(0)]' \\ . & \text{subj. to} & \mathbf{G}_0\mathbf{U}_0 \leq \mathbf{w}_0 + \mathbf{E}_0\mathbf{x}(0), \end{array} \tag{5.36}$$

with $\mathbf{G}_0$, $\mathbf{w}_0$, and $\mathbf{E}_0$ are defined in (5.34) and $\mathbf{H}$, $\mathbf{F}$, and $\mathbf{Y}$ are defined in (5.13), additionally as $J_0(\mathbf{x}(0), \mathbf{U}_0) \geq 0$ it follows that $\begin{bmatrix} \mathbf{H} & \mathbf{F}' \\ \mathbf{F} & \mathbf{Y} \end{bmatrix} \succeq 0$.
To obtain problem (5.36) elimination of equality constraints can be obtained

by successive substitution of $\mathbf{x}_{k+1} = \mathbf{A}\mathbf{x}_k + \mathbf{B}\mathbf{u}_k$, so only an input sequece as decision variables of $\mathbf{U}_0 = [\mathbf{u}_0, \ldots, \mathbf{u}_{N-1}]$ and $\mathbf{x}(0)$ is left as a parameter vector. In general, it might be more efficient to solve the problem the equality and inequality constraints, so that sparsity can be exploited. To aim this, for this lets define the set of inputs and states as $\tilde{\mathbf{z}} = [\mathbf{x}_1', \ldots, \mathbf{x}_N', \mathbf{u}_0', \ldots, \mathbf{u}_{N-1}']$ and rewrite (5.35) as:

$$\begin{aligned} J_0^*(\mathbf{x}(0)) \quad &= \quad [\mathbf{U}_0'\mathbf{x}'(0)] \begin{bmatrix} \mathbf{H} & \mathbf{F}' \\ \mathbf{F} & \mathbf{Y} \end{bmatrix} [\mathbf{U}_0'\mathbf{x}'(0)]' \\ . \text{ subj. to } \quad & \mathbf{G}_{0,eq}\tilde{\mathbf{z}} = \mathbf{E}_{0,eq}\mathbf{x}(0) \\ & \mathbf{G}_{0,in}\tilde{\mathbf{z}} \leq \mathbf{w}_{0,in} + \mathbf{E}_{0,in}\mathbf{x}(0), \end{aligned} \tag{5.37}$$

where $\mathbf{G}_{0,eq}$, and $\mathbf{E}_{0,eq}$, are the equality constraint matrices, and $\mathbf{G}_{0,in}$, $\mathbf{E}_{0,in}$, and $\mathbf{w}_{0,in}$ are the inequality constraint matrices respectively:

$$\mathbf{G}_{0,eq} = \left[\begin{array}{ccccc|cccc} \mathbf{I} & & & & & -\mathbf{B} & & & \\ -\mathbf{A} & \mathbf{I} & & & & & -\mathbf{B} & & \\ & -\mathbf{A} & \mathbf{I} & & & & & \ddots & \\ & & \ddots & \ddots & & & & & \ddots \\ & & & -\mathbf{A} & \mathbf{I} & & & & -\mathbf{B} \end{array}\right], \mathbf{E}_{0,eq} = \begin{bmatrix} \mathbf{A} \\ 0 \\ \vdots \\ 0 \end{bmatrix},$$

$$\mathbf{G}_{0,in} = \left[\begin{array}{ccccc|ccccc} 0 & & & & & 0 & & & & \\ \mathbf{A}_x & 0 & & & & 0 & & & & \\ & \mathbf{A}_x & & & & & 0 & & & \\ & & \ddots & \ddots & & & & \ddots & & \\ & & & \mathbf{A}_x & & & & & 0 & \\ & & & & \mathbf{A}_f & & & & & 0 \\ \hline 0 & & & & & \mathbf{A}_u & & & & \\ & 0 & & & & & \mathbf{A}_u & & & \\ & & \ddots & & & & & \ddots & & \\ & & & 0 & & & & & \mathbf{A}_u & \\ & & & & 0 & & & & & \mathbf{A}_u \end{array}\right], \mathbf{w}_{0,in} = \left[\begin{array}{c} \mathbf{b}_x \\ \mathbf{b}_x \\ \vdots \\ \mathbf{b}_x \\ \mathbf{b}_f \\ \hline \mathbf{b}_u \\ \mathbf{b}_u \\ \vdots \\ \mathbf{b}_u \\ \mathbf{b}_u \end{array}\right],$$

$$\mathbf{E}_{0,in} = \begin{bmatrix} -\mathbf{A}_x' & 0 & \ldots & 0 \end{bmatrix}, \tag{5.38}$$

and the constructed cost matrix $\mathbf{H}$ as:

$$\bar{\mathbf{H}} = \left[\begin{array}{cccc|ccc} \mathbf{Q} & & & & & & \\ & \ddots & & & & & \\ & & \mathbf{Q} & & & & \\ & & & \mathbf{P} & & & \\ \hline & & & & \mathbf{R} & & \\ & & & & & \ddots & \\ & & & & & & \mathbf{R} \end{array}\right]. \tag{5.39}$$

In the following the state feedback solution starting from the presumed initial state for one minimizing instance $J_0^*(\mathbf{x}(0))$ shall be displayed for the constrained quadratic control problem (5.35) as (5.37), with $\mathbf{G}_0$, $\mathbf{E}_0$ $\mathbf{w}_0$ as the

constraint describing matrices as defined in (5.34) starting from $\mathbf{x}(0)$, and $\mathbf{H}$, $\mathbf{F}$, and $\mathbf{Y}$ as the substitute matrices described in (5.13), to acquire the optimal solution.
We view the initial state $\mathbf{x}(0)$ as the vector of parameters as our goal to solve (5.35) for all values of the set of initial states $\mathbf{x}(0) \in \mathcal{X}_0$ and make this dependence explicit, with the computation of $\mathcal{X}_0$ in terms of feasibility, described in (5.32).
For convenience let us define the substitutive term $\mathbf{z}$ as:

$$\mathbf{z} \;=\; \mathbf{U}_0 + \mathbf{H}^{-1}\mathbf{F}'\mathbf{x}(0), \tag{5.40}$$

where $\mathbf{z} \in \mathbb{R}^s$ and with this transform (5.35) to obtain the equivalent control problem:

$$\begin{array}{rcl} \hat{J}^*(\mathbf{x}(0)) & = & J_0^*(\mathbf{x}(0)) - \mathbf{x}(0)'(\mathbf{Y} - \mathbf{F}\mathbf{H}^{-1}\mathbf{F}')\mathbf{x}(0) \\ & = & \min_{\mathbf{z}} \mathbf{z}'\mathbf{H}\mathbf{z} \\ & \text{subj. to} & \mathbf{G}_0\mathbf{U}_0 \leq \mathbf{w}_0 + \mathbf{S}_0\mathbf{x}(0), \end{array} \tag{5.41}$$

where $\mathbf{S}_0 = \mathbf{E}_0 + \mathbf{G}_0\mathbf{H}^{-1}\mathbf{F}'$. In this transformed problem the initial parameter vector $\mathbf{x}(0)$ appears only on right hand side of constraints. In this case (5.41) is a multi parametric constrained quadratic optimal program that can be solved explicitly by using geometrical means described first by the authors in [113]. This shall be discussed in section (5.8).

Receiding horizon control

All this said, even if we calculate the best optimal step sequence for solving the constrained control problem, there are still uncertainties for the future. Optimization over a finite horizon has the following disadvantages:

- Unforeseen problems may occur after the fixed optimization horizon, which may cancel the sequence of order for the calculated finished horizon.
- After reaching the time defined by the horizon, the law of command is no longer optimal.
- Finite horizon optimization is usually used because of the limited computing power is available, and not for theoretical reasons

To prevent this problem, the notion of optimization is introduced on a moving horizon. In each sample k , an optimization problem is solved over a defined horizon $k, \dots, k+N$ to calculate the appropriate command sequence, and only the first command is applied. This results in a moving optimization horizon, which eliminates the issues listed before displayed on Fig.(5.11).

The Formulation of the optimal control problem with moving horizon [114] in the system (5.6) with input and output constraints as mentioned in (5.29) with the cost function to minimize:

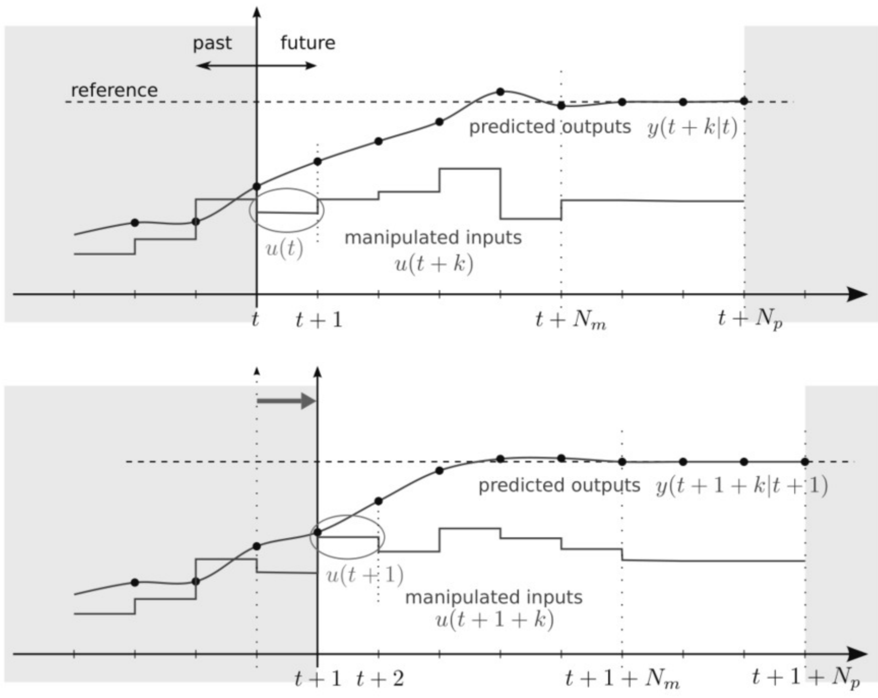

Figure 5.11: Graphycal display of receiding horison control (RHC) idea [102].

$$
\begin{aligned}
J(\mathbf{U}, \mathbf{x}(q)) \quad &= \quad \min_{\mathbf{U}_{q\to q+N|q}} J_q(\mathbf{x}(q), \mathbf{U}_{q\to q+N|q}) \\
&= \quad \mathbf{x}'_{q+N_y|q}\mathbf{P}\mathbf{x}_{q+N_y|q} + \textstyle\sum_{k=0}^{N_y-1} \mathbf{x}'_{q+k|q}\mathbf{Q}\mathbf{x}_{q+k|q} + \mathbf{u}'_{q+k}\mathbf{R}\mathbf{u}_{q+k}, \\
\text{subj. to} \quad & \mathbf{x}_N \in \mathcal{X}_f, \mathbf{x}_k \in \mathcal{X}^x, \mathbf{u}_k \in \mathcal{U}^u \\
& \mathbf{x}_{q|q} = \mathbf{x}(q), \\
& \mathbf{x}_{q+k+1|q} = \mathbf{A}\mathbf{x}_{q+k|q} + \mathbf{B}\mathbf{u}_{q+k}, \\
& \mathbf{u}_{q+k} = -K\mathbf{x}_{q+k|q}, N_u \le k \le N_y,
\end{aligned}
\tag{5.42}
$$

where $\mathbf{Q} = \mathbf{Q}' \geq 0$, $\mathbf{R} = \mathbf{R}' \geq 0$, $\mathbf{P} \geq 0$, $(\mathbf{C}, \mathbf{A})$ is observable, and $N_u \leq N_y$, $N_c \leq N_y - 1$. One trivial possibility to choose $K = 0$ and $\mathbf{P}$ to satisfy the Lyapunov equation:

$$\mathbf{P} \quad = \quad \mathbf{A}'\mathbf{P}\mathbf{A} + \mathbf{Q} \tag{5.43}$$

This means that after N_u samples the control stops and the system is evolving to an open loop form. It is obvious that the choice only makes sense if the open loop system is stable. The second option would as described with the method (5.27), but this involves to use an unconstrained control for N_u LQR samples. As a result, the MPC law calculates the optimal command sequence:

$$\mathbf{U}^*(q) \quad = \quad \left\{\mathbf{u}^*_q, \ldots, \mathbf{u}^*_{q+N_u-1}\right\}, \tag{5.44}$$

and only the first control input is applied:

$$\mathbf{u}(q) = \mathbf{u}_q^*. \tag{5.45}$$

The optimal control inputs estimated for future samples are not taken into account and the algorithm is repeated on the basis of new measurements or a new estimation of the states.

Stability of MPC

The problem of closed system stability with the predictive control has been extensively studied e.g. in [115], [116]. In the first generation of model based controllers, stability was achieved more experimentally by choosing parameters based on previous studies and experiences. In 1988 the Lyapunov stability method for discrete systems were introduced [117], and in 1990 for continuous systems [118] also for continuous systems.
While asymptotic convergence $\lim_{k\to\infty} \mathbf{x}_k = 0$ is a desirable property, it is generally not sufficient in practice. We would also like a system to stay in a small neighborhood of the origin when it is disturbed by a little. Formally this is expressed as Lyapunov stability.
For the autonomous system:

$$\mathbf{x}_{k+1} \;=\; g(\mathbf{x}_k) \tag{5.46}$$

where $g(0) = 0$. The definition of Lyapunov stability is for the equilibrium point $\mathbf{x} = 0$ of system (5.46) is:

- stable if, for each $\epsilon > 0$, there is a $\varphi > 0$ such that:

$$\|\mathbf{x}_0\| < \varphi \text{ s.t.: } \|\mathbf{x}_k\| < \epsilon, \ \forall k \geq 0. \tag{5.47}$$

- unstable if not stable
- asymptotically stable if in the set $\mathbf{\Omega} \subseteq \mathbb{R}^n$ if its stable and:

$$\lim_{k\to\infty} \mathbf{x}_k = 0, \ \forall \mathbf{x}_0 \in \mathbf{\Omega}. \tag{5.48}$$

- globally asymptotically stable if it is asymptotically stable and $\mathbf{\Omega} = \mathbb{R}^n$
- exponentially stable if it is stable and there exist constants $\chi > 0$ and $\psi \in (0, 1)$ such that:

$$\|\mathbf{x}_0\| < \varphi \text{ s.t.: } \|\mathbf{x}_k\| \leq \chi \|\mathbf{x}_0\| \psi^k, \ \forall k \geq 0. \tag{5.49}$$

Usually to show Lyapunov stability of the origin for a particular system one constructs a so called Lyapunov function, i.e., a function satisfying the conditions of the following theorem:
Consider the equilibrium point $\mathbf{x} = 0$ of system (5.46). Let $\mathbf{\Omega} \subset \mathbb{R}^n$ be a closed and bounded set containing the origin. Assume there exists a function $V : \mathbb{R}^n \to \mathbb{R}$ continuous at the origin, finite for every $\mathbf{x} \in \mathbf{\Omega}$ and such that:

$$
\begin{aligned}
V(0) &= 0 && (5.50a)\\
V(\mathbf{x}) &> 0,\ \forall \mathbf{x} \in \mathbf{\Omega}\backslash\{0\} && (5.50b)\\
V(\mathbf{x}_{k+1}) - V(\mathbf{x}_k) &\leq -\chi(\mathbf{x}_k),\ \forall \mathbf{x} \in \mathbf{\Omega}\backslash\{0\}, && (5.50c)
\end{aligned}
$$

where $\chi : \mathbb{R}^n \rightarrow \mathbb{R}$ is a continuous positive definite function, then $\mathbf{x} = 0$ is asymptotically stable. As such a function satisfying (5.50) is called a Lyapunov function.
A similar theorem can be derived for global asymptotic stability i.e.: $\mathbf{\Omega} = \mathbb{R}^n$: Consider the equilibrium point $\mathbf{x} = 0$ of system (5.46). Let $\mathbf{\Omega} \subset \mathbb{R}^n$ be a closed and bounded set containing the origin. Assume there exists a function $V : \mathbb{R}^n \rightarrow \mathbb{R}$ continuous at the origin, finite for every $\mathbf{x} \in \mathbf{\Omega}$ and such that:

$$
\begin{aligned}
\|\mathbf{x}\| \rightarrow \infty,\ \text{s.t.: } V(\mathbf{x}) &\rightarrow \infty && (5.51a)\\
V(0) &= 0 && (5.51b)\\
V(\mathbf{x}) &> 0,\ \forall \mathbf{x} \neq 0 && (5.51c)\\
V(\mathbf{x}_{k+1}) - V(\mathbf{x}_k) &\leq -\chi(\mathbf{x}_k),\ \forall \mathbf{x} \neq 0, && (5.51d)
\end{aligned}
$$

where $\chi : \mathbb{R}^n \rightarrow \mathbb{R}$ is a continuous positive definite function, then $\mathbf{x} = 0$ is globally asymptotically stable.
For linear systems a simple and effective Lyapunov function can be:

$$
V(\mathbf{x}) = \mathbf{x}'\mathbf{P}\mathbf{x}, \mathbf{P} \succ 0, \tag{5.52}
$$

In order to test the satisfaction of the last point of (5.51), we compute:

$$
\begin{aligned}
V(\mathbf{x}_{k+1}) - V(\mathbf{x}_k) &= \mathbf{x}'_{k+1}\mathbf{P}\mathbf{x}_{k+1} - \mathbf{x}'_k\mathbf{P}\mathbf{x}_k\\
&= \mathbf{x}'_k(\mathbf{A}'\mathbf{P}\mathbf{A})\mathbf{x}_k - \mathbf{x}'_k\mathbf{P}\mathbf{x}_k\\
&= \mathbf{x}'_k(\mathbf{A}'\mathbf{P}\mathbf{A} - \mathbf{P})\mathbf{x}_k,
\end{aligned} \tag{5.53}
$$

therefore, if (5.52) holds true then:

$$
\mathbf{A}'\mathbf{P}\mathbf{A} - \mathbf{P} = -\mathbf{Q}, \mathbf{Q} \succ 0, \tag{5.54}
$$

which is referred as discrete time Lyapunov equation.

5.8 Geometric approach to multi parametric programming

In this section the goal is to explain how to solve multi-parametric optimization problems (mp-OP). By start lets consider the following linear multip-parametric problem:

$$
\begin{aligned}
J^*(\mathbf{x}) &= \min_{\mathbf{z}} J(\mathbf{x}, \mathbf{z}) = \mathbf{c}'\mathbf{z}\\
\text{subj. to} &\quad \mathbf{G}\mathbf{z} \leq \mathbf{w} + \mathbf{S}\mathbf{x},
\end{aligned} \tag{5.55}
$$

where $\mathbf{z} \in \mathbb{R}^s$ is the vector of the optimization variables, $\mathbf{x} \in \mathbb{R}^n$ is the vector of parameters, and of course $J(\mathbf{x}, \mathbf{z}) : \mathbb{R}^{s+n} \to \mathbb{R}$ is the objective or cost function. Additionally $\mathbf{G} \in \mathbb{R}^{m \cdot s}$, $\mathbf{w} \in \mathbb{R}^m$, $\mathbf{c} \in \mathbb{R}^s$ and $\mathbf{S} \in \mathbb{R}^{m \cdot n}$ as described in section (5.7.1). Next we define a closed convex parameter set $\mathbf{K} \subset \mathbb{R}^n$ such as:

$$\mathbf{K} = \{\mathbf{x} \in \mathbb{R}^n : \mathbf{Tx} \leq \mathbf{Z}\}, \tag{5.56}$$

where $\mathbf{K}^* \subseteq \mathbf{K}$ is the set where (5.55) is feasible, and $\mathbf{x}^* \in \mathbf{K}^*$ where $\mathbf{x}^*$ is the optimum. It is further assumed that:

1. the constraint $\mathbf{x} \in \mathbf{K}$ is included in the constraints of $\mathbf{Gz} \leq \mathbf{w} + \mathbf{Sx}$.
2. $\mathbf{K}$ is a full dimensional polytope, or the problem can be reformulated to $\mathbf{K}$ to be full dimensional with a smaller set of parameters.
3. $\mathbf{S}$ is on full rank, or the problem can be reformulated to $\mathbf{S}$ to be full rank with a smaller set of parameters.

As such $\mathbf{J}^* : \mathbf{K}^* \to \mathbb{R}$ is a function which gives the optimum by $\mathbf{x}$. That said let $\mathbf{Z}^* : \mathbf{K}^* \to \mathbb{R}^s$ the function which gives the set of optimizers namely $\mathbf{z}^* \in \mathbf{Z}^*$. The task is to find a $\mathbf{K}^* \subseteq \mathbf{K}$ set and a $\mathbf{z}^* \in \mathbf{Z}^*$ optimizer and the value of the optimum.
Beside of the systematic linear and quadratic program solutions [102] there is a direct geometrical solution for the problem which uses critical regions for describing the parameter space. The critical regions are convex subsets of the parameter space where the optimum is constant based on the function of the parameters. Consider the multi parametric program (5.55), and let $\mathcal{I}_c = \{1, \ldots, m\}$ be the set of constraint indices. For any $\mathcal{A} \subseteq \mathcal{I}_c$, let $\mathbf{G}_\mathcal{A}$, and $\mathbf{S}_\mathcal{A}$ be the subsets of $\mathbf{G}$, and $\mathbf{S}$, respectively, compromising the rows indexed by $\mathcal{A}$, and denote with $\mathbf{G}_j$, $\mathbf{S}_j$ and $\mathbf{w}_j$, the j^{th} row of $\mathbf{G}$, $\mathbf{S}$ and $\mathbf{w}$. We define $\mathcal{C}_\mathcal{A}$ as the set of states $\mathbf{x}$ for which the same set $\mathcal{A}$ of constraints is active at the optimum. Formally, the *optimal partition* of $\mathcal{I}_c$ at $\mathbf{x}$ is the optimal partition of $(\mathcal{A}(x), \mathcal{A}^N(x))$, where:

$$\begin{aligned} \mathcal{A} &= \{j \in \mathcal{I}_c : \mathbf{G}_j \mathbf{z}^*(x) - \mathbf{S}_j \mathbf{x} = \mathbf{w}_j \forall \mathbf{z}^* \in \mathbf{Z}^*(x)\} \\ \mathcal{A}^N &= \{j \in \mathcal{I}_c : \exists \mathbf{z}^* \in \mathbf{Z}^*(x) \text{ s.t.: } \mathbf{G}_j \mathbf{z}^*(x) - \mathbf{S}_j \mathbf{x} < \mathbf{w}_j\}. \end{aligned} \tag{5.57}$$

It can be noticed, that $\mathcal{A}$ and $\mathcal{A}^N$ are disjoint (the intersection of $\mathcal{A}$ and $\mathcal{A}^N$ is an empty set) and they union is $\mathcal{I}_c$. As such consider a set $\mathcal{A} \subseteq \mathcal{I}_c$, then the *critical region* associated with the set of active constraints $\mathcal{A}$ is defined as:

$$\mathcal{C}_\mathcal{A} = \{\mathbf{x} \in \mathbf{K}^* : \mathcal{A}(x) = \mathcal{A}\}. \tag{5.58}$$

With the above the critical region $\mathcal{C}_\mathcal{A}$ is the set of all $\mathbf{x}$ states such that constraints indexed by $\mathcal{A}$ are active at the optimum of problem (5.55). Furthermore it can be proven, that the optimum is an affine function in the domain of $\mathbf{K}$ adn unique for every critical region. As such the problem can be separated into two parts:

1. Find the least dimension subset of $\mathbf{K}$ which contains $\mathbf{K}^*$.
2. Partition $\mathbf{K}^*$ into critical regions and find the optimum for every critical region.

The graphical representation of critical regions can be observed at Fig.(5.12). The algorithm starts from a starting point $\mathbf{x}_0$ and solves the linear programming problem and find $\mathbf{z}^*(\mathbf{x}_0)$. After this find the active constrains and define the corresponding critical region $\mathcal{C}_{\mathcal{A}}(\mathbf{x}_0)$. Its clear from the definition of one critical region that J^* is constant for any $\mathbf{x} \in \mathcal{C}_{\mathcal{A}}(\mathbf{x}_0)$. Next we find the optimum and the optimizer's value for $\mathbf{x} \in \mathcal{C}_{\mathcal{A}}(\mathbf{x}_0)$. and move on to the next critical region. If the optimum problem is not degenerate then finding the critical regions is straightforward, but in the contrary the outcome is defined by the algorithm's starting direction.

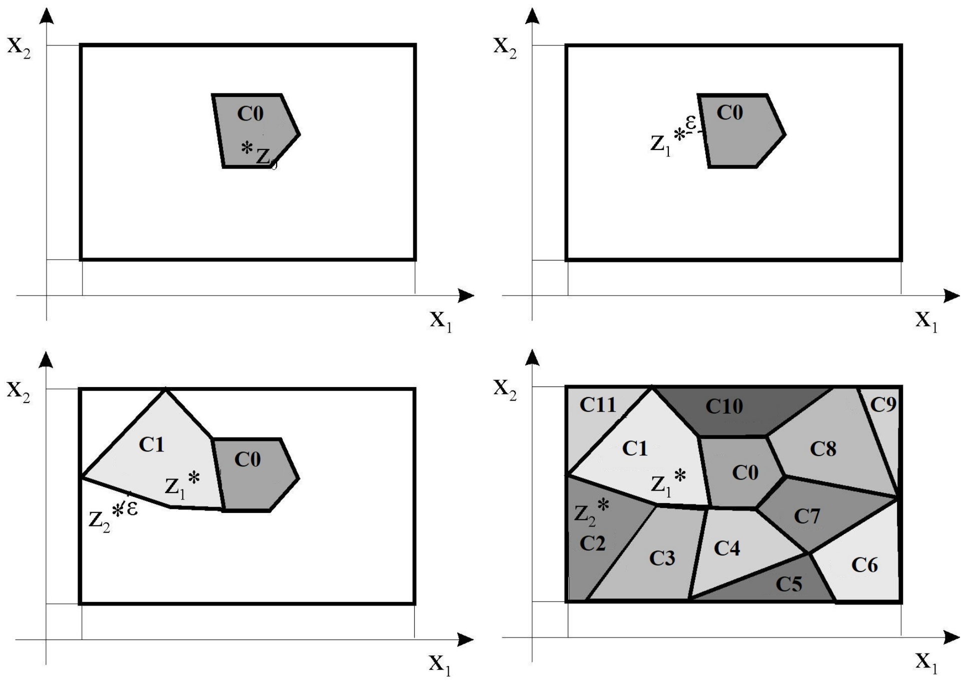

Figure 5.12: Partitioning incrementally the two dimensional parameter space to critical regions from $C0$ to $C11$.

As it shall be described in section 4.4, the if the linear optimization could be described with quadratic programming the process yield more computational cost efficient results in a lot of cases. As such it is advised to apply above geometrical approach in a multi-parametric quadratic programming (mp-QP) environment, as it would be used in the explicit MPC. Consider a multi parametric quadratic program:

$$\begin{aligned} J^*(\mathbf{x}) \quad &= \quad \min_{\mathbf{z}} J(\mathbf{x},\mathbf{z}) = \tfrac{1}{2}\mathbf{z}'\mathbf{H}\mathbf{z} \\ \text{subj. to} \quad &\mathbf{G}\mathbf{z} \le \mathbf{w} + \mathbf{S}\mathbf{x}, \end{aligned} \tag{5.59}$$

and the variables are defined as by (5.55) additionally it is assumed that $\mathbf{H} \succ 0$. The goal is to find the value function $J^*(\mathbf{x})$ and the optimizer function

$\mathbf{z}^*(\mathbf{x})$ in $\mathbf{K}^*$. The search of these functions proceeds by partitioning the set of feasible states into critical regions as before. Note that the more general problem with $J(\mathbf{x},\mathbf{z}) = \frac{1}{2}\mathbf{z}'\mathbf{H}\mathbf{z} + \mathbf{x}'\mathbf{F}\mathbf{x}$ can always be transformed into (5.59) using the variable substitution $\tilde{\mathbf{z}} = \mathbf{z} + \mathbf{H}^{-1}\mathbf{F}'\mathbf{x}$.
As previously let be j the j^{th} row of a matrix or the j^{th} element in a vector, also $\mathcal{J} = \{1,\dots,m\}$ be the set of constraint indices and for any $\mathcal{A} \subseteq \mathcal{I}_c$, also $\mathbf{G}_{\mathcal{A}}$, $\mathbf{w}_{\mathcal{A}}$, and $\mathbf{S}_{\mathcal{A}}$ be the submatrices of $\mathbf{G}$, $\mathbf{w}$ and $\mathbf{S}$ respectively, consisting rows, indexed by $\mathcal{A}$, and $\mathbf{K}^*$ is full dimensional. with the definition displayed in (5.57), and (5.58) it can be showed that the critical regions of a multi parametric quadratic program are polyhedra. Let $(\mathcal{A},\mathcal{A}^N) = (\mathcal{A}(\bar{\mathbf{x}}),\mathcal{A}^N(\bar{\mathbf{x}}))$ for some $\bar{\mathbf{x}} \in \mathbf{K}^*$, where for any given $\bar{\mathbf{x}} \in \mathbf{K}^*$, $J^*(\bar{\mathbf{x}})$ denotes the minimum value of the objective function for $\mathbf{x} = \bar{\mathbf{x}}$. Then:

1. the closure of $\mathcal{C}_{\mathcal{A}}$ is a polyhedron.

2. $\mathbf{z}^*(\mathbf{x})$ is an affine function of the state inside $\mathcal{C}_{\mathcal{A}}$, i.e.: $\mathbf{z}^*(\mathbf{x}) = \mathbf{F}_i\mathbf{x} + \mathbf{g}_i$ for all $\mathcal{C}_{\mathcal{A}}$.

3. $J^*(\mathbf{x})$ is a quadratic function of the state inside $\mathcal{C}_{\mathcal{A}}$, i.e.: $J^*(\mathbf{x}) = \mathbf{x}'\mathbf{M}_i\mathbf{x} + \mathbf{c}_i\mathbf{x} + \mathbf{d}_i$ for all $\mathbf{x} \in \mathcal{C}_{\mathcal{A}}$.

For proving the above, the first order Karush-Kuhn-Tucker (KKT) conditions (described in [102] in detail) for multi parameter quadratic programs are:

$$\mathbf{H}\mathbf{z}^* + \mathbf{G}'\mathbf{u}^* = 0,\ \mathbf{u} \in \mathbb{R}^m \tag{5.60a}$$
$$\mathbf{u}_i^*(\mathbf{G}_i\mathbf{z}^* - \mathbf{w}_i - \mathbf{S}_i\mathbf{x}) = 0,\ i = 1,\dots,m \tag{5.60b}$$
$$\mathbf{u}^* \geq 0 \tag{5.60c}$$
$$\mathbf{G}\mathbf{z}^* - \mathbf{w} - \mathbf{S}\mathbf{x} \leq 0. \tag{5.60d}$$

With the KKT conditions (5.60) the constraints of quadratic problem (5.59) can be written as:

$$\begin{aligned} \frac{dL}{d\mathbf{z}} &\geq 0 \\ \frac{dL}{d\lambda} &\geq 0 \\ \mathbf{z}\frac{dL}{d\mathbf{z}} &= 0 \\ \lambda g_l(\mathbf{x}) &= 0 \\ \mathbf{z} \geq 0\,, \lambda &\geq 0 \end{aligned} \quad \Longleftrightarrow \quad \begin{aligned} \mathbf{z}'\mathbf{H} + \lambda\mathbf{G} &\geq 0 \\ \mathbf{G}\mathbf{z} - \mathbf{w} - \mathbf{S}\mathbf{x} &\leq 0 \\ \mathbf{z}'(\mathbf{H}\mathbf{z} + \mathbf{G}'\lambda) &= 0 \\ \mathbf{z} \geq 0\,, \lambda \geq 0&, \end{aligned} \tag{5.61}$$

where λ is the Lagrange multiplier, L is the Lagrange function and $g(\mathbf{x})$ is the equality constraint. Then can be applied to the active constraints of (5.59) applied on the critical region of $\mathcal{C}_{\mathcal{A}}$:

$$\begin{aligned} \mathbf{Hz} + \mathbf{G}'_{\mathcal{A}}\lambda_{\mathcal{A}} &= 0 \\ \lambda_{\mathcal{A}}(\mathbf{G}_{\mathcal{A}}\mathbf{z} - \mathbf{w}_{\mathcal{A}} - \mathbf{S}_{\mathcal{A}}\mathbf{x}) &= 0 \\ \mathbf{Gz} - \mathbf{w} - \mathbf{Sx} &\leq 0 \\ \lambda_{\mathcal{A}} &\geq 0. \end{aligned} \tag{5.62}$$

From (5.8) it follows:

$$\begin{aligned} \mathbf{z} &= -\mathbf{H}^{-1}\mathbf{G}'_{\mathcal{A}}\lambda_{\mathcal{A}} \\ 0 &= \lambda_{\mathcal{A}}(-\mathbf{G}_{\mathcal{A}}\mathbf{H}^{-1}\mathbf{G}'_{\mathcal{A}} - \mathbf{w}_{\mathcal{A}} - \mathbf{S}_{\mathcal{A}}\mathbf{x}), \end{aligned} \tag{5.63}$$

which then implies that:

$$\begin{aligned} \lambda_{\mathcal{A}} &= (-\mathbf{G}_{\mathcal{A}}\mathbf{H}^{-1}\mathbf{G}'_{\mathcal{A}})^{-1}(\mathbf{w}_{\mathcal{A}} + \mathbf{S}_{\mathcal{A}}\mathbf{x}) \\ \mathbf{z} &= -\mathbf{H}^{-1}\mathbf{G}'_{\mathcal{A}}(-\mathbf{G}_{\mathcal{A}}\mathbf{H}^{-1}\mathbf{G}'_{\mathcal{A}})(\mathbf{w}_{\mathcal{A}} + \mathbf{S}_{\mathcal{A}}\mathbf{x}). \end{aligned} \tag{5.64}$$

In this case $\mathbf{z}$ serves as the optimum if the KKT conditions are fulfilled. Substituting into yields:

$$\begin{aligned} (-\mathbf{G}_{\mathcal{A}}\mathbf{H}^{-1}\mathbf{G}'_{\mathcal{A}})^{-1}(\mathbf{w}_{\mathcal{A}} + \mathbf{S}_{\mathcal{A}}\mathbf{x}) &\geq 0 \\ (\mathbf{G}_{\mathcal{A}} - \mathbf{H}^{-1}\mathbf{G}'_{\mathcal{A}})(-\mathbf{G}_{\mathcal{A}}\mathbf{H}^{-1}\mathbf{G}'_{\mathcal{A}})^{-1}(\mathbf{w}_{\mathcal{A}} + \mathbf{S}_{\mathcal{A}}\mathbf{x}) &\leq \mathbf{w} + \mathbf{Sx}. \end{aligned} \tag{5.65}$$

This inequality of (5.65) expresses the critical region of $\mathcal{C}_{\mathcal{A}}$, and for said region the optimizer can be expressed as:

$$\mathbf{z}^* = (-\mathbf{H}^{-1}\mathbf{G}'_{\mathcal{A}})(-\mathbf{G}_{\mathcal{A}}\mathbf{H}^{-1}\mathbf{G}'_{\mathcal{A}})^{-1}(\mathbf{w}_{\mathcal{A}} + \mathbf{S}_{\mathcal{A}}\mathbf{x}). \tag{5.66}$$

With this in hand the quadratic multi parametric program (5.59) can be solved the same way as the linear multi parametric program (5.55), an the optimum value can be calculated for every critical region explicitly, as the affine function of parameters.

5.8.1 Storage of critical regions

The issue of iterative model based controllers is that they require a lot of computational resource. The CPU load and required ROM consumption could increase exponentially the longer the more steps the control horizon is calculated. For this reason explicit model bssed predictive controllers (EMPC) were developed, where only the storage the critical regions and the signal coefficients for each critical region, so the matrices $\mathbf{H}$, $\mathcal{K}$, $\mathbf{F}$, $\mathbf{G}$ are required. The on-line part of control consists of searching the critical region for the current states and calculating the necessary inputs for them. One method of storing entire critical regions in order to calculate them, and that is in the order in which the MP-LP or MP-QP problem is resolved. It has the disadvantage, that the search time can be high, as such starting from the top of the list, a linear search is not effective. The efficient method is to store critical regions already in a binary tree [119], [120], [121], [122]. The method of generating the binary tree is shown in (Fig.(5.13).).
The basic idea is to sort the critical regions depending on their adjacent sides.

For example, in (Fig.(5.13).a.) side j_1 divides the state space into two, at the right of it are the regions $X_{2,3,4,5}$ and to the left are the regions $X_{1,2,6}$. They make up the nodes adjacent to the base node I_1 of the binary tree. Next the another side from the space is chosen defined by each node I_2 respectively I_3, and the algorithm is continued until all the regions in the current node correspond to the same control signal, denoted by F on the shaft in fig. (Fig.(5.13).b.) Thus with this search pattern logarithmic search time can be achieved.

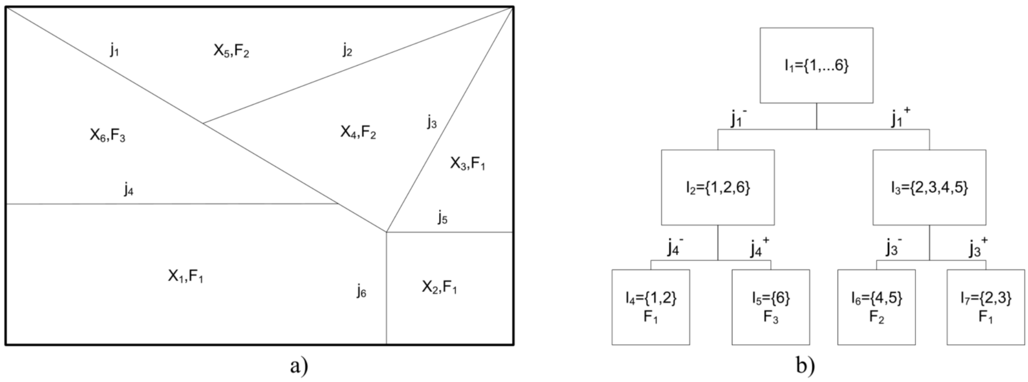

Figure 5.13: Basic search three of an EMPC where, a) are the critical regions for a space of 2D parameters, b) the related binary tree.

The implementation of MPC in explicit form is very efficient up to a certain number of critical regions, because they do not require calculations but only search in a table. For more complex problems or fast systems the method requires longer search time.

5.9 Notations used in the appendix

$\mathbf{A}$	State matrix of a linear time invariant model
$\mathbf{A}_x$	Constraint state matrix
$\mathbf{A}_u$	Constraint input matrix
$\mathbf{A}_f$	Constraint state matrix at the end of the horizon
$\mathcal{A}$	Set if indices in states where the constraints are active
$\mathcal{A}^N$	Set if indices in states where the constraints are inactive
$\mathbf{B}$	Input matrix of a linear time invariant model
$\mathcal{C}_{\mathcal{A}}$	Critical region associated with the active constraints
$\mathcal{D}$	APPS set of step directions
d_i	APPS direction of active process
$\mathbf{E}$	Unified constraint state matrix
$\mathcal{E}$	APPS set of external sucesses
$\mathbf{F}$	State coefficient matrix for calculating the optimal input
$\mathbf{G}$	Unified constraint input matrix
g	Autonomous function where there are no inputs
$\mathbf{H}$	Supplementary quadratic optimizer matrix
I_i	i^{th} node in critical region storage
$\mathcal{I}_c$	Set if indices of constraints
J	Cost (or value) function to optimize
J^*	Optimal cost value
$\mathcal{J}$	Set if indices of active constraints
$\mathbf{K}$	Controller gain
$\mathcal{K}$	Set of states respective to constraints
$\mathcal{K}^*$	Set of feasible states respective to constraints
k	Time step on the horizon N
L	Lagrange function
N	Defined horizon of MPC
N_c, N_u, N_y	Defined control, input, and output horizon respectively
$\mathbf{P}$	Terminal penalising weight matrix
$\mathcal{P}$	APPS set of processes
$\mathcal{P}^c$	Set of all (input and state) constraints at time instance
$\mathbf{p}$	APPS search pattern
$\mathbf{Q}$	State penalising weight matrix
$\mathcal{Q}$	APPS set of sidestep indices
$\mathbf{R}$	Input penalising weight matrix
$\mathbf{S}$	General state constraint coefficient
$\mathcal{S}$	APPS set of successful iterations
$\mathcal{S}^x$	Set of all possible future state matrices stepping through the horizon
$\mathcal{S}^u$	Set of all possible future input matrices stepping through the horizon
$\mathbf{U}_0^*$	Optimal vector of future inputs starting from the initial state
$\mathcal{U}$	APPS set of unsuccessful steps
$\mathcal{U}^u$	Set of inputs not violating constraints
$\mathbf{u}^*$	Optimal vector of input
V	Lyapunov function
$\mathbf{w}$	Unified constraint vector
X_i	i^{th} critical region in critical region search
$\mathcal{X}^x$	Set of all possible future states stepping through the horizon
$\mathbf{x}$	State vector of a linear time invariant model
$\bar{\mathbf{x}}$	Minimum state value of the objective function
x_i^{best}	APPS best reached state, where x_i^{best} is a minima
$\mathbf{Y}$	Supplementary matrices
$\mathbf{Z}^*$	Set of optimizers leading to feasible states
$\mathbf{z}$	Optimizer of linear multi parametric problem
$\mathbf{z}^*$	Optimizer, leading to a feasible state
$\tilde{\mathbf{z}}$	Set of all future states and inputs over the horizon
Δ	APPS step length control parameter
Δ_i^{best}	APPS best reached step size
λ	Lagrange multiplier
θ	APPS system specific tunable parameter
ρ	APPS infinite sequence iterator

5.10 Abbrevations

AC: Alternating current
ACSI: Asymmetrical current source inverter
APPS: Asynchronous Parallel Pattern Search
CPU: Central processing unit
CSI: Current Source Inverter
CSR: Current source rectifier
CVUF: Complex voltage unbalance factor
DC: Direct current
EMPC: Explicit model predictive control
HPF: High pass filter
IGBT: Insulated gate bipolar transistor
MAC: Multiply and accumulate
MIMO Multiple input, multiple output
MPC: Model predictive coltrol
MPT: Model predictive control toolbox
MPPT: Maximum power point tracking
MP-LP: Multi paramteric linear programming
MP-QP: Milti parametric quadratic programming
ROM: Read only memory
SFC: State feedback control
SVM: Space vector modulation
SVPWM Space vector pulse width modulated
THD: Total harmonic distortion
SHE: Selective harmonic elimination
TPWM: Trapezoidal pulse width modulation
VSR: Voltage source rectifier
VU: Voltage unbalance
VUF: Voltage unbalance factor (i.e. TDV)

Bibliography

Related Publications

[P1] **L. Neukirchner**, A. Göllei, P. Görbe, and A. Magyar, "Carbon footprint reduction via voltage asymmetry compensation of three-phase low voltage grid utilizing small domestic power plants," *Chemical Engineering Transactions*, vol. 45, pp. 283–288, 2015.

[P2] **L. Neukirchner**, P. Görbe, and A. Magyar, "Examination of different voltage asymmetry norms under transient behavior of three-phase low voltage power systems containing small domestic power plants," in *PowerTech, 2015 IEEE Eindhoven*, IEEE, 2015, pp. 1–6.

[P3] **L. Neukirchner**, P. Görbe, and A. Magyar, "Voltage unbalance reduction in the domestic distribution area using asymmetric inverters," *Journal of cleaner production*, vol. 142, pp. 1710–1720, 2017.

[P4] **L. Neukirchner**, A. Göllei, P. Görbe, and A. Magyar, "Voltage unbalance reduction of a local transformer area with domestic asymmetrical inverter and optimal control design," *Int. J. of Thermal & Environmental Engineering*, vol. 12, no. 2, pp. 129–134, 2016.

[P5] **L. Neukirchner**, A. Magyar, A. Fodor, N. D. Kutasi, and A. Kelemen, "Constrained predictive control of three-phasebuck rectifiers," *Acta Polytechnica Hungarica*, vol. 17, no. 1, 2020.

Literature

[1] S. A. Shezan, S Julai, M. Kibria, *et al.*, "Performance analysis of an off-grid wind-pv (photovoltaic)-diesel-battery hybrid energy system feasible for remote areas," *Journal of Cleaner Production*, vol. 125, pp. 121–132, 2016.

[2] F. Cucchiella, I. D'Adamo, and S. L. Koh, "Environmental and economic analysis of building integrated photovoltaic systems in italian regions," *Journal of Cleaner Production*, vol. 98, pp. 241–252, 2015.

[3] J. Kaldellis, M Simotas, D Zafirakis, and E Kondili, "Optimum autonomous photovoltaic solution for the greek islands on the basisof energy pay-back analysis," *Journal of Cleaner Production*, vol. 17, no. 15, pp. 1311–1323, 2009.

[4] M. Ortega, J. Hernández, and O. García, "Measurement and assessment of power quality characteristics for photovoltaic systems: Harmonics, flicker, unbalance, and slow voltage variations," *Electric Power Systems Research*, vol. 96, pp. 23–35, 2013.

[5] L. H. Saw, Y. Ye, and A. A. Tay, "Integration issues of lithium-ion battery into electric vehicles battery pack," *Journal of Cleaner Production*, vol. 113, pp. 1032–1045, 2016.

[6] P. D. Lund, J. Mikkola, and J Ypyä, "Smart energy system design for large clean power schemes in urban areas," *Journal of Cleaner Production*, vol. 103, pp. 437–445, 2015.

[7] M. C. R. Paz, R. G. Ferraz, A. S. Bretas, and R. C. Leborgne, "System unbalance and fault impedance effect on faulted distribution networks," *Computers & Mathematics with Applications*, vol. 60, no. 4, pp. 1105–1114, 2010.

[8] P. Gnaciński, M. Pepliński, D. Hallmann, and P. Jankowski, "Induction cage machine thermal transients under lowered voltage quality," *IET Electric Power Applications*, vol. 13, no. 4, pp. 479–486, 2019.

[9] M. Savaghebi, A. Jalilian, J. C. Vasquez, and J. M. Guerrero, "Secondary control scheme for voltage unbalance compensation in an islanded droop-controlled microgrid," *IEEE Transactions on Smart Grid*, vol. 3, no. 2, pp. 797–807, 2012.

[10] A. Siddique, G. Yadava, and B. Singh, "Effects of voltage unbalance on induction motors," in *Conference Record of the 2004 IEEE International Symposium on Electrical Insulation*, IEEE, 2004, pp. 26–29.

[11] T. Brekken, N. Mohan, and T. Undeland, "Control of a doubly-fed induction wind generator under unbalanced grid voltage conditions," in *2005 European Conference on Power Electronics and Applications*, IEEE, 2005, 10–pp.

[12] C.-Y. Lee, B.-K. Chen, W.-J. Lee, and Y.-F. Hsu, "Effects of various unbalanced voltages on the operation performance of an induction motor under the same voltage unbalance factor condition," *Electric Power Systems Research*, vol. 47, no. 3, pp. 153–163, 1998.

[13] B. Meersman, B. Renders, L. Degroote, T. Vandoorn, and L. Vandevelde, "Three-phase inverter-connected dg-units and voltage unbalance," *Electric Power Systems Research*, vol. 81, no. 4, pp. 899–906, 2011.

[14] Y. Ates, M. Uzunoglu, A. Karakas, A. R. Boynuegri, A. Nadar, and B. Dag, "Implementation of adaptive relay coordination in distribution systems including distributed generation," *Journal of cleaner production*, vol. 112, pp. 2697–2705, 2016.

[15] M. T. Bina and A Kashefi, "Three-phase unbalance of distribution systems: Complementary analysis and experimental case study," *International Journal of Electrical Power & Energy Systems*, vol. 33, no. 4, pp. 817–826, 2011.

[16] P. Görbe, A. Magyar, and K. M. Hangos, "Reduction of power losses with smart grids fueled with renewable sources and applying ev batteries," *Journal of cleaner production*, vol. 34, pp. 125–137, 2012.

[17] P. Görbe, A. Fodor, A. Magyar, and K. M. Hangos, "Experimental study of the nonlinear distortion caused by domestic power plants," *Applied Thermal Engineering*, vol. 70, no. 2, pp. 1288–1293, 2014.

[18] N. Korovkin, Q. Vu, and R. Yazenin, "A method for minimization of unbalanced mode in three-phase power systems," in *2016 IEEE NW Russia Young Researchers in Electrical and Electronic Engineering Conference (EIConRusNW)*, IEEE, 2016, pp. 611–614.

[19] A. D. Martin, R. S. Herrera, J. R. Vazquez, P. Crolla, and G. M. Burt, "Unbalance and harmonic distortion assessment in an experimental distribution network," *Electric Power Systems Research*, vol. 127, pp. 271–279, 2015.

[20] P. G. Kini, R. C. Bansal, and R. S. Aithal, "A novel approach toward interpretation and application of voltage unbalance factor," *IEEE transactions on industrial electronics*, vol. 54, no. 4, pp. 2315–2322, 2007.

[21] H. Wen, D. Cheng, Z. Teng, S. Guo, and F. Li, "Approximate algorithm for fast calculating voltage unbalance factor of three-phase power system," *IEEE Transactions on Industrial Informatics*, vol. 10, no. 3, pp. 1799–1805, 2014.

[22] L. R. Araujo, D. Penido, S. Carneiro, and J. L. R. Pereira, "A three-phase optimal power-flow algorithm to mitigate voltage unbalance," *IEEE Transactions on Power Delivery*, vol. 28, no. 4, pp. 2394–2402, 2013.

[23] A. Von Meier, *Electric power systems: a conceptual introduction.* John Wiley & Sons, 2006.

[24] J. Cobben, "Power quality: About the problems and solutions," 2012.

[25] C. Eugene, "A new simple and effective approximate formulation for determination of three-phase unbalance by the voltmeter method," in *CIGRE 1986*, 1986, p. 11.

[26] A Robert and J Marquet, "Assessing voltage quality with relation to harmonics, flicker and unbalance," in *International Conference on Large High Voltage Electric Systems*, vol. 2, 1992, pp. 36–203.

[27] C. L. Fortescue, "Method of symmetrical co-ordinates applied to the solution of polyphase networks," *Transactions of the American Institute of Electrical Engineers*, vol. 37, no. 2, pp. 1027–1140, 1918.

[28] A. H. Bonnett and G. Soukup, "Understanding the nema motor-generator standards of section mg-1-1993, revision 3, three-phase induction motors," in *Record of Conference Papers. IEEE Industry Applications Society 44th Annual Petroleum and Chemical Industry Conference*, IEEE, 1997, pp. 225–238.

[29] "IEEE recommended practice for electric power distribution for industrial plants (ieee red book)," 1986, pp. 1–609.

[30] "IEEE standard for inverse-time characteristics equations for overcurrent relays," 2019, pp. 1–25.

[31] "IEEE guide for self-commutated converters," 1987.

[32] P Pillay and M Manyage, "Definitions of voltage unbalance," *IEEE Power Engineering Review*, vol. 21, no. 5, pp. 50–51, 2001.

[33] R. C. Dugan, M. F. McGranaghan, and H. W. Beaty, "Electrical power systems quality," *New York, NY: McGraw-Hill,| c1996*, 1996.

[34] Y.-J. Wang, "An analytical study on steady-state performance of an induction motor connected to unbalanced three-phase voltage," in *2000 IEEE Power Engineering Society Winter Meeting. Conference Proceedings (Cat. No. 00CH37077)*, IEEE, vol. 1, 2000, pp. 159–164.

[35] L Pierrat and J. Meyer, "Unbalance factor it is as simple as abc," *Revue Générale de l'Électricité*, vol. 1, no. 6, pp. 18–26, 1987.

[36] Y.-J. Wang, "Analysis of effects of three-phase voltage unbalance on induction motors with emphasis on the angle of the complex voltage unbalance factor," *IEEE Transactions on energy conversion*, vol. 16, no. 3, pp. 270–275, 2001.

[37] A. K. Singh, G. Singh, and R Mitra, "Some observations on definitions of voltage unbalance," in *2007 39th North American Power Symposium*, IEEE, 2007, pp. 473–479.

[38] T.-H. Chen, C.-H. Yang, and N.-C. Yang, "Examination of the definitions of voltage unbalance," *International Journal of Electrical Power & Energy Systems*, vol. 49, pp. 380–385, 2013.

[39] R. Betz, T Summers, T Furney, *et al.*, "Symmetry compensation using a h-bridge multilevel statcom with zero sequence injection," in *Industry Applications Conference, 2006. 41st IAS Annual Meeting. Conference Record of the 2006 IEEE*, vol. 4, 2006, pp. 1724–1731.

[40] J. Hang, J. Zhang, M. Cheng, and J. Huang, "Online interturn fault diagnosis of permanent magnet synchronous machine using zero-sequence components," *IEEE Transactions on Power Electronics*, vol. 30, no. 12, pp. 6731–6741, 2015.

[41] S. Arnborg, G. Andersson, D. J. Hill, and I. A. Hiskens, "On undervoltage load shedding in power systems," *International Journal of Electrical Power & Energy Systems*, vol. 19, no. 2, pp. 141–149, 1997.

[42] Y.-J. Wang and L. Pierrat, "A method integrating deterministic and stochastic approaches for the simulation of voltage unbalance in electric power distribution systems," *IEEE Transactions on Power Systems*, vol. 16, no. 2, pp. 241–246, 2001.

[43] D. Schwanz, F. Möller, S. K. Rönnberg, J. Meyer, and M. H. Bollen, "Stochastic assessment of voltage unbalance due to single-phase-connected solar power," *IEEE Transactions on Power Delivery*, vol. 32, no. 2, pp. 852–861, 2016.

[44] J. Xu, J. Wang, S. Liao, *et al.*, "Stochastic multi-objective optimization of photovoltaics integrated three-phase distribution network based on dynamic scenarios," *Applied Energy*, vol. 231, pp. 985–996, 2018.

[45] Y. Li, D. M. Vilathgamuwa, and P. C. Loh, "Microgrid power quality enhancement using a three-phase four-wire grid-interfacing compensator," *IEEE transactions on industry applications*, vol. 41, no. 6, pp. 1707–1719, 2005.

[46] K. Lee, T. M. Jahns, T. A. Lipo, and V. Blasko, "New control method including state observer of voltage unbalance for grid voltage-source converters," *IEEE Transactions on Industrial Electronics*, vol. 57, no. 6, pp. 2054–2065, 2009.

[47] Y. Xu, L. M. Tolbert, J. D. Kueck, and D. T. Rizy, "Voltage and current unbalance compensation using a static var compensator," *IET Power Electronics*, vol. 3, no. 6, pp. 977–988, 2010.

[48] V. Vekhande, V. Kanakesh, and B. G. Fernandes, "Control of three-phase bidirectional current-source converter to inject balanced three-phase currents under unbalanced grid voltage condition," *IEEE Transactions on power electronics*, vol. 31, no. 9, pp. 6719–6737, 2015.

[49] Z. Wang, B. Wu, D. Xu, M. Cheng, and L. Xu, "Dc-link current ripple mitigation for current-source grid-connected converters under unbalanced grid conditions," *IEEE Transactions on Industrial Electronics*, vol. 63, no. 8, pp. 4967–4977, 2016.

[50] X. Guo, Y. Yang, and X. Zhang, "Advanced control of grid-connected current source converter under unbalanced grid voltage conditions," *IEEE Transactions on Industrial Electronics*, vol. 65, no. 12, pp. 9225–9233, 2018.

[51] J. Hu, M. Marinelli, M. Coppo, A. Zecchino, and H. W. Bindner, "Coordinated voltage control of a decoupled three-phase on-load tap changer transformer and photovoltaic inverters for managing unbalanced networks," *Electric Power Systems Research*, vol. 131, pp. 264–274, 2016.

[52] A. El-Naggar and I. Erlich, "Control approach of three-phase grid connected pv inverters for voltage unbalance mitigation in low-voltage distribution grids," *IET Renewable Power Generation*, vol. 10, no. 10, pp. 1577–1586, 2016.

[53] P. P. Dash and M. Kazerani, "Dynamic modeling and performance analysis of a grid-connected current-source inverter-based photovoltaic system," *IEEE Transactions on Sustainable Energy*, vol. 2, no. 4, pp. 443–450, 2011.

[54] D. M. Olsson and L. S. Nelson, "The nelder-mead simplex procedure for function minimization," *Technometrics*, vol. 17, no. 1, pp. 45–51, 1975.

[55] P. D. Hough, T. G. Kolda, and V. J. Torczon, "Asynchronous parallel pattern search for nonlinear optimization," *SIAM Journal on Scientific Computing*, vol. 23, no. 1, pp. 134–156, 2001.

[56] T. G. Kolda and V. J. Torczon, "Understanding asynchronous parallel pattern search," in *High Performance Algorithms and Software for Nonlinear Optimization*, Springer, 2003, pp. 323–342.

[57] S. Kirkpatrick, C. D. Gelatt, and M. P. Vecchi, "Optimization by simulated annealing," *science*, vol. 220, no. 4598, pp. 671–680, 1983.

[58] S. Boyd, L. Xiao, and A. Mutapcic, "Subgradient methods," *lecture notes of EE392o, Stanford University, Autumn Quarter*, vol. 2004, pp. 2004–2005, 2003.

[59] A. Von Jouanne and B. Banerjee, "Assessment of voltage unbalance," *IEEE transactions on power delivery*, vol. 16, no. 4, pp. 782–790, 2001.

[60] D. Smith, H. Braunstein, and J. Borst, "Voltage unbalance in 3-and 4-wire delta secondary systems," *IEEE transactions on power delivery*, vol. 3, no. 2, pp. 733–741, 1988.

[61] N. Kutasi, A. Kelemen, and M. Imecs, "Constrained optimal control of three-phase ac-dc boost converters," in *2010 IEEE International Conference on Automation, Quality and Testing, Robotics (AQTR)*, IEEE, vol. 1, 2010, pp. 1–6.

[62] Y. Zhang, Y. Yi, P. Dong, F. Liu, and Y. Kang, "Simplified model and control strategy of three-phase pwm current source rectifiers for dc voltage power supply applications," *IEEE Journal of Emerging and Selected Topics in Power Electronics*, vol. 3, no. 4, pp. 1090–1099, 2015.

[63] I. Vajda, Y. N. Dementyev, K. N. Negodin, N. V. Kojain, L. S. Udut, I. A. Chesnokova, *et al.*, "Limiting static and dynamic characteristics of an induction motor under frequency vector control," *Acta Polytechnica Hungarica*, vol. 14, no. 6, pp. 7–27, 2017.

[64] B. Ghalem and B. Azeddine, "Six-phase matrix converter fed double star induction motor," *Acta Polytechnica Hungarica*, vol. 7, no. 3, pp. 163–176, 2010.

[65] S. Gupta and R. K. Tripathi, "Two-area power system stability improvement using a robust controller-based csc-statcom," *Acta Polytechnica Hungarica*, vol. 11, no. 7, pp. 135–155, 2014.

[66] D. Chen, J. Jiang, Y. Qiu, J. Zhang, and F. Huang, "Single-stage three-phase current-source photovoltaic grid-connected inverter high voltage transmission ratio," *IEEE Transactions on Power Electronics*, vol. 32, no. 10, pp. 7591–7601, 2016.

[67] B. Exposto, R. Rodrigues, J. Pinto, V. Monteiro, D. Pedrosa, and J. L. Afonso, "Predictive control of a current-source inverter for solar photovoltaic grid interface," in *2015 9th International Conference on Compatibility and Power Electronics (CPE)*, IEEE, 2015, pp. 113–118.

[68] M. Chebre, A. Meroufel, and Y. Bendaha, "Speed control of induction motor using genetic algorithm-based pi controller," *Acta Polytechnica Hungarica*, vol. 8, no. 6, pp. 141–153, 2011.

[69] R. Salloum, B. Moaveni, and M. R. Arvan, "Robust pid controller design for a real electromechanical actuator," *Acta Polytechnica Hungarica*, vol. 11, no. 5, pp. 125–144, 2014.

[70] F. Tahri, A. Tahri, A. Allali, and S. Flazi, "The digital self-tuning control of step a down dc-dc converter," *Acta Polytechnica Hungarica*, vol. 9, no. 6, pp. 49–64, 2012.

[71] H. Gao, D. Xu, B. Wu, and N. R. Zargari, "Model predictive control for five-level current source converter with dc current balancing capability," in *IECON 2017-43rd Annual Conference of the IEEE Industrial Electronics Society*, IEEE, 2017, pp. 8230–8235.

[72] Y. Han, L. Xu, M. M. Khan, and C. Chen, "Control strategies, robustness analysis, digital simulation and practical implementation for a hybrid apf with a resonant ac-link," *Acta polytechnica hungarica*, vol. 7, no. 5, 2010.

[73] H. Feroura, F. Krim, B. Tabli, and A. Laib, "Finite-set model predictive voltage control for islanded three phase current source inverter," in *2017 5th International Conference on Electrical Engineering-Boumerdes (ICEE-B)*, IEEE, 2017, pp. 1–5.

[74] Z. Yan, X. Xu, Z. Yang, X. Wu, and Y. Wang, "Study of effective vector synthesis sequence for three-phase current rectifier," in *2015 Fifth International Conference on Instrumentation and Measurement, Computer, Communication and Control (IMCCC)*, IEEE, 2015, pp. 1065–1070.

[75] Z. Bai, H. Ma, D. Xu, B. Wu, Y. Fang, and Y. Yao, "Resonance damping and harmonic suppression for grid-connected current-source converter," *IEEE Transactions on Industrial Electronics*, vol. 61, no. 7, pp. 3146–3154, 2013.

[76] J. C. Wiseman and B. Wu, "Active damping control of a high-power pwm current-source rectifier for line-current thd reduction," *IEEE Transactions on Industrial Electronics*, vol. 52, no. 3, pp. 758–764, 2005.

[77] H. Zheng, X. Zhou, N. Yang, and Y. Ding, "Current source rectifier based on fuzzy two closed loop control system," in *2010 International Conference on Computer, Mechatronics, Control and Electronic Engineering*, IEEE, vol. 5, 2010, pp. 103–106.

[78] A. Chatterjee, R. Chatterjee, F. Matsuno, and T. Endo, "Augmented stable fuzzy control for flexible robotic arm using lmi approach and neuro-fuzzy state space modeling," *IEEE transactions on industrial electronics*, vol. 55, no. 3, pp. 1256–1270, 2008.

[79] T. Haidegger, L. Kovács, R.-E. Precup, B. Benyó, Z. Benyó, and S. Preitl, "Simulation and control for telerobots in space medicine," *Acta Astronautica*, vol. 81, no. 1, pp. 390–402, 2012.

[80] S. Vrkalovic, E.-C. Lunca, and I.-D. Borlea, "Model-free sliding mode and fuzzy controllers for reverse osmosis desalination plants," *Int. J. Artif. Intell*, vol. 16, no. 2, pp. 208–222, 2018.

[81] C. B. Regaya, A. Zaafouri, and A. Chaari, "A new sliding mode speed observer of electric motor drive based on fuzzy-logic," *Acta Polytechnica Hungarica*, vol. 11, no. 3, pp. 219–232, 2014.

[82] K. Széll and P. Korondi, "Mathematical basis of sliding mode control of an uninterruptible power supply," *Acta Polytechnica Hungarica*, vol. 11, no. 03, pp. 87–106, 2014.

[83] S. F. Ahmed, C. F. Azim, H. Desa, and A.-S. T. Hussain, "Model predictive controller-based single phase pulse width modulation (pwm) inverter for ups systems," *Acta Polytechnica Hungarica*, vol. 11, no. 6, pp. 23–38, 2014.

[84] P. Correa and J. Rodriguez, "A predictive control scheme for current source rectifiers," in *2008 13th International Power Electronics and Motion Control Conference*, IEEE, 2008, pp. 699–702.

[85] N. Muthukumar, S. Srinivasan, K. Ramkumar, K. Kannan, and V. E. Balas, "Adaptive model predictive controller for web transport systems," *Acta Polytechnica Hungarica*, vol. 13, no. 3, pp. 181–194, 2016.

[86] A. Kelemen, N. Kutasi, M. Imecs, and I. I. Incze, "Constrained optimal direct power control of voltage-source pwm rectifiers," in *2010 IEEE 14th International Conference on Intelligent Engineering Systems*, IEEE, 2010, pp. 249–254.

[87] M Rivera, S Kouro, J Rodriguez, *et al.*, "Predictive current control in a current source inverter operating with low switching frequency," in *4th International Conference on Power Engineering, Energy and Electrical Drives*, IEEE, 2013, pp. 334–339.

[88] A. Godlewska and A. Sikorski, "Predictive control of current source rectifier," in *2015 Selected Problems of Electrical Engineering and Electronics (WZEE)*, IEEE, 2015, pp. 1–6.

[89] J. W. Kolar, H. Ertl, and F. C. Zach, "Design and experimental investigation of a three-phase high power density high efficiency unity power factor pwm (vienna) rectifier employing a novel integrated power semiconductor module," in *Proceedings of Applied Power Electronics Conference. APEC'96*, IEEE, vol. 2, 1996, pp. 514–523.

[90] N. Zargari and G Joos, "A current-controlled current source type unity power factor pwm rectifier," in *Conference Record of the 1993 IEEE Industry Applications Conference Twenty-Eighth IAS Annual Meeting*, IEEE, 1993, pp. 793–799.

[91] Y. Sato and T. Kataoka, "State feedback control of current-type pwm ac-to-dc converters," *IEEE transactions on industry applications*, vol. 29, no. 6, pp. 1090–1097, 1993.

[92] T. Nussbaumer, M. Baumann, and J. W. Kolar, "Comprehensive design of a three-phase three-switch buck-type pwm rectifier," *IEEE Transactions on Power Electronics*, vol. 22, no. 2, pp. 551–562, 2007.

[93] L. Malesani and P. Tenti, "Three-phase ac/dc pwm converter with sinusoidal ac currents and minimum filter requirements," *IEEE Transactions on Industry Applications*, no. 1, pp. 71–77, 1987.

[94] R Itoh, "Steady-state and transient characteristics of a single-way step-down pwm gto voltage-source convertor with sinusoidal supply currents," in *IEE Proceedings B (Electric Power Applications)*, IET, vol. 136, 1989, pp. 168–175.

[95] D. J. Tooth, S. J. Finney, and B. W. Williams, "Effects of using dc-side average current-mode control on a three-phase converter with an input filter and distorted supply," *IEE Proceedings-Electric Power Applications*, vol. 147, no. 6, pp. 459–468, 2000.

[96] M. Salo, "A three-switch current-source pwm rectifier with active filter function," in *2005 IEEE 36th Power Electronics Specialists Conference*, IEEE, 2005, pp. 2230–2236.

[97] M. Baumann, U. Drofenik, and J. W. Kolar, "New wide input voltage range three-phase unity power factor rectifier formed by integration of a three-switch buck-derived front-end and a dc/dc boost converter output stage," in *INTELEC. Twenty-Second International Telecommunications Energy Conference (Cat. No. 00CH37131)*, IEEE, 2000, pp. 461–470.

[98] M. Baumann and J. W. Kolar, "A novel control concept for reliable operation of a three-phase three-switch buck-type unity-power-factor rectifier with integrated boost output stage under heavily unbalanced mains condition," *IEEE Transactions on Industrial Electronics*, vol. 52, no. 2, pp. 399–409, 2005.

[99] L. Moussaoui and A. Moussi, "An open loop space vector pwm control for csi-fed field-oriented induction motor drive with improved performances and reduced pulsating torque," *WSEAS Trans.-Circuits and Systems*, vol. 1, no. 2, pp. 71–77, 2005.

[100] M. Herceg, M. Kvasnica, C. Jones, and M. Morari, "Multi-Parametric Toolbox 3.0," in *Proc. of the European Control Conference*, `http://control.ee.ethz.ch/~mpt`, Zürich, Switzerland, 2013, pp. 502–510.

[101] J. C. Wiseman, B. Wu, and G. Castle, "A pwm current-source rectifier with active damping for high power medium voltage applications," in *2002 IEEE 33rd Annual IEEE Power Electronics Specialists Conference. Proceedings (Cat. No. 02CH37289)*, IEEE, vol. 4, 2002, pp. 1930–1934.

[102] F. Borrelli, A. Bemporad, and M. Morari, *Predictive control for linear and hybrid systems*. Cambridge University Press, 2017.

[103] **L. Neukirchner**. "Constrained predictive control of three-phase buck rectifiers simulation details." (2019), [Online]. Available: `http://virt.uni-pannon.hu/ver/index.php/en/projects/30-empc-csr,2019`.

[104] M. Kheraluwala, R. W. Gascoigne, D. M. Divan, and E. D. Baumann, "Performance characterization of a high-power dual active bridge dc-to-dc converter," *IEEE Transactions on industry applications*, vol. 28, no. 6, pp. 1294–1301, 1992.

[105] S. Inoue and H. Akagi, "A bidirectional dc–dc converter for an energy storage system with galvanic isolation," *IEEE Transactions on Power Electronics*, vol. 22, no. 6, pp. 2299–2306, 2007.

[106] J. A. Rossiter, *Model-based predictive control: a practical approach*. CRC press, 2017.

[107] W. H. Kwon and S. H. Han, *Receding horizon control: model predictive control for state models*. Springer Science & Business Media, 2006.

[108] M. Baotic, "Optimal control of piecewise affine systems: A multi-parametric approach," Ph.D. dissertation, ETH Zurich, 2005.

[109] M. Herceg, "Real-time explicit model predictive control of processes," Ph.D. dissertation, PhD thesis, 2009.

[110] A. Grancharova and T. A. Johansen, "Survey of explicit approaches to constrained optimal control," in *Switching and Learning in Feedback Systems*, Springer, 2005, pp. 47–97.

[111] P. Antoniewicz, "Predictive control of three phase ac/dc converters," Ph.D. dissertation, The Institute of Control and Industrial Electronics, 2009.

[112] T. Geyer, *Low complexity model predictive control in power electronics and power systems*. Cuvillier Verlag, 2005.

[113] A. Bemporad, M. Morari, V. Dua, and E. N. Pistikopoulos, "The explicit linear quadratic regulator for constrained systems," *Automatica*, vol. 38, no. 1, pp. 3–20, 2002.

[114] G. Goodwin, M. M. Seron, and J. A. De Doná, *Constrained control and estimation: an optimisation approach*. Springer Science & Business Media, 2006.

[115] D. Q. Mayne, J. B. Rawlings, C. V. Rao, and P. O. Scokaert, "Constrained model predictive control: Stability and optimality," *Automatica*, vol. 36, no. 6, pp. 789–814, 2000.

[116] P. Grieder, M. Kvasnica, M. Baotić, and M. Morari, "Stabilizing low complexity feedback control of constrained piecewise affine systems," *Automatica*, vol. 41, no. 10, pp. 1683–1694, 2005.

[117] S. a. Keerthi and E. G. Gilbert, "Optimal infinite-horizon feedback laws for a general class of constrained discrete-time systems: Stability and moving-horizon approximations," *Journal of optimization theory and applications*, vol. 57, no. 2, pp. 265–293, 1988.

[118] D. Q. Mayne and H. Michalska, "Receding horizon control of nonlinear systems," *IEEE Transactions on automatic control*, vol. 35, no. 7, pp. 814–824, 1990.

[119] C. N. Jones, P. Grieder, and S. V. Raković, "A logarithmic-time solution to the point location problem for parametric linear programming," *Automatica*, vol. 42, no. 12, pp. 2215–2218, 2006.

[120] P. Tøndel, T. A. Johansen, and A. Bemporad, "Evaluation of piecewise affine control via binary search tree," *Automatica*, vol. 39, no. 5, pp. 945–950, 2003.

[121] P. Tøndel and N Trondheim, "Constrained optimal control via multiparametric quadraticprogramming.," Ph.D. dissertation, Citeseer, 2003.

[122] N. Kutasi, A. Kelemen, and M. Imecs, "Vector control of induction motor drives with model based predictive current controller," in *2008 IEEE International Conference on Computational Cybernetics*, IEEE, 2008, pp. 21–26.